ACTIVATION AND INHIBITOR STUDIES ON METHYL-COENZYME M

REDUCTASE AND PURIFICATION OF A NEW HYDROXYLAMINE

OXIDOREDUCTASE FROM *METHYLOMICROBIUM ALBUM*

ATCC 33003

Except where reference is made to the work of others, the work described in this
dissertation is my own or was done in collaboration with my advisory committee.
This dissertation does not include proprietary or classified information.

_____
Na Yang

Certificate of Approval:

_____   _____
Douglas C. Goodwin   Evert C. Duin, Chair
Associate Professor   Assistant Professor
Chemistry and Biochemistry   Chemistry and Biochemistry

_____   _____
Holly R. Ellis   Edward J. Parish
Associate Professor   Associate Professor
Chemistry and Biochemistry   Chemistry and Biochemistry

_____
Joe F. Pittman
Interim Dean
Graduate School

ACTIVATION AND INHIBITOR STUDIES ON METHYL-COENZYME M

REDUCTASE AND PURIFICATION OF A NEW HYDROXYLAMINE

OXIDOREDUCTASE FROM *METHYLOMICROBIUM ALBUM*

ATCC 33003

Na Yang

A Dissertation

Submitted to

the Graduate Faculty of

Auburn University

in Partial Fulfillment of the

Requirements for the

Degree of

Doctor of Philosophy

Auburn, Alabama
May 10, 2008

ACTIVATION AND INHIBITOR STUDIES ON METHYL-COENZYME M

REDUCTASE AND PURIFICATION OF A NEW HYDROXYLAMINE

OXIDOREDUCTASE FROM *METHYLOMICROBIUM ALBUM*

ATCC 33003

Na Yang

_____

Signature of Author

_____

Date of Graduation

VITA

Na Yang, daughter of Yufan Yang and Ping Wang, was born on October 16, 1977, in Shanghai, People's Republic of China. She graduated from Nanjing University of Technology (the former Nanjing University of Chemical Technology) with a Bachelor degree of Biochemical Engineering in July of 2000. From 2000 to 2002, she worked as a research assistant in Shanghai Institute of Biochemistry and Cell Biology, Chinese Academy of Sciences. In August 2002, she entered graduate school at Auburn University in the Department of Chemistry and Biochemistry for pursuing a Ph.D. degree.

ACTIVATION AND INHIBITOR STUDIES ON METHYL-COENZYME M

REDUCTASE AND PURIFICATION OF A NEW HYDROXYLAMINE

OXIDOREDUCTASE FROM *METHYLOMICROBIUM ALBUM*

ATCC 33003

Na Yang

Doctor of Philosophy, May 10, 2008
(B.E., Nanjing University of Technology, 2000)

196 Typed Pages

Directed by Evert C. Duin

Methyl-coenzyme M reductase (MCR) catalyzes the formation of methane from methyl-coenzyme M (CH_3-S-CoM) and coenzyme B (HS-CoB) in methanogenic archaea. In order to manage the overproduction of methane in the environment, the exploration of the cellular regulation of MCR activity and catalytic mechanism of MCR is necessary. Two cellular components, A2 and A3a are involved in the activation of MCR in *Methanothermobacter thermoautotrophicus*. The effect of A2 and A3a on the activation of MCR from *Methanothermobacter marburgensis* was tested. MCRsilent and A2 were purified to homogeneity. A3a was purified to 70% purity and it might contain an iron-sulfur cluster. With the presence of minimal required components and the electron donor Ti(III) citrate, there was no significant activity detected in MCR from *M*.

marburgensis. Efforts to reconstitute the cluster content of A3a did not result in the higher activity of MCR. It was concluded that the components A2 and A3a are not involved in or are not sufficient for the activation of MCRsilent from *M. marburgensis.* There are several hypothetical catalytic mechanisms proposed for MCR. The major difference between these mechanisms is the initial interaction between the substrate methyl-coenzyme M and the nickel atom in the MCR active site, being either a metalloorganic nickel-methyl or a nickel-thiolate complex. With EPR and ENDOR spectroscopic techniques, we were able to show the presence of a Ni(III)-CH$_3$ species in MCR after reaction with bromomethane. This is no proof, but the result give plausibility to hypothetical mechanisms that include such an intermediate in the reaction. Additionally, it was shown by both EPR and NMR spectroscopy that incubation of the Ni(III)-CH$_3$ species with the substrate analog coenzyme M resulted in the formation of methyl-coenzyme M, which is the first evidence for reverse methanogenesis as has been proposed to take place in archaea conducting anaerobic methane oxidation.

Hydroxylamine Oxidoreductase from the nitrifier *Nitrosomonas europaea* is a multi-heme containing protein and has been extensively studied. It is known for long that methanotrophs are also able to oxidize ammonia to nitrate. An HAO-like gene was recently found in the genome of the methanotroph, *Methylomicrobium album* ATCC 33003. A protein that was capable of oxidizing hydroxylamine was purified from this strain and preliminary characterization showed that this enzyme is a heterodimer and does not contain a heme prosthetic group or iron-sulfur cluster. The properties of this new HAO are compared with known HAOs from various microorganisms.

ACKNOWLEDGEMENTS

This dissertation could not have been written without the great help of the people I would like to thank. First, I acknowledge my profound gratitude to my advisor, Dr. Evert C. Duin, for his invaluable support, encouragement, supervision and useful suggestions throughout the entire research work. My dissertation would not be possible without his help and guidance. Secondly, I am highly thankful to my committee members, Dr. Douglas C. Goodwin, Dr. Holly R. Ellis, Dr. Edward Parish and Dr. Sang-Jin Suh for their academic comments and instructive guidance to my research and dissertation; Also, I would like to thank the following: Bärbel Buchenau from the Max-Planck-Institute for providing the A2 plasmid; Dr. Peter Livant for NMR assistance; Tom Carrington for instrument assistance; my lovely lab colleagues, Mi Wang, Weiya Xu and Dolapo A. Adedeji for their generous support; my colleagues as well as friends Na Song, Chengdong Huang, Xiaoxun Li for their kindly help. Special thanks giving to my dear friends Chao Xu, Scottie Feng, Yinhui Xu for always being there to be supportive. I am also grateful to the Department of Chemistry and Biochemistry, Auburn University, and Petroleum Research Fund for their financial support during my research.

Finally, I am greatly indebted to my parents for their continuous love and understanding through my graduate study at Auburn.

Style manual used: <u>Biochemistry</u>

Computer software used: <u>Microsoft Word 2003, WinEPR, ChemDraw, Origin7,</u>
<u>CorelDraw11, Endnote X.</u>

TABLE OF CONTENTS

LIST OF TABLES

LIST OF FIGURES

CHAPTER ONE

LITERATURE REVIEW

1. 1 METHYL-COENZYME M REDUCTASE

1.1.1 Tetrapyrroles

Tetrapyrroles are compounds that contain four pyrrole rings that are interconnected in a linear or cyclic fashion through one-carbon bridges except for corrins. Many naturally occurring macrocyclic tetrapyrroles have been discovered that have important biological functions as well as enticing structural features. One striking feature is the presence of a ligand metal atom in the center of the cyclic tetrapyrrole. To date, five different types of metals have been found in tetrapyrroles: nickel in coenzyme F_{430}, iron in hemes and siroheme, magnesium in chlorophylls, cobalt in corrinoids, and copper in turacin (*1*).

The biosynthesis of different tetrapyrroles from L-glutamate has been described in the literature in much detail (*2*). Figure 1.1 gives a schematic presentation of the synthetic pathways for different type of tetrapyrroles found in nature. As shown, all tetrapyrroles are derived from the common precursor, uroporphyrinogen III. Conversion of uroporphyrinogen III to dihydrosirohydrochlorin is the first step towards synthesis of siroheme, cobalamin and cofactor 430 (F_{430}). On the other hand, conversion of uroporphyrinogen III into protoporphyrinogen IX leads ultimately to the formation of
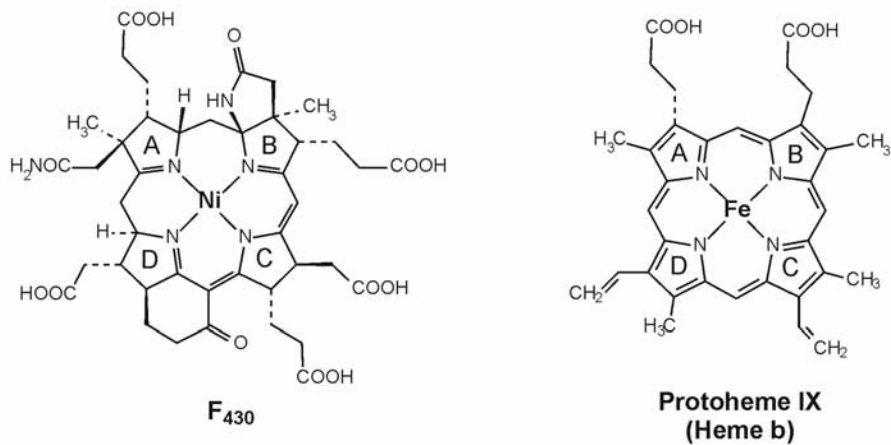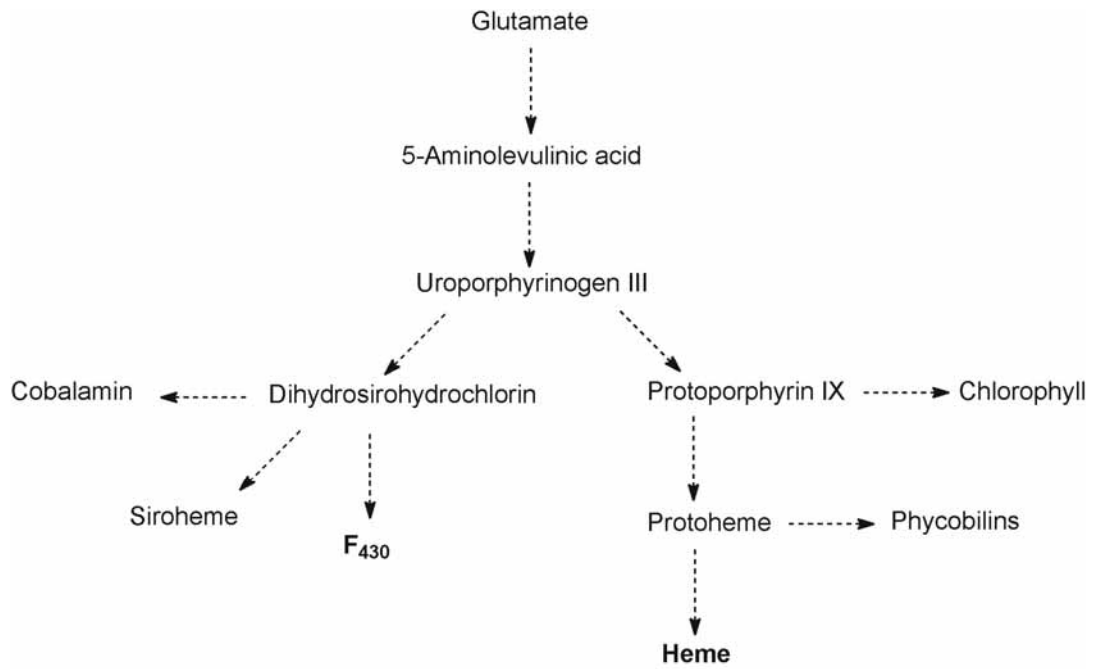
Figure 1.1 Schematic representation of the synthetic pathways leading to the different tetrapyrroles found in nature and the structures of cofactor 430 (F_{430}) and protoheme IX.

phycobillins, chlorophyll, and heme. In each case, six of the uroporphyrinogen III side chains have been shortened by direct decarboxylation (four acetic acid groups → four methyl groups) or oxidative decarboxylation (two propionic acid groups → two vinyl groups). However, no decarboxylations occurred in siroheme, cobalamin (except for one acetic acid chain) and coenzyme F_{430} (*3*).

In this dissertation, research will be presented on two enzymes that contain tetrapyrroles, methyl-coenzyme M reductase (MCR) and hydroxylamine oxidoreductase (HAO). The first enzyme is a F_{430}-containing protein and the second enzyme is a heme-containing protein. The chemical properties of both tetrapyrroles are very different. Figure 1.2 shows the level of saturation and the extension of conjugation in the pyrrole ring of different type of tetrapyrroles. While the hemes have the highest level of unsaturation (eleven double bonds) and the largest conjugated system, F_{430} is the most highly saturated pyrrole ring system in nature and its chromophore extends over only three of the four nitrogens (*4, 5*). In that respect the chromophore of F_{430} is more like that in corrins, which formed the basis for its general name, corphin, since it combines characteristics of both porphyrins and corrins (*3*). The presence of eleven double bonds in heme makes it very rigid, while the free F_{430} is highly flexible.

As described in chapter 2, the activation of MCR is an important problem. In the early MCR research no methods were available to obtain active enzyme or to reactivate the purified but inactive enzyme. As a result, much research has been done on the free $F_{430.}$ However, most data that have been obtained for the native F_{430}, can not be directly translated to F_{430} in the protein environment. For example, native F_{430} is thermally unstable. It tends to epimerize to form the 13-monoepimer and finally the
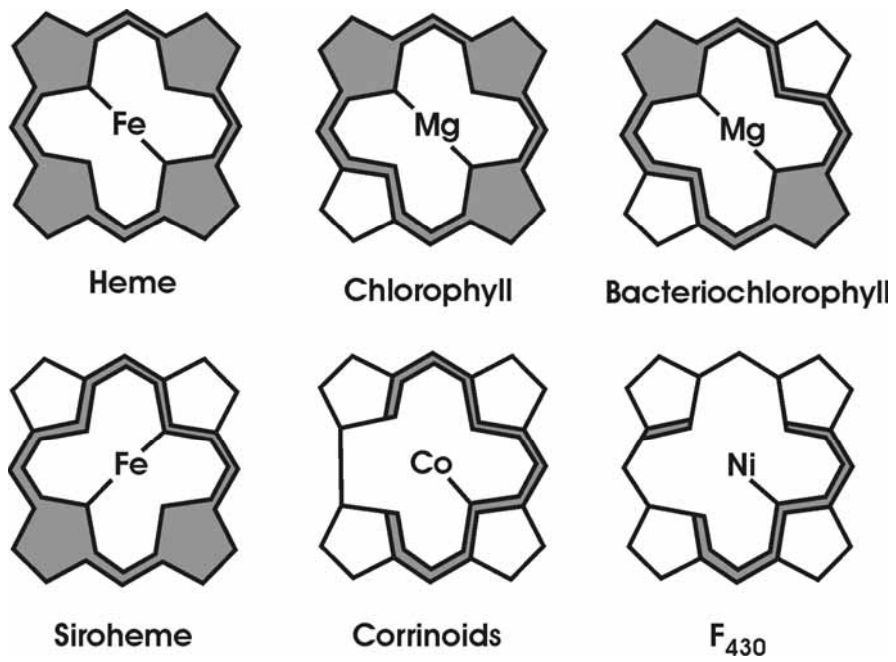
Figure 1.2. Schematic comparison of the conjugated systems of the different tetrapyrroles (*8*).

12, 13-diepimer at room temperature and it gradually oxidizes to 12,13-didehydro-F_{430} in the presence of air (*6*). This epimerization does not take place when bound in a protein. Experimental data and molecular mechanics calculations show that thermodynamically the Ni(II)-diepimer is more stable than native Ni(II)F_{430} outside of the protein. The native Ni(II)F_{430} has a lower energy conformation when bound in MCR (*7*).

It has also been known for a long time that the free F_{430} is unable to react with the MCR substrate methyl-coenzyme M (see below) and produce methane. It has been proposed that the nickel of F_{430} would react with methyl-coenzyme M to form a nickel-methyl intermediate. Only in the presence of strong methylating compounds such as methyliodine could a nickel-methyl species be observed. Additional protonation would then result in the formation of methane (*8*). Although the work on free F_{430} formed the basis of one of the hypothetical reaction mechanism for MCR, there was considerable doubt about whether such a species would indeed be formed on F_{430} in the enzyme. Recently, however, we showed that such a species can exist in the active site (see chapter 3) to create a more solid base for a hypothetical mechanism that includes such an intermediate.

1.1.2 Methanogens and Methanogenesis

Methane is known as a potent green-house gas and the most abundant organic gas in the atmosphere. In spite of its current lower concentration in the atmosphere compared with carbon dioxide, methane absorbs terrestrial radiation in the infrared region more efficiently than does carbon dioxide, and contributes to global warming (*9*). With the development of rice production and livestock cultivation, more and more methane

escapes into the atmosphere, which is of great concern. Therefore, controlling methane production tops the agenda of many researchers.

As we also know, methane is the end product of anaerobic microbial decomposition of bioorganic mass and fermentation. This last step of anaerobic breakdown of biomass is called methanogenesis and it usually takes place in diverse anaerobic microbial habitats such as fresh water sediment, swamps, rice paddies and the intestinal tract of animals. Methanogens, also known as methanogenic archaea, are the organisms mediating the methane-formation reactions. They play critical roles in this process by converting products from anaerobic fermentation (hydrogen, carbon dioxide, formate and acetate) as main substrates into methane. Only by such means can methanogens obtain energy to grow (*8*).

With different substrates, there are different metabolic pathways of methanogenesis. Most of the methanogens utilize carbon dioxide and molecular hydrogen as substrates to produce methane (Figure 1.3). The hydrogenogenic pathway starts with reduction of carbon dioxide to formylmethanofuran (CHO-MFR). Then the formyl group is transferred from formylmethanofuran to tetrahydromethanopterin (CH-H$_4$MPT), which carries the C1 unit for the next three steps, formation of methenyltetrahydromethanopterin (CH$\equiv$H$_4$MPT), reduction with H$_2$ to methylenetetrahydromethanopterin (CH$_2$=H$_4$MPT) and reduction with H$_2$ to methyltetrahydromethanopterin (CH$_3$-H$_4$MPT). The next to last step in the pathway is methylation of coenzyme M, the smallest coenzyme known, to form methyl-coenzyme M (CH$_3$-S-CoM). Methyl-coenzyme M could also be obtained from methanol or methylamine through the methylothrophic pathway. The other major pathway is the

6
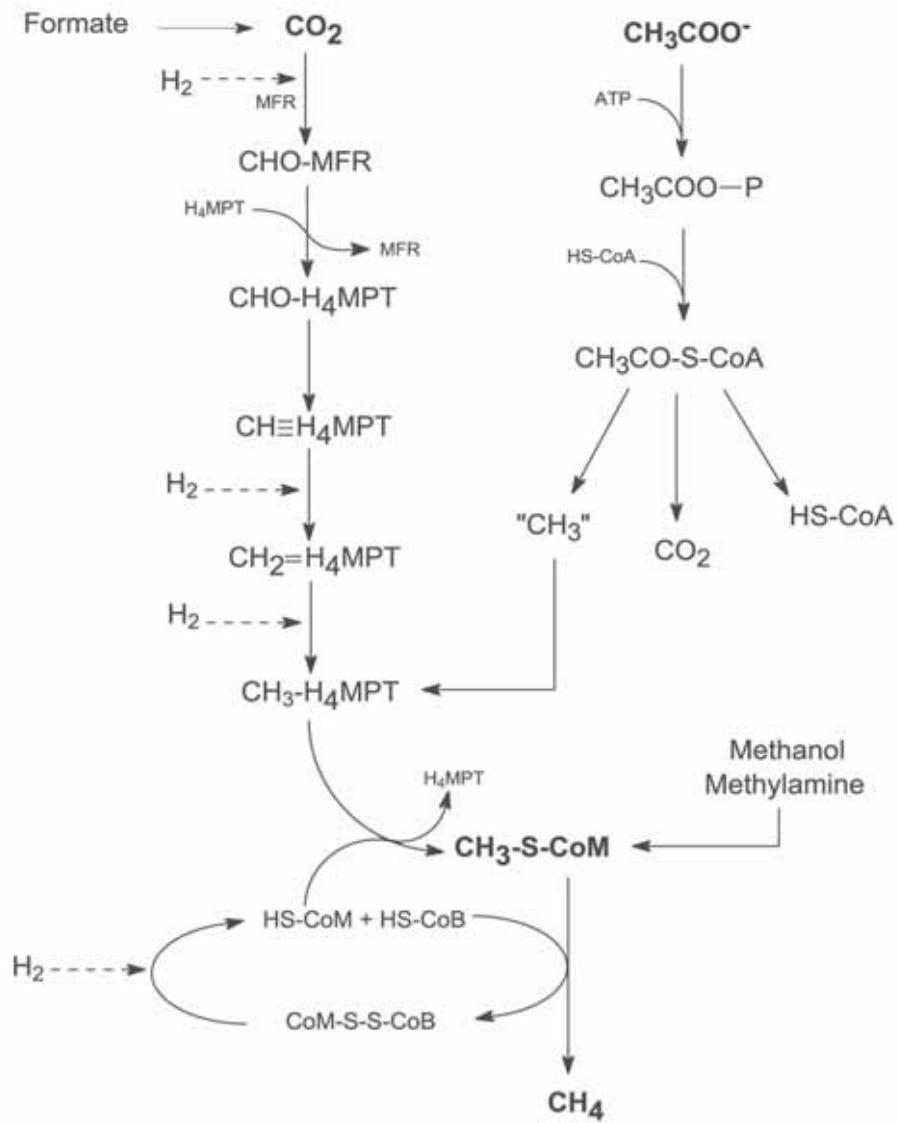
Figure 1.3. Metabolic pathways of methanogenesis. (See text in section 1.1.2 for details)

acetoclastic pathway that starts with the phosphorylation of acetate (CH_3COO^-) which is coupled to coenzyme A. Acetyl-coenzyme A is broken down by the carbon monoxide dehydrogenase/acetyl CoA synthase complex into two one-carbon units. The carbon monoxide unit is oxidized to carbon dioxide at the same enzyme complex, while the methyl group is transferred to tetrahydromethanopterin. As shown in Figure 1.3, methyl-coenzyme M is a unique intermediate, which is important in the final steps of methane formation. Methyl-coenzyme M reductase, the enzyme catalyzing the last step of methane formation from methyl-coenzyme M, is the subject of this part of the review.

1.1.3 The Nickel Enzymes

It was first discovered as early as 1979 that growth of *Methanothermobacter marburgensis* was dependent on nickel when grown on hydrogen and carbon dioxide. This was unexpected because at that moment the only enzyme known to contain nickel was urease and it was also known that methanogens did not need urea for growth (*10*). Shortly, *M. marburgensis* was found to contain eight nickel-containing enzymes based on biochemical and genetic studies (*8, 11*): methyl-coenzyme M reductase isoenzyme I and II, F_{420}-reducing [Ni-Fe]-hydrogenase, F_{420}-nonreducing [Ni-Fe]-hydrogenase, energy converting [Ni-Fe]-hydrogenase isoenzyme I and II, carbon monoxide dehydrogenase and acetyl-CoA synthase.

Amongst the eight nickel enzymes in *M. marburgensis* (strain Marburg), methyl-coenzyme M reductase isoenzymes, isoenzyme I (McrABG) and isoenzyme II (MrtABG) require the biggest amount of the nickel which is incorporated into the cofactor 430, the prosthetic group of the methyl-coenzyme M reductase (*12*). F_{430} is a nickel-containing

tetrapyrrole with a unique structure, dubbed corphin (Figure 1.2). The nickel presence in MCR F_{430} was discovered by Ellefson *et al.* (*13*). MCR is not only characteristic of methanogenic archaea but also of the methanotrophic archaea which are capable of catalyzing anaerobic oxidation of methane to carbon dioxide in anoxic marine sediments (*14, 15*). The methanogenic archaea are phylogenetically closely related to methanotrophic archaea (*16*).

1.1.4 Methyl-Coenzyme M Reductase and Its Active Site

Methyl-coenzyme M reductase is a nickel-containing enzyme that catalyzes the final step of methane production in the energy metabolism of methanogenic archaea as introduced above. In this step, methyl-coenzyme M and coenzyme B are substrates for MCR and they are converted to methane and the heterodisulfide of coenzyme M and coenzyme B (for structures see Figure 1.4).

$$CH_3\text{-S-CoM} + HS\text{-CoB} \longrightarrow CH_4 + CoM\text{-S-S-CoB}$$
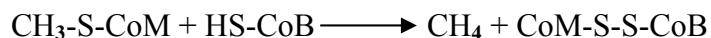
MCR has a molecular mass of around 300 kDa and it has a $\boldsymbol{\alpha_2\beta_2\gamma_2}$ structure (Figure 1.5). Each molecule of enzyme contains two non-covalently but tightly bound coenzymes F_{430} (structure see Figure 1.2). Three subunits are tightly associated with each other especially between subunits α and α′, β and β′ forming the active-site channel. The MCR is a functional dimer with two identical, but independent, F_{430}-containing active sites which are 50 Å apart from each other. Each cofactor F_{430} is embedded within the protein and could be accessed from the outside by a 50 Å long, pocket-like channel, through which the substrates could reach F_{430}. The crystal structure of MCRox1-silent and MCRsilent were resolved at 1.16 Å (*17*). In the MCRox1-silent form, coenzyme B could

a. H_3C-S-CH$_2$CH$_2$-SO$_3^-$

b. HS-CH$_2$CH$_2$-SO$_3^-$

c.
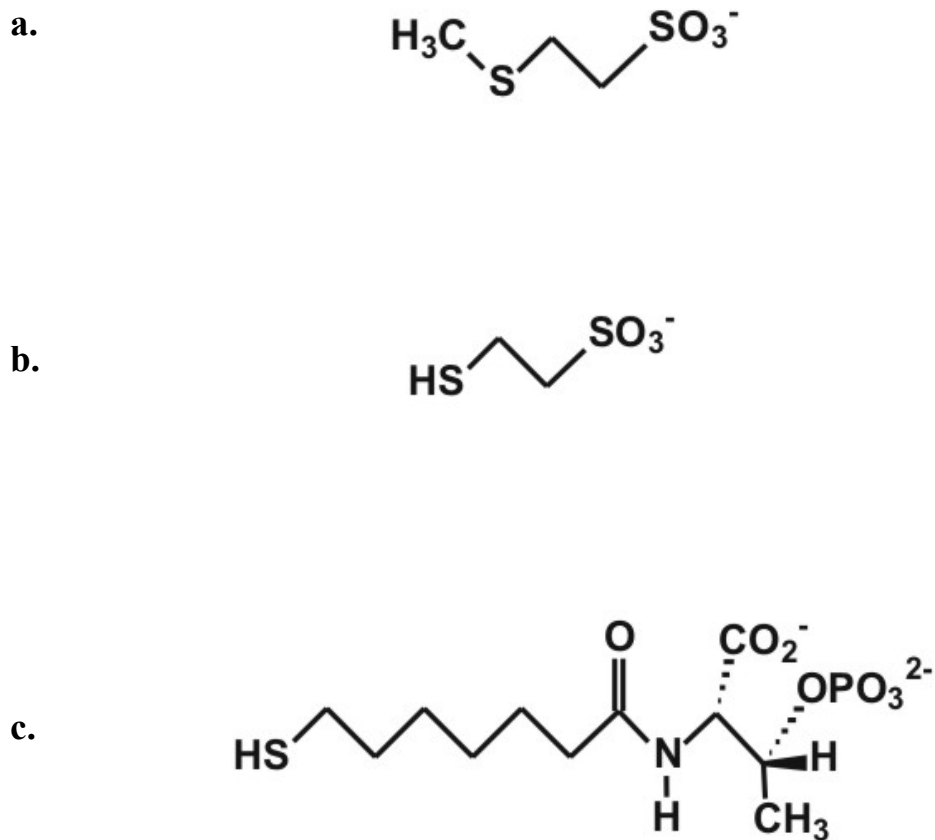
Figure 1.4. Structures of: a) methyl-coenzyme M (CH$_3$-S-CoM, 2-(methylthio) ethanesulfonate). b) Coenzyme M (HS-CoM, 2-mercaptoethanesulfonate); c) Coenzyme B (HS-CoB, *N*-7-mercaptoheptanoyl-O-phospho-L-threonine).
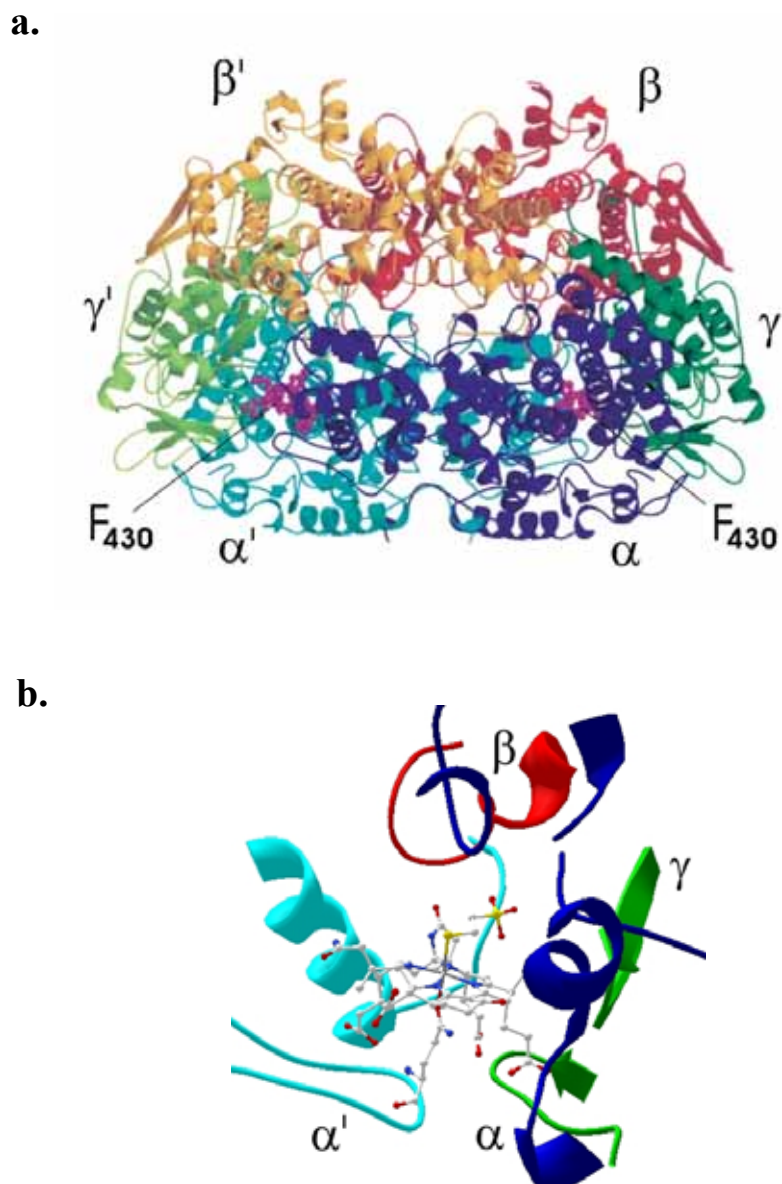
Figure 1.5. Schematic representation of the MCR structure: a) MCR overall crystal structure. b) MCR active site structure. Each of the two coenzymes F_{430} is bound to subunits α, α', β and γ, or α', α, β' and γ'.

fit into the narrow channel with its long aliphatic side-chain reaching up to 8 Å from the nickel (Figure 1.6 A). Coenzyme M coordinates with the nickel from the proximal side of F_{430} with its thiol group. In addition, the oxygen from a glutamine residue ($Gln^{\alpha'147}$) coordinates the nickel from the back side, which is observed in all MCR crystals. Figure 1.6 B shows the crystal structure of MCRsilent. Heterodisulfide, coordinates to the nickel in the active site (*17*). Comparing the positioning of the coenzyme B and coenzyme M moieties with that in Figure 1.6 A, we find that the coenzyme B moiety of heterodisulfide in the MCRsilent structure aligns almost perfectly with coenzyme B in MCRox1-silent while coenzyme M moves to a position where one oxygen atom of the sulfonate is able to be axially coordinated to the nickel. It would be reasonable to picture the structures with methyl-coenzyme M replacing coenzyme M in Figure A, which would represent a possible starting point in the catalytical reaction (*5*).

F_{430} is a yellow compound which has a maximal absorbance at 430 nm. It has a molecular mass of ~905 Da as do all the nickel corphin cofactors in methanogenic archaea (*10*). The EPR spectra shown in Figure 1.7 are for the free $F_{430}M$, the pentamethyl ester form of F_{430}, in three different oxidation states. $F_{430}M$ is soluble in nonpolar, noncoordinating solvent. This property helped resolve the structure of F_{430} with nuclear magnetic resonance (NMR) spectroscopy (*5*) since the nickel ion tends to form coordinated complexes in both F_{430} and $F_{430}M$ in the presence of donor ligands. These forms are paramagnetic while the uncoordinated forms are not. $Ni(II)F_{430}M$ in acetonitrile, dry dichloromethane, chloroform is in low spin state and $Ni(II)F_{430}$ in acetonitrile could be oxidized to $Ni(III)$ $F_{430}M$ (*18*). Both $Ni(II)$ $F_{430}M$ in acetonitrile and $Ni(II)F_{430}$ in water could be reduced to the $Ni(I)$ state at a redox potential ($E^{\circ'}$)
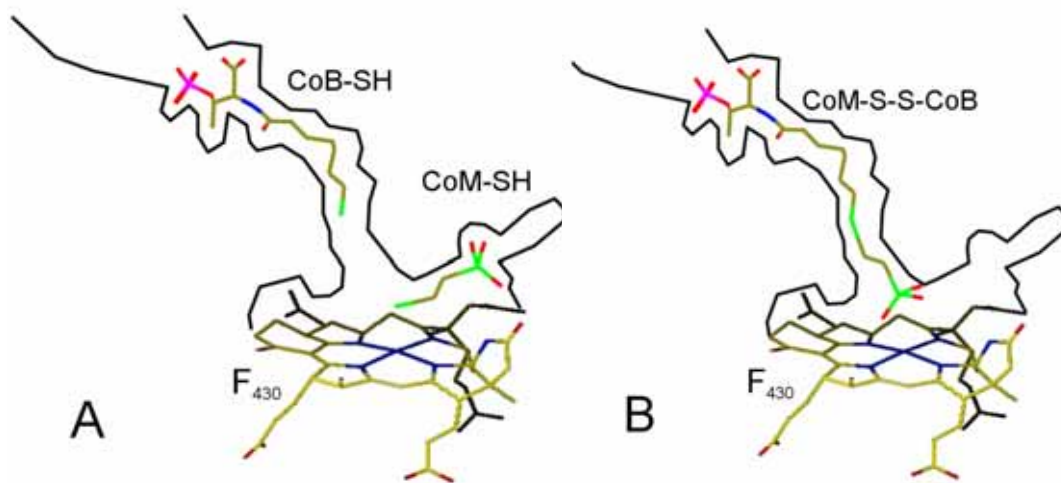
Figure 1.6. Schematic representation of the active sites of MCRox1-silent (A) and MCRsilent (B).
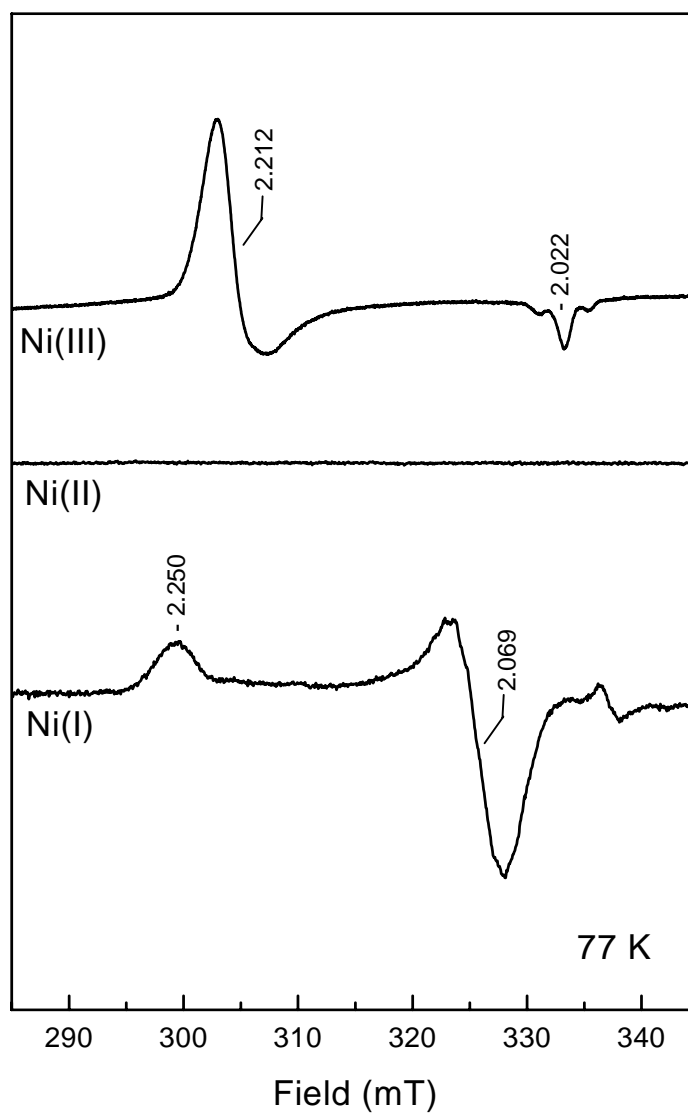
Figure 1.7. EPR spectra of cofactor $F_{430}M$ in different oxidation states. $F_{430}M$ is the pentamethyl ester form of F_{430}.

of - 600 mV/NHE (*19, 20*).

1.1.5 EPR Signals of MCR Redox Forms

Electron Paramagnetic Resonance (EPR) spectroscopy is one of the best ways to study biological metalloenzymes by interpretating the energy difference between atomic or molecular states. MCR exhibits different EPR signals for different states of the enzyme. Only states that have a free / unpaired electron, paramagnetic species with spin 1/2, 3/2, 5/2 etc, are EPR active and can be detected using standard EPR measuring techniques. The forms with the nickel in the 3+ (d^7) and 1+ (d^9) oxidation states are EPR active. Figure 1.8 shows an overview of the different EPR spectra that can be detected in MCR. The conditions needed to induce these different EPR spectra will be described below. MCR with the nickel in the 2+ (d^8) oxidation state is not EPR active. The spin state, however, is $S = 1$ (*21*) and not the more common spin state $S = 0$. Still, this form does not show an EPR spectrum in either perpendicular or parallel EPR modes.

When *M. marburgensis* is grown on 80% H_2 and 20% CO_2, no EPR signal is exhibited, which is designated as MCRsilent. If the gas mixture is switched to 100% H_2 prior to the harvesting, a MCRred1 EPR signal indicating the only active MCR form, is induced within 5 min. Upon continuous gassing with 100% H_2, another EPR signal, named MCRred2, is induced (*22*). The reason for the names of MCRred1 and MCRred2 is that both of EPR signals are detected in whole cells or cell extracts under these relative reducing conditions.

Likewise, another important EPR signal, MCRox1, can be induced before harvesting by switching the gas phase to 80% N_2 and 20% CO_2, creating a more
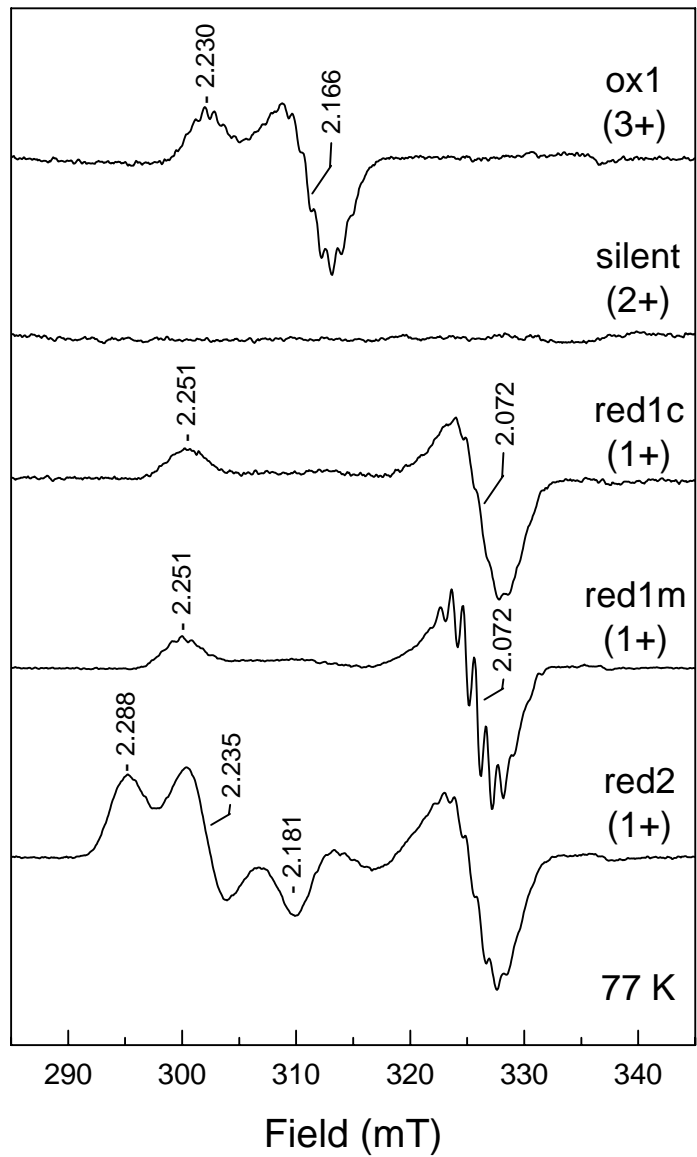
Figure 1.8. EPR spectra of the methyl-coenzyme M reductase in different forms with their respective oxidation states.

oxidizing environment instead. The enzyme in the MCRox1 form has no activity. However, MCR purified in the MCRox1 state can be activated to the MCRred1 state with a high specific activity of 100 U/mg under incubation with Ti(III) citrate at pH 10.0 and 65 °C (*23*).

There are several EPR-silent forms of MCR which have been characterized via X-ray absorption and crystallization experiments: MCRred1-silent, MCRox1-silent, MCRred2-silent. The conditions for induction of MCRsilent have been described. As for MCRred1-silent, MCRox1-silent, MCRred2-silent, they could be gradually formed from their respective EPR-active forms by exposure to oxygen.

Figure 1.8 shows two types of MCRred1 signals. One is called MCRred1**c**, indicating MCRred1 in presence of **c**oenzyme M in the solution. The other is named MCRred1**m**, designating MCRred1 in presence of **m**ethyl-coenzyme M in the solution. The slight difference between these two is that MCRred1m shows much more resolved superhyperfine structure, resulting from the nuclear spin (I=1) of the four nitrogen nuclei which are coordinated to the nickel center, than MCRred1c. This effect is due to the presence of methyl-coenzyme M, 3.08 Å away from the nickel. The EPR spectrum of MCRred2 looks more complicated than others since it has both an axial component and a rhombic component. The signal could be induced in vitro from MCRred1 form by addition of coenzyme M and coenzyme B (*24*).

Comparison of Figure 1.8 and Figure 1.7 shows identical spectra for MCRred1 and Ni(I)F_{430}M and it is concluded that the nickel in MCRred1 is in 1+ oxidation state. It also shows the similarity between the EPR spectrum of MCRox1 and one of Ni(I)F_{430}M, which was also found in electron nuclear double resonance (ENDOR) measurements (*25*).

17

This led to the proposal that the nickel in this state is also 1+. However, it was also proposed to be Ni(III) since the signal could be formed under more oxidizing conditions in the cell and is relatively stable against oxygen. The UV/visible spectrum of MCRox1 is more similar to Ni(II)F_{430} than Ni(I)F_{430} or Ni(III)F_{430} (*26*). At this point, the discussion of the nickel oxidation state of MCRox1 heated up and more techniques were applied to solve this puzzle: Cryoreduction experiment (*27*), X-ray absorption spectroscopy (XAS) studies (*28*) and Magnetic circular dichroism (MCD) measurements (*21, 29*). The redox state of the nickel in MCRox1 is formally 3+, which was confirmed by density functional theory (DFT) calculations (*30*). Although most of the electron density of the unpaired electron are found on the nickel, some of the other electron density can also be found on the sulfur and nitrogen ligands making the nickel behave more like a Ni(II) in spectroscopic techniques.

1.1.6 Activation and Inactivation of Methyl-Coenzyme M Reductase

MCR has different states as mentioned above and some have been detected in whole cells. These various forms were also artificially prepared in vitro and were characterized with spectroscopic techniques since all of these forms might be involved in reaction mechanism as well as the activation process. Among these forms, only the MCRred1 form is active. How these MCR forms are related to each other and how to convert inactive MCR forms to active MCRred1 is of great importance for MCR research since it has direct impact on the control of methane production. Figure 1.9 illustrates the "MCR conversion cycle", which describes the important relationship between different MCR forms as studied in vitro. As shown, the active form, MCRred1,

18
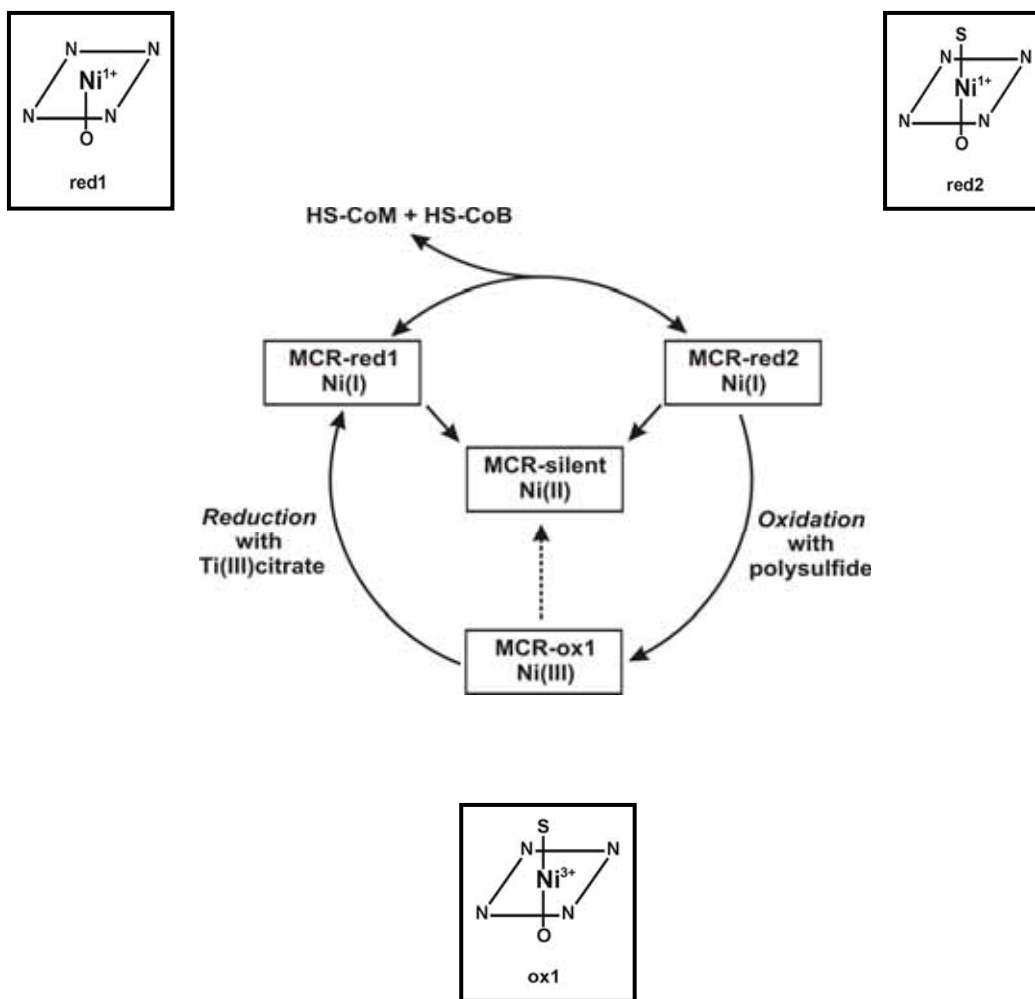
Figure 1.9. MCR conversion cycle *in vitro* between MCRred1, MCRred2, and MCRox1.

can be converted to MCRred2 when incubated with coenzyme M and coenzyme B in a reversible step (*24*). As for MCRred2, it can be converted to an inactive but important form, MCRox1, by addition of the oxidant polysulfide (*31*). The MCRox1 form can be activated to form MCRred1 by incubation with the artificial reductant titanium(III) citrate at pH 9.0 and 65°C (*23*). It is not clear what reductant and/or oxidant is used by the cell.

MCRred1 is highly oxygen sensitive and it will be converted into a MCRsilent form immediately upon contact with oxygen or other oxidants. MCRred2 is also oxygen sensitive. MCRox1 is relatively oxygen stable and the signals would quench given longer time. It might be interesting to elucidate the mechanisms by which the cell protects to launch a protection mechanism to keep MCR from oxygen by converting MCRred1 to other MCR forms except for MCRsilent. It is safe to assume that when methanogens are under certain microaerobic conditions, hydrogen production from fermentation process would slow down, and the pathway for methyl-coenzyme M formation would be blocked so that the amount of coenzyme M would start to accumulate *in vivo* (Figure1.1). Together with the coenzyme B available in the cell, this could lead to MCRred2 formation and finally MCRox1 formation.

To date, no methods have been found to convert MCRsilent or MCRred1-silent into MCRred1 *in vitro*. It was reported in 1988 that the inactive MCR purified from *Methanothermobacter thermoautothrophicus* could be activated *in vitro* with the addition of two protein components called A2, A3a and ATP as well as Ti(III) citrate. The observed activity, however, was less than 0.1% of the theoretical specific activity of MCR (*8*). The MCR purified from *M. marburgensis*, has residual activity about 0.1 U/mg

by itself (*32*). When A2, A3a and reductant are present, the specific activity reaches 1 U/mg, about 2% of the *in vivo* activity (*33*). These enzyme preparations are essentially MCRsilent as shown by EPR spectroscopic measurements.

In the published work (*34*), A2 was purified to homogeneity and overexpressed in *E.coli*. The predicted amino acid sequence of the A2 protein indicates it is a ATP-binding protein that belongs to the ATP-binding cassette (ABC) family of energy-dependent transport systems (*34*). A3a has been partially purified, and it appears to be a large iron-sulfur cluster containing aggregate with a molecular weight of 500 kDa. It is rather oxygen sensitive and proposed as electron provider for the reductive activation of MCR (*35*). The low percentage of activation, however, cast some doubt about the involvement of these proteins in the activation of MCR.

Inactive MCR form has two moles of coenzyme M tightly bound in the active site (*36*). When inactive MCR was incubated with the activating system including A2, A3a, ATP and electron donor together with isotopically labeled methyl-coenzym M (*methyl*-^{3}H, *thio*-^{35}S) and coenzyme B, the coenzyme M moiety of methyl-coenzyme M slowly exchanged to MCR-bound coenzyme M during turnover. Upon exchanging of two moles coenzyme M to enzyme, there is 150 mol/ (mole enzyme) methane formed already (*36*). In the absence of the activating system and substrate coenzyme B, no exchange or methane formation was found. The finding that it needs more than 150 turnovers to reach only 0.1% of specific activity *in vivo* means that only small part of MCR molecules were activated and they might lose activity immediately after a couple of turnovers, which made the work even more difficult (*8*) .

1.1.7 Catalytic Mechanism of Methyl-Coenzyme M Reductase

Although there is a body of structural, spectroscopic, kinetic, biochemical and computational data available to point out different directions for catalytic mechanism of methyl-coenzyme M reductase, basically it could be narrowed down to two radically different models that are consistent with most data (*8, 37*).

Mechanism I is shown in Figure 1.10. Ni(I)-MCRred1 reacts with methyl-coenzyme M to form a methyl-Ni(III) intermediate by nucleophilic attack. The formed methyl-Ni(III) intermediate withdraws an electron from coenzyme M to generate a methyl-Ni(II) intermediate and a coenzyme M thiyl radical. The methyl-Ni(II) species is then protonated with electrophilic substitution to produce methane. At the same time the coenzyme M thiyl radical reacts with coenzyme B to produce the heterodisulfide anion radical. Finally, the excess electron goes back to nickel and converts Ni(II) back to Ni(I) (*38*).

Mechanism I was proposed on the basis of the cobalamin biochemistry and supported by the findings that include: ethyl-coenzyme M reduction catalyzed by MCR proceeds with inversion of the stereo configuration at the carbon atom of the ethyl group (*39*); Ni(I) F_{430} in inactivated MCR reacts with 3-bromopropane sulfonate to form an alkyl-Ni(III) species (*40*); In aprotic solvents, free Ni(I)F_{430} reacts with methyl iodide to form methyl-Ni(II) F_{430} which is subsequently protonolyzed to methane and Ni(II)F_{430} (*41, 42*); and the fact that the catalytic efficiency of methyl-coenzyme M reduction is much lower than the reduction of ethyl-coenzyme M indicating the catalytic cycle starts with a nucleophilic substitution (*43*). Nevertheless, according to the density functional calculation, mechanism I turns out to be energetically unfavorable (*44, 45*).

22
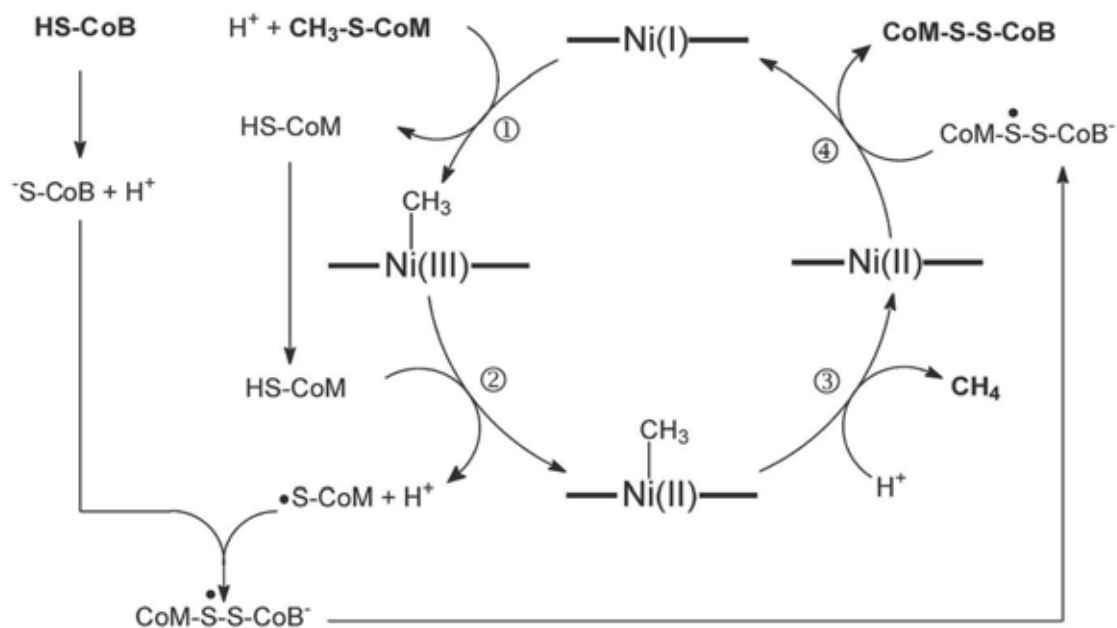
Figure 1.10. MCR mechanism I.

Mechanism II (Figure 1.11) was proposed based on quantum mechanical calculations. The key step involves an attack of Ni (I) at the thioether sulfur instead of the methyl group of methyl-coenzyme M, yielding a Ni (II) thiolate and a free methyl radical which withdraws a hydrogen atom from the sulfhydryl group of coenzyme B to form methane. The formed coenzyme B thiyl radical reacts with coenzyme M thiolate to the heterodisulfide radical anion which returns the excess electron to the nickel (*38*). This alternative mechanism is energetically much more favorable than Mechanism I in term of formation of the methyl-Ni(II) intermediate (*44*) and is also consistent with the finding that when coenzyme B is around, coenzyme M is reversibly coordinated to Ni(I) F_{430} in active MCR with its thiol sulfur (*46*). However, the model could not explain the finding of the low catalytic efficiency of the reduction of ethyl-coenzyme M and even zero catalytic efficiency of the reduction of allyl-coenzyme M catalyzed by MCR (*10*). Thus, the mechanism of MCR is still not clarified. Neither of the mechanisms takes into account of the reversibility of the role MCR may play in the anaerobic oxidation of methane (see below). For instance, in mechanism I, methane oxidation has to start with the attack of methane by Ni(II)F_{430}, which is extremely difficult because of its low electrophilicity suggested by the low redox potential of -0.6 V of the Ni(II)F_{430}/Ni(I)F_{430} couple (*26*). As for Mechanism II, likewise, it is also energetically unfavorable for the attack of methane by coenzyme B thiyl radical since the bond dissociation energy of the C-H bond in methane is higher than that of the S-H bond (*10*).

In summary, the reaction mechanism of methyl-coenzyme M reductase is still a mystery. We are still looking for convincing evidence to prove or modify the proposed mechanisms or any new perspectives that could lead to more realistic mechanisms.

CH$_3$-S-CoM

Ni (I)

HS-CoB $\dot{C}$H$_3$

Ni (II)-S-CoM

CH$_4$ $\dot{S}$-CoB

CoM-S-S-CoB

Ni (II)

CoM-$\dot{S}$-S-CoB$^-$
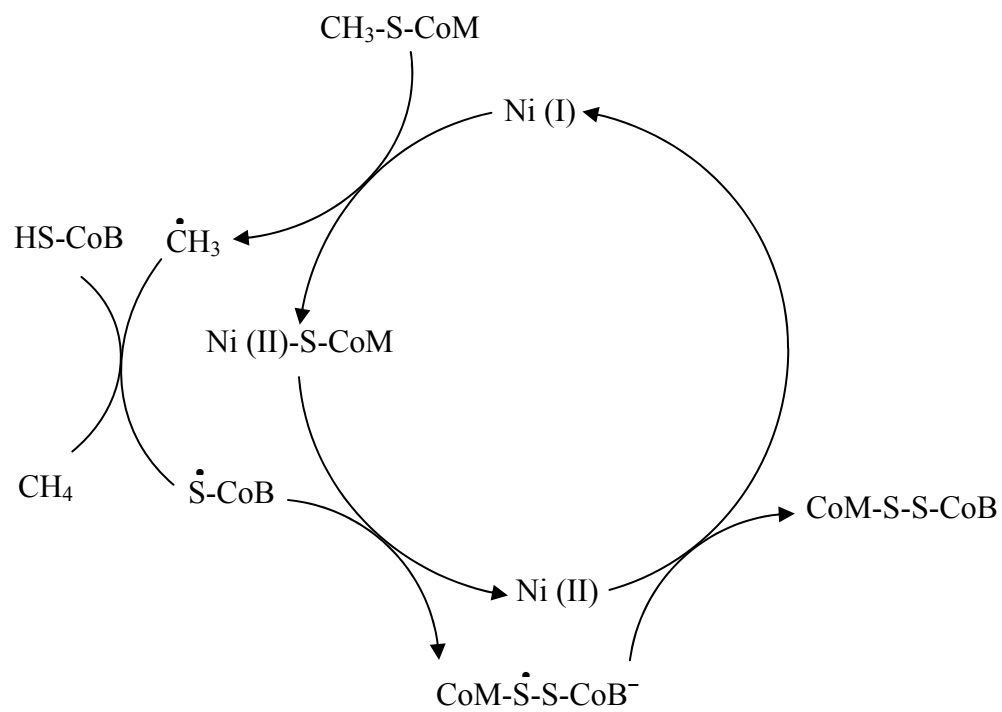
Figure 1.11. MCR Mechanism II (*38*).

1.1.8 Anaerobic Oxidation of Methane (AOM)

Another aspect that is important for proposing a hypothetical mechanism is that MCR may be involved in the anaerobic oxidation of methane (AOM). Methanotrophic archaea that are able to catalyze AOM in the Black Sea contain MCR (*47*). It was found that there were at least two methyl-coenzyme M reductases present. One contained the regular cofactor F_{430} with a molecular mass of 905 Da while the other contained a modified F_{430} with a molecular mass of 951 Da, which could be the origin of the differences in the catalytical properties of the enzyme from methanotrophic archaea and that from methanogenic archaea (*10*).

There is a thermodynamics aspect related to the very slow pace of the methane oxidation process (*48, 49*). The standard free energy change $\Delta G°$ associated with the methane production step is about -30 kJ/mol (CH_4). Under physiological conditions, ΔG $=\Delta G° + RT\ln$ [products]/ [substrates] = -30 + 5.7 log [products]/ [substrates]. From this equation, it can be derived that the reaction catalyzed by MCR will become reversible only when the ratio of the products to substrates concentration is around 10^5, which is physiologically feasible (*10*). Additionally, it was proposed that sulfate-reducing bacteria helped to make methane oxidation process thermodynamically favorable based on the observation that the first-found microbial consortium being responsible for anaerobic methane oxidation contains archaea surrounded by sulfate-reducing bacteria (*5, 14*). So the reversibility of the reaction cycle catalyzed by MCR needs to be taken into account for catalytically mechanistic proposals if this is known for certain.

1.1.9 Summary

Methane, the well-known important green-house gas, a final product of anaerobic degradation of organic biomass in anaerobic microbial environments, is produced from carbon dioxide, molecular hydrogen, acetate and C1 compounds by methanogenic archaea in an energy-conserving process called methanogenesis. This pathway ends up with the same step for methane production despite different starting points. MCR is a unique nickel-containing enzyme that catalyzes this final step in which methyl-coenzyme M and coenzyme B are converted into methane and the heterodisulfide of coenzyme M and coenzyme B. MCR contains the nickel porphinoid F_{430} as its prothetic group which has to be in the nickel (I) oxidation state for the enzyme to be active. The recent development of methods to purify highly active protein allows us to explore two main aspects of this important enzyme, activation and the reaction mechanism, with diverse spectroscopic techniques. In previous activation studies, it showed that the inactive MCRsilent form could be activated by a reconstitution system containing two required components A2 and A3a in addition to the inactive enzyme and appropriate reductant in *Methanothermobacter thermoautotrophicus* but with very low activity. Our detailed efforts trying to reconstitute and optimize the activation system in *Methanothermobacter marburgensis* will be described in chapter 2. For the MCR reaction mechanism, there are mechanism models available based on data gathered over the last twenty years. Model I is rooted on a nucleophilic attack of Ni(I) to the methyl group from CH_3-S-CoM forming a methyl-Ni(III) intermediate and model II mainly differs in the first reaction step where Ni(I) reacts with the thioether sulfur of CH_3-S-CoM to form a Ni(II)-S-CoM intermediate and a methyl radical. The recent observation of a new role that MCR might play in

anaerobic oxidation of methane opens up new possibilities of reversibility while adding more rules to the hypothetical mechanism. Spectroscopic studies on a methyl-nickel species in MCR will be described in chapter 3 of this dissertation.

1. 2 HYDROXYLAMINE OXIDOREDUCTASE

1.2.1 Heme-Proteins

Heme, or iron-porphyrin complex, is one of the most pervasive cofactors in nature. It is a prosthetic group having an iron atom in the center of a porphyrin. Heme-containing proteins could be classified by diverse functions, ranging from oxygen transport and storage (hemoglobin and myoglobin), electron transfer (cytochromes), catalysis (catalases and peroxidases), to ligand binding, signal transduction and regulation of gene expression (FixL, CooA) (*50-52*). These distinctive biological functions are achieved by modification of the heme environments within the protein. Therefore, a huge amount of effort has been put into the investigation of the structure-function relationships in heme-proteins for the past half decade and it continues to draw great attention because of many recent exciting discoveries of heme-proteins with novel functions such as guanylate cyclase (*53*), heme chaperone CcmE (*54*), first heme-protein in Archea Hem-AT etc. (*55*)

Structually, hemes could be classified by major types, heme *a, b, c, d, o*. In each type, the tetrapyrrole ring has iron at the center which is coordinated with four porphyrin nitrogen ligands in the plane of heme and two axial ligands above and below the plane. Among these, heme *b* is the most common one and is found in many biologically important heme-proteins such as catalases, peroxidases, cytochromes *b*, globins and signaling proteins. Other important types are heme *a* and heme *c*. Heme *a* differs from heme *b* in that a methyl group at ring position 8 is oxidized into a formyl group, and one of the vinyl groups, at ring position 2, has been substituted by an isoprenoid chain. The typical example of an iron protein containing heme *a* is the last protein in the electron transport chain, cytochrome *c* oxidase (*56*). Heme *c* is also derived from heme *b* but by

replacement of two vinyl groups by thioether bonds covalently bonded to surrounding protein (Figure 1.12). Cytochrome *c* and hydroxylamine oxidoreductase are protein examples that contain *c*-type hemes.

1.2.2 Multiheme c-type Cytochromes

Cytochromes can be defined as proteins having one or several heme groups that are responsible for electron or proton transportation. In the 1920s, the word cytochrome (cellular pigment) was created by David Keilin to imply essential components involved in the electron transfer chain, which marked the beginning of studies on what was later called the respiratory chain (*57, 58*). Today, more than half of the known heme-containing proteins are cytochromes for either carrying out an electron transfer process or catalyzing a chemical redox reaction. The presence of different type of hemes gives rise to different type of cytochromes and c-type cytochromes represent one of the largest families of heme-proteins (*59*). Hemes in *a*-type and *b*-type cytochromes are noncovalently bound in the major protein groups while *c*-type cytochromes have *c*-hemes that are covalently bound to the major protein group through two thioether bonds between two cysteine residues and the α-carbons of the vinyl groups of the heme. The two cysteins are present in a conserved CxxCH motif referred as "fingerprint peptide" (*52*). In some rare cases, the association is in the form of a CXXXCH, CXXXXCH or CXXCK motif (*60*). It is amazing that the formation of the thioether bonds has such a big effect on the chemical and thermal stability of the protein. As for the axial ligands in c-type cytochromes, one of them is always either H or K coordinated to the heme iron, and the second one is always either a methionine or histidine, which has different impacts
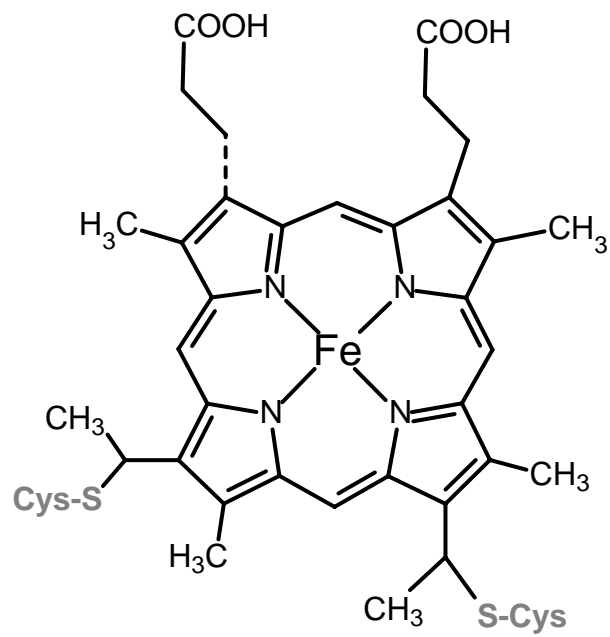
Figure 1.12. Heme *c*

on the reduction potential (*61*).

Mitochondrial cytochrome *c* represents the universal cytochrome *c* folding topology having a simple and predominantly α-helical globular fold while some other interesting *c*-type cytochromes include cytochrome *f*, cytochrome c_3, cytochrome c_{554}, hydroxylamine oxidoreductase, have an unusual fold. For example, cytochrome *f*, a *c*-type cytochrome of plant thylakoids, has the heme covalently attached to a β-sheet fold (*62, 63*). Cytochrome c_3 has both an unusual fold and a multiheme arrangement. This molecule consists of a single polypeptide chain wrapped around a core of four hemes (*64*). Cytochrome c_{554}, also a tetra-heme molecule, folds in different way by having four hemes arranged in two pairs (*65*). Hydroxylamine oxidoreductase (HAO) is known for its remarkably complicated structure, having seven *c*-type hemes and a P460 heme in the active site. The crystal structure of HAO was resolved to 2.8 Å resolution in 1997 (*66*).

A striking feature of many multiheme *c*-type cytochromes, such as hydroxylamine oxidoreductase, is that they have a conformationally related close packing of the hemes, in spite of little sequence similarity (*60*). All *c*-type cytochromes bind heme through a CXXCH motif. There are two apparent differences between multiheme cytochromes and most monoheme *c*-type cytochromes. One is that their heme environments differ notably despite the same heme-proteins binding region. The other is that the iron is usually coordinated by histidines in multiheme cytochromes while histindine and methionine ligands are applied in most monoheme *c*-type cytochromes. Both of the differences contribute to the variance of the redox midpoint potential of the heme in these proteins.

1.2.3 Hydroxylamine Oxidoreductase

The nitrifying chemolithoautotrophic bacterium, *Nitrosomonas europaea*, obtains energy for growth through the oxidation of ammonia to nitrite, a two-step process which contains two key enzymes, ammonia monooxygenase (AMO) and hydroxylamine oxidoreductase (HAO) (*67*). AMO is a membrane-bound enzyme that catalyzes the first reaction step as follows (Eq.1):

$$NH_3 + O_2 + 2e^- + 2H^+ \longrightarrow NH_2OH + H_2O \qquad\qquad (Eq.1)$$
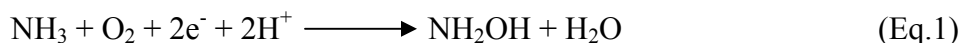
It involves the oxidation of ammonia to the intermediate hydroxylamine. HAO, an enzyme found in the periplasm, catalyzes the second step, the oxidation of hydroxylamine to nitrite (Eq.2)(*68*):

$$NH_2OH + H_2O \longrightarrow NO_2 + 4e^- + 5H^+ \qquad\qquad (Eq.2)$$
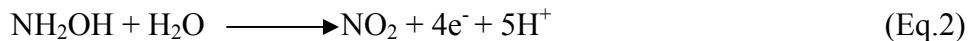
The electrons produced in this step have different paths: two electrons are passed onto an electron transport chain containing cytochrome c_{554}, cytochrome c_{552} and cytochrome *c* oxidase for gaining energy. The other two electrons seem to go in reverse direction towards AMO for hydroxylamine production or are used for ATP-dependent reverse electron transport for NAD(P)H production (*69*). Obviously hydroxylamine oxidoreductase is a key enzyme as the starting point for the essential energy flow distribution in the electron transport chain.

Hydroxylamine oxidoreductase is one of the most complex hemeproteins known. It is a trimer of polypeptides with its monomer of 67k Da molecular weight (*70*). Each monomer contains totally eight hemes covalently bound via cystein thioether bonds present in the CXYCH sequences. Seven of them are *c*-type heme groups and the remaining one is an unusual novel heme named P460 which contains a novel

33

chromophore with an absorption maximum at 463nm in the fully reduced form and has been shown to be reactive with CO, which suggests it is a high-spin, five-coordinate heme that functions in catalysis (*71*).

The crystal structure of HAO was resolved to 2.8 Å resolution (*66*). The trimeric structure is shown in Figure 1.13. Each subunit has two distinct domains, an N-terminal domain (residue 1-269) and a central domain (residues 270-499). The former comprises 14 α-helices, a short two-stranded β-sheet, along with five c-type hemes and P460 heme. The latter consists of ten α-helices and contains two c-type hemes. The most striking feature of HAO is the remarkable complex arrangement of the total 24 hemes, eight hemes for each subunit. In Figure 1.13, the hemes are located in the bottom half of the structure. The three P460 hemes are found above the plane of a "heme-ring" comprising eighteen c-type hemes (*66*).

In each subunit, six of the *c*-hemes have α-band absorption maxima at 553 nm in the ferrous form and their reduction potentials are within -412 mV to +288 mV (vs NHE) (*72*). The seventh c-heme which has α-band absorption maximum at 559 nm has its midpoint potential value at +11 mV and the active-site heme P460 has been found to have a midpoint potential of -260 mV (*69*).

The function of these seven *c*-hemes is thought as a sink to transfer electrons away from the catalytic site P460 heme where ligand binding is believed to take place. The complex arrangement of totally 24 hemes creates strong redox power for oxygen reduction into water in both the AMO pathway and ATP-synthesis process (*59*). EPR studies also indicate that there are strong interactions between these hemes (*69*).
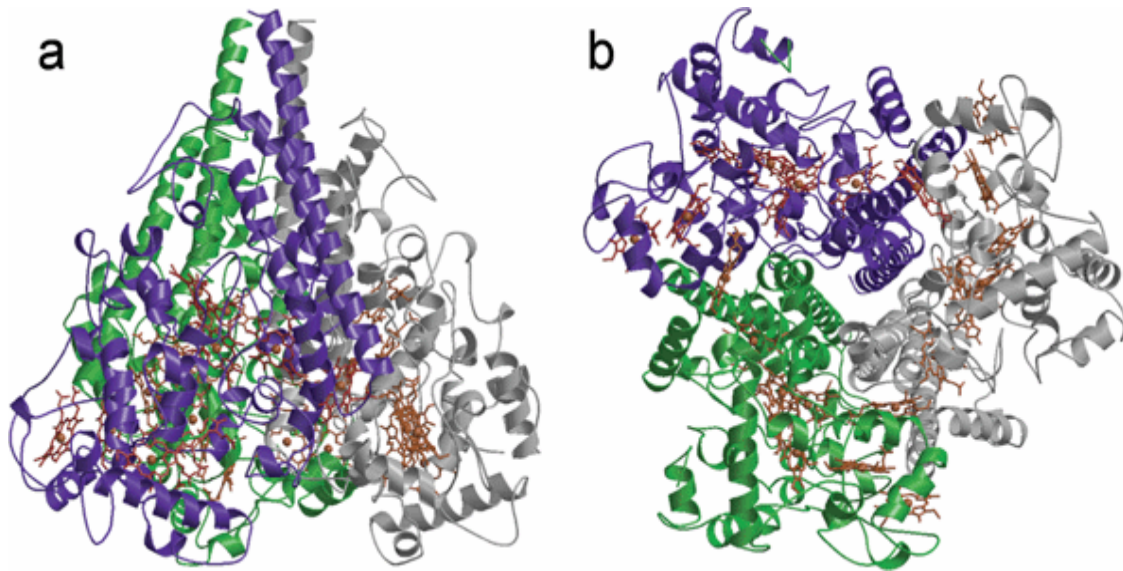
Figure 1.13. The crystal structure of hydroxylamine oxidoreductase from *Nitrosomonas europaea* [PDB ID 1FGJ] (*66*). The three subunits are coloured purple, green, and grey respectively. Hemes are located at the bottom of the trimer a) the view from the side, b) the view from the base of the trimer (*59*).

Methanotrophs and ammonia-oxidizing bacteria share a number of morphological, physiological and biochemical similarities (*73*). It has been long known that methanotrophs are capable of oxidizing ammonia to nitrite. The first step of this process is the oxidation of ammonia to hydroxylamine, catalyzed by the methane monooxygenase (MMO) (*74, 75*). The second step is the oxidative conversion of hydroxylamine to nitrate catalyzed presumably by either cytochrome P460 or hydroxylamine oxidoreductase (HAO) enzymes (*75-77*). Little is known about how the enzyme catalyzes this reaction in methanotroph. Recently, an HAO-like gene was sequenced from *Methylomicrobium album,* ATCC 33003 (*78*). This strain was used to purify and characterize the first HAO protein from a methanotrophic bacterium to demonstrate its function in hydroxylamine oxidation (chapter 4).

1. 3 ELECTRON PARAMAGNETIC RESONANCE

1.3.1 Introduction

Electron Paramagnetic Resonance (EPR) or Electron Spin Resonance (ESR) spectroscopy is a technique that measures the absorption of microwave radiation by an unpaired electron when it is placed in a strong magnetic field. It characterizes the properties and probes the environment of this paramagnetic center (*79*). EPR spectroscopy has become a particularly important instrument in studies of biological systems that naturally contain paramagnetic species like metal ions, substrate radicals, and redox-active centers in proteins (*80*). EPR is able to focus its measurement on the paramagnetic active sites without interference from diamagnetic species. Since the tertiary structure of metalloproteins is normally diamagnetic, EPR is an exceptional technique to look into the structure of the paramagnetic cofactor in the free enzyme, intermediates and product complex (*81*). It can also be applied to collect kinetic information on paramagnetic species (*80*).

1.3.2 Basic Principles

Spectroscopy provides the way to measure and interprete the energy difference between different atomic and molecular states. On the basis of Plank's law, electromagnetic radiation is absorbed [Eq. (1)]

$$\Delta E = h\nu \tag{1}$$

Where h is Plank's constant and ν is the radiation frequency. The absorption energy is the reason that transition would occur between lower and higher energy states. And the energy absorption comes from the interaction between the magnetic dipole moment of an

unpaired electron and an applied magnetic field, which is called the Zeeman effect. The Zeeman energy of the spin states is due to the magnitude of the applied magnetic field and a proportionality constant called the *g* factor [Eq.(2)]:

$$\text{Zeeman energy} = g\beta B_0 m_s \tag{2}$$

Where β is a conversion constant called electron Bohr magneton, B_0 is the magnetic field, and m_s is the electron spin quantum number that can be either +1/2 (parallel state) or -1/2 (antiparallel state) when the paramagnetic species contains one unpaired electron (S=1/2).

The *g* factor is also called spectroscopic splitting factor, the free-electron *g* factor is isotropic and its precise value is 2.0023. As for paramagnetic molecules or ions, the *g* factor is a tensor quantity, indicating that value depends on the orientation of the molecule in applied magnetic field (*80*). Therefore, the amount of *g* anisotropy relies on the degree of spin-orbit coupling. Small organic radicals with only O, H, N and C atoms have *g* factors close to the free-electron *g* factors while spin-orbit coupling could be large for transition metal ions, leading to *g* factors that differ significantly from free-electron *g* factors.

In EPR measurements, the paramagnetic species is placed in a magnetic field which splits the energy levels of the ground states (Figure 1.14). The *g* factor could be determined by the energy between the two spin levels since β is a constant and B_0 could be obtained. Normally, the *g* value can be converted and calculated as following [Eq.(3),(4)]:

$$\Delta E = h\nu = g\beta B_0 \tag{3}$$

$$g = h\nu / \beta B_0 = 714.484 \, [\nu \, (\text{GHz})] / [B_0 \, (\text{gauss})] \tag{4}$$

where h is Planck's constant and ν is the microwave frequency.
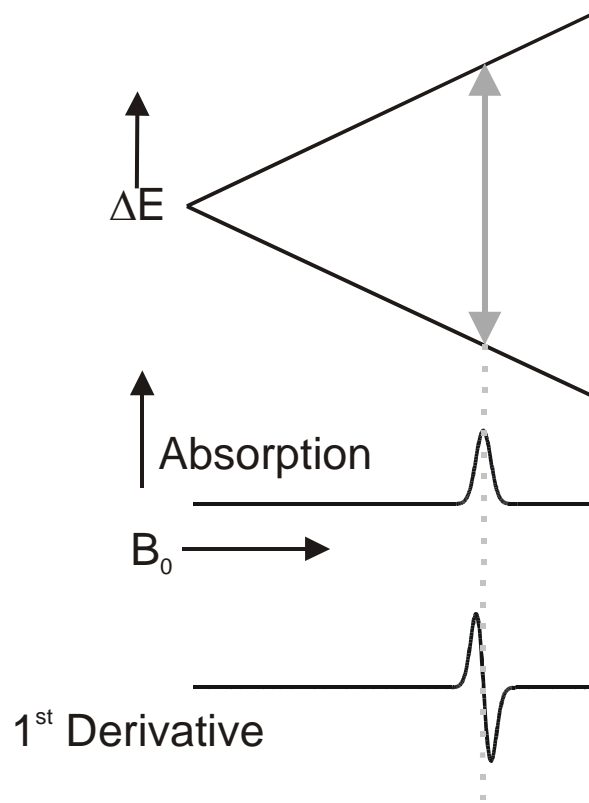
Figure 1.14. Schematic illustration of the splitting of the electron spin states with absorption and first-order derivative.

From basic physics theory, we know that a bar magnet would align itself in an outside magnetic field and the energy of the bar magnet could be affected by the interaction with another bar magnet within certain distance. A similar interaction occurs between an unpaired electron and a neighboring magnetic nucleus, which is termed as *nuclear hyperfine interaction* (Figure 1.15). It is called **hyperfine** if it is due to the nucleus where the unpaired electron originates and is called **superhyperfine** if it results from a neighboring nucleus. Therefore we could add this term to the energy expression above [Eq. (3)] as [Eq. (5)]:

$$\Delta E = h\nu = g\beta B_0 + hAm_I \tag{5}$$

where A is designated as Hyperfine Coupling Constant (measured in cm^{-1} or MHz), m_I is the magnetic quantum number for the nucleus and A is called Hyperfine Splitting Constant. Each nuclear spin would split the EPR line into $2I+1$ hyperfine lines of equal intensity since there are $2I+1$ possible m_I values. Table 1.1 listed some of the nuclei that are important in biological research (*82*).

As mentioned, the deviation of the measured *g* factor from that of the free electron (g_e) originates from spin-orbit coupling between ground state and excited states. Because orbitals are oriented in the molecule in different ways, the magnitude of this mixing is direction-dependent, or named anisotropic. If a molecule is tumbling quickly enough, as in a low-viscosity solution, the anisotropic effect is averaged to zero. However, when all the paramagnetic molecules are in an immobilized orientation, for instance, in a single crystal, the *g* factor would change with different positioning due to anisotropy. Consequently, for every paramagnetic molecule, there is a unique axis system called the "principle axis system". The *g* factors measured along the axes are "principal *g* factors"
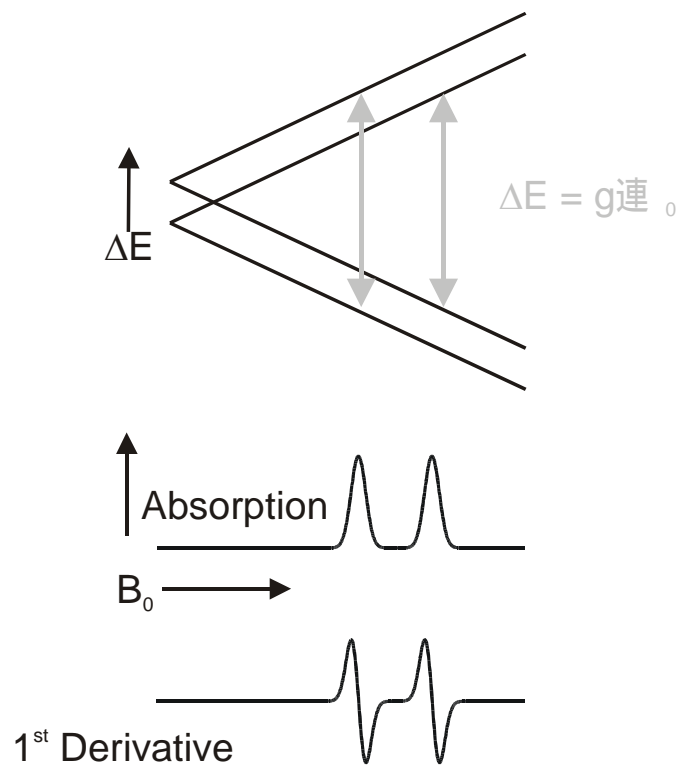
Figure 1.15. Schematic illustration of the interaction between a single electron and magnetic nucleus with nuclear spin 1/2.

Isotope	Nuclear Spin (I)	% Abundance
^{1}H	1/2	99.9
^{2}H	1	0.02
^{12}C	0	98.9
^{13}C	1/2	1.1
^{14}N	1	99.6
^{15}N	1/2	0.37
^{16}O	0	99.8
^{17}O	5/2	0.037
^{32}S	0	95.0
^{33}S	3/2	0.76
^{51}V	7/2	99.8
^{55}Mn	5/2	100
^{56}Fe	0	91.7
^{57}Fe	1/2	2.19
^{59}Co	7/2	100
^{58}Ni & ^{61}Ni	0	68 & 26
^{61}Ni	3/2	1.19
^{63}Cu & ^{65}Cu	3/2	69 & 31
^{95}Mo & ^{97}Mo	5/2	16 & 9
^{183}W	1/2	14.4

Table 1.1. The nuclear spin of some nuclei that are important in biological research.

and designated as g_x, g_y and g_z respectively (*83-85*).

The nuclear hyperfine interaction contains both an isotropic and an anisotropic contribution. For small molecules in solution, the anisotropic contribution to the nuclear hyperfine interaction is averaged out so that the EPR spectra of small molecules in solution would exhibit finely resolved nuclear hyperfine structure arising only from the isotropic effect (*80*).

Most EPR spectra of biological transition metals are measured as frozen solution samples. The act of freezing immobilizes the molecules in all probable orientations. Therefore, the EPR spectrum of a frozen sample representing the summation of all probable orientations is referred to "powder spectrum".

There are three different classes of anisotropy, isotropic, axial and rhombic according to the "principal axis system." In the first class, **isotropic**, all of the principal *g* factors are the same in different directions, $g_x = g_y = g_z$ and therefore, the spectrum has a single symmetric shape line. In the second one, **axial**, there exists a unique axis ($g_x = g_y \neq g_z$). The *g* factor along the unique axis is said to be parallel with it, $g_z = g_\parallel$ while the other two are perpendicular to it, $g_x = g_y = g_\perp$. As for the last class, **rhombic,** all the *g* factors are different ($g_x \neq g_y \neq g_z$) (Figure 1.16) (*83-85*).
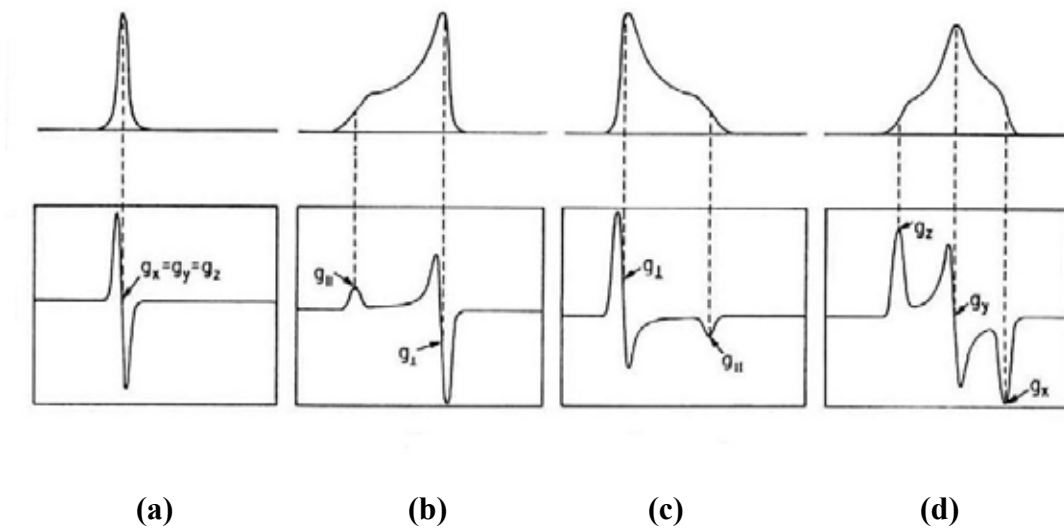
Figure1.16. Absorption and first-derivative spectra of three different classes of anisotropy (a) isotropic, $g_x = g_y = g_z$, (b) axial, $g_x = g_y < g_z$, $g_{//} > g$, (c) axial, $g_x = g_y > g_z$, $g_{//} < g$ (d) rbomic, $g_x \neq g_y \neq g_z$ (Adopted from (79)).

1.3.3 Example of a Nickel EPR Spectrum

There are a number of proteins known to contain nickel including urease, nickel hydrogenases, carbon-monoxide dehydrogenase, acetyl-coenzyme A synthesase, methyl-coenzyme M Reductase, Ni-superoxide dismutase, glyoxalase I and *cis-trans* isomerase. (*81*). The most common redox state, 2+, is EPRsilent (S = 0 or S = 1). The oxidized Ni(III) form and the reduced Ni(I) form are both EPR active (S = 1/2).

In methyl-coenzyme M reductase, nickel is coordinated by four nitrogen atoms in the active site (Figure 1.1) and the nuclei of these nitrogen atoms have a nuclear spin S = 1. In the Figure 1.17, the top spectrum shows the typical EPR signal of methyl-coenzyme M in the MCRred1 form with the nickel in the 1+ oxidation state, obtained from cells growing with natural abundance of nickel. The superhyperfine lines resulting from the four nitrogen ligands are clearly detected on the $g_\perp$ peak. The hyperfine structure on $g_{//}$ peak is not that obvious but still recognizable. As an example of hyperfine structure, *M. marburgensis* cells were grown on [61]Ni which has a nuclear spin 3/2. In the MCRred1 signal an additional split is detectable on the g_z ($g_{//}$) due to the nuclear spin of [61]Ni.
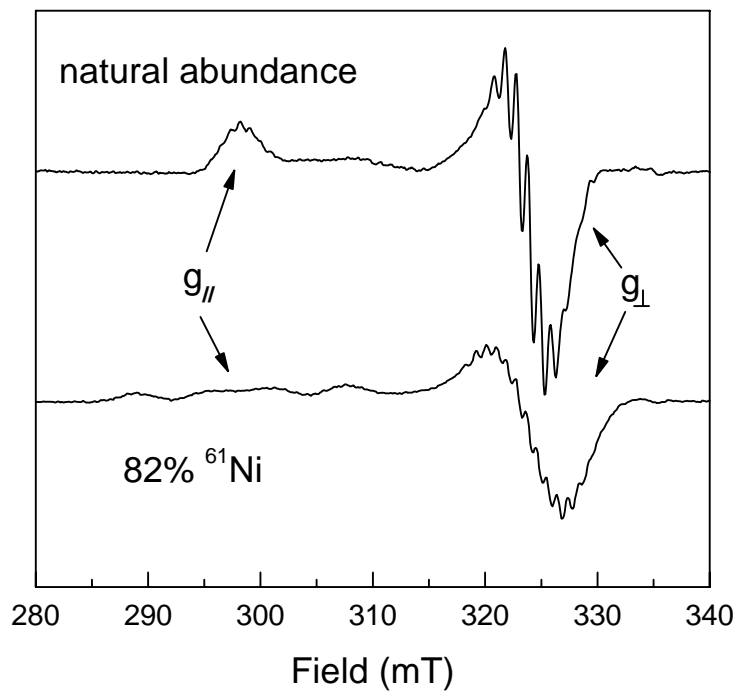
Figure 1.17. EPR spectra of methyl-coenzyme M in the red1 state from *Methanothermobacter marburgensis*. a) Cells grown with natural abundance nickel. b) Cell grown on [61]Ni.

1. 4 ELECTRON NUCLEAR DOUBLE RESONANCE

1.4.1 Introduction

Electron-nuclear double resonance (ENDOR) was first established by Feher in 1956 (*86*) and was first used on metalloproteins by Eisenberger and Pershan (*87*). It complements the EPR technique by recovering the hyperfine coupling constants for nuclei at paramagnetic center unresolved in the EPR signal. It measures the nuclear magnetic resonance (NMR) spectra of nuclei associated with the electron spin (*88*). The occurrence of a nuclear resonance transition is not detected in a direct form but as an intensity change in the EPR signal. Therefore this technique is classified as a double resonance technique which has two major advantages: direct stimulation of NMR transitions enhances the spectral resolution by orders of magnitude compared with EPR; detection of the effect utilizing the Boltzmann population difference of electron spin energy levels increases the sensitivity by orders of magnitude compared with NMR (*89*). Therefore, ENDOR lines are usually sharper than EPR lines. The hyperfine coupling constants, undetectable by ordinary EPR spectroscopy, can often be determined by ENDOR. Further, ENDOR spectrum is only of paramagnetic species without interference from diamagnetic molecules.

The technique of ENDOR could provide answers to the questions such as what kind of nuclei interact with the unpaired electron? How do the hyperfine coupling constants for these different nuclei change with changes in pH value, solvent, or during substrate binding in catalysis? In addition to protons, a multiple of magnetic nuclei can be studied by ENDOR, such as: ^{2}H, ^{13}C, and ^{14}N and some first investigated signals from ^{17}O, ^{33}S, ^{61}N, $^{63,65}Cu$ and $^{95,97}Mo$ nuclei that exist as components of active site in

metalloenzyme or as part of a bound ligand or substrate (*89*). The ENDOR technique is not restricted to monoradicals, but can also be applied to multi-radicals in spin states of higher multiplicities (triplet, quartet, or quintet state). It has opened up new vistas for investigations of the primary process of photosynthesis, the mode of action of derivatives of vitamin E and K, and the mechanism of the enzymatic catalysis of flavoenzymes in biological redox-chains (*90*).

1.4.2 Basic Principles

The general theory of ENDOR has been covered in detail by Swartz *et al*., Atherton, Dorio and Freed, Schweiger (*91-94*). Therefore, only the basic theory necessary for understanding the work presented in this dissertation is described here.

Based on classic Schödinger equation and conventional "Spin Hamiltonian" (*95*) and considering nuclear spins factor, the spin Hamiltonian for the simplest system with effective electron spin $S' = 1/2$ and a single nuclear with $I = 1/2$ could be described as:

$$H = g\,\beta_e\,B\,S' - g_n\,\beta_n\,B\,I + S'A\,I \tag{1}$$

Where β_e, β_n are the conversion constants, electronic and nuclear magnetons, g, g_n are the electronic and nuclear *g*-tensor describing the anisotropic interaction between the magnetic field B and the electronic spin S', and A is the anisotropic hyperfine tensor describing the interaction between the electronic and nuclear spins. In this equation, the first term is the electronic Zeeman interaction, the second is the nuclear Zeeman interaction, and the third is the hyperfine interaction. The effects of these three terms are showed in Figure 1.18 and a detailed explanation can be found in (*96*).

m_s m_s, m_l m_s, m_l

+1/2, -1/2

+1/2, -1/2

+1/2

EPR

ENDOR
ν_n +A/2

~

EPR

+1/2, +1/2

+1/2, +1/2

EPR

-1/2, -1/2

-1/2, -1/2

~

-1/2

ENDOR
ν_n -A/2

-1/2, +1/2

-1/2, +1/2

Electronic
Zeeman
Interaction

Nuclear
Zeeman
Interaction

Hyperfine
Interaction
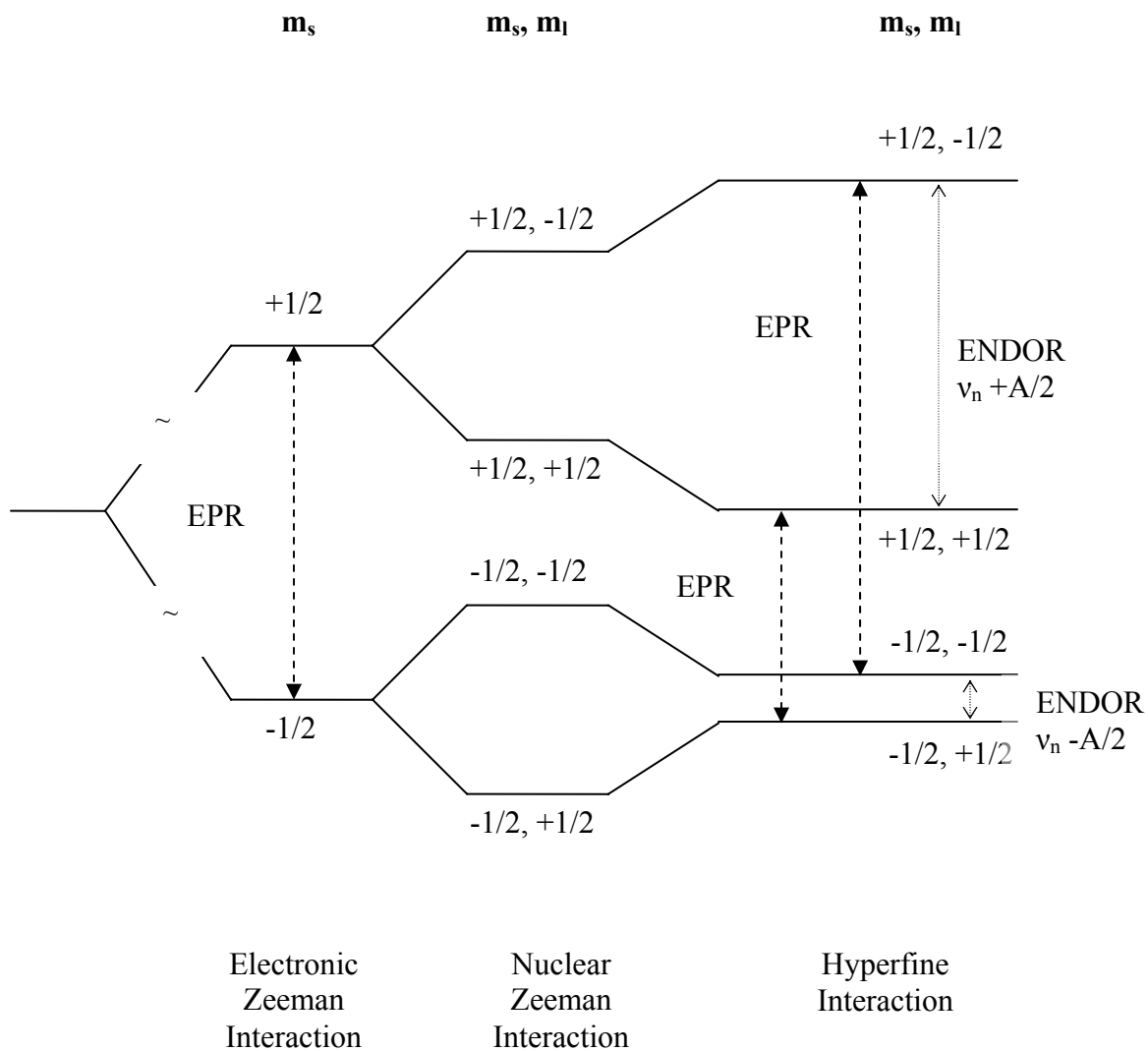
Figure1.18. Schemic illustration of the effects of electronic and nuclear Zeeman interactions

and of the hyperfine interaction on the simplest system with S=1/2, I=1/2.

(---), the allowed EPR transitions; (····), ENDOR transitions.

In Figure 1.18, the energy level diagram is calculated from Eq. (1) and the splitting of the spin states is resulted from the successively smaller interactions for a magnetic field of approximately 330 mT (3300G). Usually, the energies follow the order of: electron Zeeman (~ 10 GHz) > nuclear Zeeman (1-15 MHz) ≈ electron-nuclear hyperfine (0-10 MHz). As it can be seen, the relative magnitude of the nuclear Zeeman (g_n β_n B I) and nuclear hyperfine (S´AI) energy terms in Eq. (1) have marked effects on the ENDOR spectra. It is the $\Delta m_l = \pm 1$ transitions that ENDOR is able to detect while the $\Delta M_s = \pm 1$ is detected in EPR. The radiofrequencies where the ENDOR lines are observed ($v_\pm$) are related to the NMR nuclear Lamor frequency (v_n) of the magnetic nucleus and the hyperfine coupling constant (A) by: $v_\pm = | v_n \pm A/2 |$. In the case when $| v_n | > | A/2 |$, it means the nuclei is weakly coupled, whereas $| v_n | < |A/2 |$ indicates strongly coupled nuclei. And the middle case when $| v_n | = | A/2 |$ is named cancellation condition.

In CW ENDOR, the EPR signal at a given field is partially saturated by an increase of microwave power (*86*). When the radio frequency matches a nuclear frequency, in another word, when a nuclear transition is induced, the population of the partially saturated EPR transition will be changed and the recovery of this signal will be realized by detecting net mw absorption. Therefore it allows us to determine the hyperfine coupling constant (*97*).

ENDOR spectra are supposed to be sharper than the original EPR spectra because of the long relaxation times of most nuclei, which provide us with more information of hyperfine splittings that were undetectable in the EPR spectrum. It is indeed a technique with great advantage to interpret broad lines in EPR spectra with better resolved hyperfine structure.

CHAPTER TWO

ACTIVATION OF METHYL-COENZYME M REDUCTASE

2. 1 INTRODUCTION

Methyl-coenzyme M reductase (MCR) catalyzes the reaction of methyl-coenzyme M (CH_3-S-CoM) and coenzyme B (HS-CoB) to form methane (CH_4) and the heterodisulfide of coenzyme M and coenzyme B (CoM-S-S-CoB). This unique reaction is the last step for methane production in methanogenesis, which takes place in several strictly anaerobic environments (*8*). It is widely known that methane is a potent green-house gas that contributes to global warming by trapping the heat in the atmosphere. Although part of the methane produced by methanogens is reoxidized by other organisms in nature, there is a steady rise of methane in atmosphere resulting from human activities such as rice-production and increasing amounts of livestock (*98*). In order to slow down the methane formation, insight into this process is needed by studying the microbial basis and the environmental regulation of methanogenesis, the reaction mechanisms of the proteins involved, and the regulation of enzyme activity.

The most common way to slow down enzymatic processes is to find appropriate inhibitors that block key steps in the reaction mechanism. However, this is not the best way to control methane production since different species of methanogens have different resistance to various chemical inhibitors (*99*). Studies showed that methane production is

51

resumed after the more sensitive species are replaced with the more resistant methanogens. A better approach could be the investigation of the cellular regulation of MCR activity, which could eventually lead to management of the methane production byregulation of the activation system. The MCR conversion cycle introduced in Figure 1.9, shows the relationship between different MCR forms, in which MCRred1 is the only active form that can directly catalyze the reaction for methane formation. The only direct method to activate MCR in significant amount is through the incubation of MCRox1 with the reductant titanium(III) citrate at pH 10.0 and 65 °C (*23*), which was a breakthrough in the studies on MCR activation.

To our knowledge, there is only one system capable of activating the MCRsilent form, which has been studied in *Methanothermobacter thermoautotrophicus* (formerly known as *Methanobacterium thermoautotrophicum*, strain ΔH). The system involves two essential components, A2 and A3a (*34, 35, 100*). In previous studies, both proteins were isolated but were not fully characterized. A2 was purified to homogeneity and it has two ATP-binding domains according to the genetic sequence (Figure 2.1). Homology studies showed it is similar to ATP binding cassette (ABC) proteins (*34*), which would indicate a function in membrane transport. However, the A2 protein seems to be a cytosolic protein. Some of the homologous proteins are ABC proteins that are not involved in transport at all, like the sulfonylurea receptor, which serves as a regulatory subunit that fine tunes the gating of a potassium channel in response to alterations in cellular metabolism. Several proteins in the hydrogenothropic pathway are associated with the membrane and contribute to H^+ and Na^+ gradients (*101, 102*). Therefore the possible association of the A2 protein with the membrane is intriguing. However, without further evidence we only
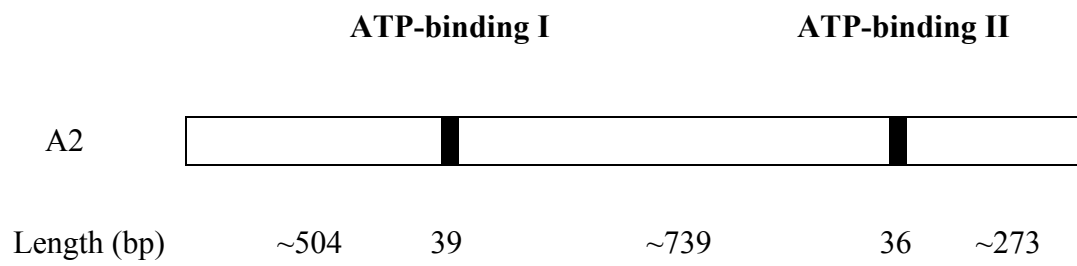
Figure 2.1. Illustration of the position of the ATP-binding domains in the A2 gene.

know with certain that the A2 protein binds ATP. A3a is an oxygen-labile, hydrophobic, iron-containing protein and was reported to have an apparent molecular weight of 500 kDa (*35*). It was proposed that component A3a might contain an iron-sulfur cluster because of its extreme oxygen sensitivity and the inhibitory effect of bathophenanthrolinedisulfonate, a specific chelator of Fe^{2+} ions (*35*). It was proposed that component A3a is an iron-sulfur-cluster-containing protein that accepts ATP provided by component A2. ATP hydrolysis occurring on A3a could create a low-potential electron that is able to bridge the potential gap between the iron-sulfur cluster and the nickel center of F_{430} (Figure 2.2) (*103*). This proposal has not been verified since the A3a has never been completely purified. In the presence of the essential components A2 and A3a, and Ti(III) citrate, the inactive MCR purified from *M. thermoautotrophicus* could be activated. However, only 2-5% of the specific activity displayed by MCR *in vivo* could be obtained (*8*).

Our goal here is to investigate the activation of the MCRsilent form in *Methanothermobacter marburgensis* (formerly known as *Methanobacterium thermoautotrophicum,* strain Marburg). The reduction of the low-potential nickel site in MCR is an interesting topic by itself. However, there is a more urgent need for understanding the activation of MCR. Site-directed mutagenesis studies are planned for the near future in an attempt to understand the role of several unique amino acids present in MCR. A genetic system is available for *Methanosarcina acetivorans* C2A that allows the insertion of a second MCR, providing the cells with one MCR for growth and another MCR that can be genetically modified. It is not sure if our current activation method of changing the gas phase of growing cells will function for the mutated enzyme. A better
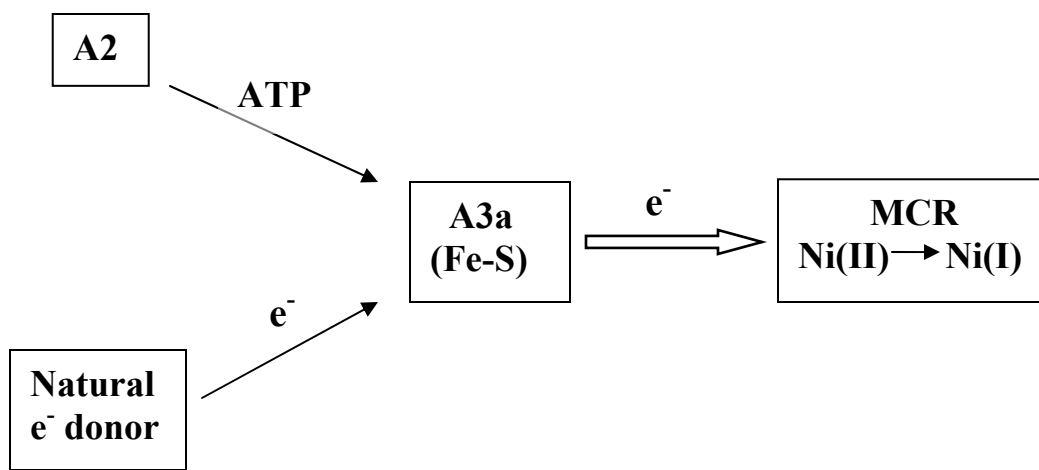
Figure 2.2. Schematic illustration of the postulated system for activation of MCRsilent.

understanding of the activation system could give valuable information of possible methods to perform an *in vitro* activation of MCR.

For the activation studies, the natural substrates of MCR were synthesized and inactive MCR was purified. The A2 component was overexpressed in *Escherichia Coli* and purified to homogeneity. Solutions containing all necessary components for the activation of MCR, with only lacking the A3a component were used to test the presence of A3a in crude fractions. No significant activity was observed in these studies. However, following a published purification protocol a protein was purified to 70% purity that showed all the typical properties of the A3a component from *M. thermoautotrophicus*. EPR measurements indicated the presence of a $[4Fe-4S]^{+/2+}$ cluster with very low signal intensity (< 5%). An effort was made to increase the cluster content, but no significant activation of MCR was observed with these preparations. We conclude that the A2 and A3a components are either not sufficient for the activation of MCRsilent or not activating components for MCR in *M. marburgensis*.

2．2 MATERIALS AND METHODS

2.2.1 Biochemical and Chemical Reagents

Glucose, dithiothreitol, sodium sulfide, kanamycin, chloramphenicol ferrous ethylenediammonium sulfate, imidazole, iron(III) chloride, sodium dithionite, potassium permanganate, methyl iodide, ammonium acetate, and isopropyl-β-D-thiogalactoside (IPTG), coenzyme M were purchased from Sigma-Aldrich (St. Louis, MO). Potassium phosphate (monobasic anhydrous and dibasic anhydrous), 2-propanol, absolute ethanol, glycerol, magnesium sulfate, magnesium chloride, tryptone, yeast extract, LB-agar, ammonium chloride, sodium chloride, ammonium sulfate and Tris-base were from Fisher Biotech (Pittsburg, PA). Diethyl amino ethyl (DEAE) sepharose, Q-sepharose, S-300 Sephacryl, Phenol Sepharose and PD-10 columns were purchased from Amersham Biosciences (Piscataway, NJ). Centricon ultrafiltration units were from Millipore (Bedford, MA).

Standard anaerobic buffers were used for all purifications and experiments. The buffers were filtered (0.22 μm) and subsequently boiled under nitrogen gas flow. They were stirred under vacuum for a period of 1-2 h. The buffers could then be used or stored under nitrogen with 0.3 atmospheric overpressure applied to the head space of the bottle.

2.2.2 Preparation of Titanium(III) Citrate Solution

A 200 mM Ti(III) citrate solution was prepared by dissolving Ti(III) chloride powder in 250 mM sodium citrate under strictly anaerobic conditions (*104*). After stirring at RT for at least 15 min the solution was neutralized by slow addition of solid $KHCO_3$ until foam production stopped and a pH of 6.0~7.0 was reached.

57

2.2.3 Synthesis and Purification of Methyl-Coenzyme M

Methyl-coenzyme M was synthesized from coenzyme M by methylation with methyl iodide (*105*). Coenzyme M (3 mmol) was incubated for 12 h with 6 mmol of methyliodide in 5 ml of a 33% aqueous ammonia solution under a 100% N_2 atmosphere. After incubation for 12 h at room temperature the reaction mixture was evaporated to almost dryness. After lyophilization the dry yellow residue was dissolved in 10 ml distilled water. Aliquots of the solution of 5 ml were loaded on a Q-Sepharose column (volume 30 ml) and a linear gradient of 0 to 1 M ammonium carbonate was used for elution. Ammonium carbonate was used instead of hydrochloric acid to elute methyl-coenzyme M from the Q-Sepharose column since methyl-coenzyme M in the non-dissociated sulfonic acid form and water form an azeotropic mixture. Eluate was collected and tested for methyl-coenzyme M by thin layer chromatography on Kieselgel 60 F_{254} (Merck) with butanol/acetic acid/water (2:1:1) as the mobile phase. Methyl-coenzyme M generally eluted from the column between 250 mM and 350 mM ammonium carbonate. Fractions containing methyl-coenzyme M were combined and lyophilized, which removes the ammonium carbonate. Subsequently, the powder in the powder (1.8 g) was obtained at the end.

2.2.4 Synthesis of Coenzyme B *(106)*

7,7'-Dithiodiheptanoic acid: 7-Mercaptoheptanoic acid was synthesized by dissolving 17.4 g (228 mmol) of thiourea in a stirred solution of 7-bromoheptanoic acid (9.6 g, 46.6 mmol) in 110 ml of ethanol. This mixture was refluxed under argon at 90°C for 17 h, cooled to room temperature, and 25 ml of a 60% aqueous solution (w/v) of sodium

hydroxide was added. The mixture was refluxed under argon for an additional 2 hours, and cooled to room temperature. The yellow/white solution was concentrated. A 100 ml aqueous solution of 1M HCl was added followed by 20 ml concentrated HCl. The thiol was extracted 3 times with 100 ml dichloromethane. The dichloromethane phase was extracted 3 times with 150 ml of an aqueous solution of 1 M sodium bicarbonate. The aqueous extract was acidified with HCl to a pH of 1-2, and extracted 3 times with 200 ml dichloromethane. The organic phase was filtered over cotton and concentrated to 70 ml. The thiol was oxidized to a disulfide by mixing the dichloromethane phase with an aqueous solution of 10% (w/v) iodine and 20% (w/v) potassium iodide until the brown color persisted. The aqueous phase was removed and the dichloromethane phase was washed 3 times with an aqueous solution of 1M sodium thiosulfate, and three times with water. The organic phase was filtered over cotton, (dried over anhydrous magnesium sulfate), and concentrated under vacuum. The product was crystallized twice from benzene (or toluene), and dried for two days under high-vacuum, to give 3.3 g (46%) of white crystals.

7,7'-dithiobis(succinimido-oxyheptanoate): 7,7'-Dithiodiheptanoic acid (388 mg, 1.2 mmol) was dissolved in 8 ml of 1,4-dioxane at room temperature and the solution was stirred while 290 mg (2.5 mmol) of N-hydroxysuccinimide was added when this dissolved, 505 mg (2.4 mmol) of dicyclohexylcarbodiimide (in 3 ml 1,4-dioxane) was added drop-wise and the solution was stirred 16 h at room temperature. The precipitated dicyclohexylurea was removed by filtration over a glass filter and the filtrate was washed 2 times with 5 ml 1,4-dioxane, and dried (to a clear oil) under vacuum. The product was

recrystallized twice from boiling 2-propanol, and dried for 1 day under high vacuum to give 384 mg (62%) of white crystals.

(+)-N,N'-(7,7'-Dithio-diheptanoyl)bis(O-phospho-L-threonine): A solution of O-phospho-L-threonine (400 mg, 2 mmol) and triethylamine (0.56 ml, 4 mmol) in 4 ml water was added with stirring to a solution of 7,7'-dithiobis(succinimido-oxyheptanoate) (362 mg, 0.7 mmol l) in 18 ml tetrahydrofuran and 4 ml acetonitrile. After stirring at room temperature under nitrogen for 36 h, the solvents were removed under vacuum at 30°C. The resulting white residue was dissolved in 1 M HCl (25 ml) and washed three times with dichloromethane (3 × 8 ml). Traces of dichloromethane were removed from the aqueous phase under vacuum. The aqueous phase was applied to a 2 × 13 cm column of polystyrene XAD-2 (equilibrated with 1 M HCl). The column was washed with 100 ml of 1 M HCl, followed by 150 ml H_2O. The product was eluted applying a methanol gradient (80 ml H_2O/MeOH, 4:1; 120 ml H_2O/MeOH, 1:1; 80 ml H_2O/MeOH, 1:4, 100 ml MeOH). TLC analysis (solvent system: n-butanol/acetic acid/H_2O, 2:1:1) of the collected fractions (10 ml each) showed that HTP-S-S-HTP (Rf = 0.35) had been completely separated from O-phosphothreonine (Rf = 0.24) and less polar products (Rf > 0.6). The combined fractions containing pure HTP-S-S-HTP were concentrated under vacuum (50°C) to 1/10 of the original volume, and 2 ml of 2 M ammonia was added to obtain the ammonium salt. After lyophilization 112 mg (20%) *(+)-N,N'-(7,7'-dithiodiheptanoyl)bis(O-phospho-L-threonine)*, a white solid, was obtained.

***N*-7-Mercaptoheptanoyl-O-phospho-L-threonin (CoB-SH):** 25 mg (32 µmol) HTP-S-S-HTP (ammonium salt) was dissolved in 0.5 ml anaerobic 50 mM potassium phosphate buffer, pH 7.0, under a nitrogen atmosphere. Subsequently, 2 ml of an anaerobic $NaBH_4$-solution (10% in 50 mM potassium phosphate buffer, pH 7.0) was added, and the solution was stirred for 16 h under nitrogen atmosphere at RT. Excess $NaBH_4$ is removed by addition of 0.5 ml 25% HCl (aq) and the acid solution (pH 0) was loaded on a Amberlite XAD-2 column (1 cm x 10 cm) equilibrated with anaerobic 1 M HCl (aq). The column was washed with anaerobic water and the H-S-HTP was eluted with anaerobic water/methanol (70:30; v/v). The collected H-S-HTP fractions were lyophilized, and the powder was dissolved in anaerobic 50 mM Tris/HCl buffer (pH 7.6). The pH was adjusted to 7.0 with a 2 M NaOH solution. The H-S-HTP concentration was determined indirectly by determining the thiol concentration with Ellman's Reagent. The concentration of H-S-HTP was 50 µmol (78%). Approximately 17 mg of coenzyme B was obtained.

2.2.5 Purification of MCR in Silent and Ox1 State

M. marburgensis was grown at 65 °C in a 13 L glass fermenter (New Brunswick) containing 10 L of growth medium. The mineral-salt medium (*107*) contained 65 mM KH_2PO_4, 50 mM NH_4Cl, 30 mM Na_2CO_3, 0.5 mM nitrilotriacetic acid, 2 mM $MgCl_2$, 50 µM $FeCl_2$, 1 µM $CoCl_2$, 1 µM Na_2MoO_4, 5 µM $NiCl_2$, and 20 µM resazurin. It was made anaerobic by gassing with 80% H_2/20% CO_2/0.1% H_2S at a rate of 1,200 ml/min. The resazurin was added to the medium to indicate when sufficient anaerobic conditions were

reached. After 1 h of equilibration, the medium was inoculated with 150–200 ml of fresh cell culture. At a ΔOD_{578} of ~4.5, the cells were harvested.

To obtain MCR in the MCRsilent state no special treatment before harvesting was necessary. The gas supply was switched to 80% N_2/20% CO_2 for 30 min to induce the MCRox1 form. The cell culture was cooled down over a 10 min period to 10 °C under continuous gas flow and the cells were subsequently harvested anaerobically by centrifugation using a flow-through centrifuge (Hettich, contifuge 17 RS). Approximately 50~60 g of wet cells were usually obtained using this procedure. All the following steps were performed in an anaerobic chamber (Coy Instruments) filled with 95% N_2/5% H_2.

After the cells were collected by centrifugation, the rotor was brought in the anaerobic tent. The cell pellet was resuspended in 50 ml 10 mM Tris-HCl buffer, pH 7.6, and sonicated 3 times for 7 min each at 100% power on ice, followed by ultra-centrifugation at 160,000 x g for 20 min at 4 °C. The supernatant was subjected to a 70% ammonium sulfate precipitation step by addition of the appropriate amount of a saturated ammonium sulfate solution. MCR stays in solution under these conditions. Precipitated protein was removed by ultra-centrifugation at 160,000 x g for 20 min at 4 °C. The supernatant was, subsequently, subjected to a 100% ammonium sulfate precipitation step by addition of the appropriate amount of solid ammonium sulfate. The 100% precipitation step separates MCR from small cofactors present in the cell extract of methanogens. After the 100% precipitation step, the pellet was resuspended in 100 ml 10 mM Tris-HCl pH 7.6 and subsequently loaded on a Q-Sepharose column equilibrated with 50 mM Tris-HCl pH 7.6. The column was developed with a step gradient using the same buffer containing 2 M NaCl. MCR eluted at about 0.52 M NaCl.

MCRsilent was purified from 80% H_2/20% CO_2 gassed cells without extra addition of any of the coenzymes to the buffers, typically yielding 150 mg of MCRsilent (in 120 ml). MCRox1 was purified from 80% N_2/20% CO_2 gassed cells with methyl-coenzyme M present in all steps. The method generally yielded approximately 150 mg MCRox1 (in 120 ml) with 0.5–0.8 spins per nickel.

2.2.6 Protein Determination and Activity Measurement

The protein concentration of MCR was determined by using the method of Bradford (*108*) with bovine serum albumin (Serva) as standard or by measuring the absorbance difference of oxidized enzyme (MCRsilent) at 420 nm using an $\varepsilon = 44,000$ $M^{-1}cm^{-1}$ for a molecular mass of 280,000 Da. Both methods yielded almost the same results. Methyl-coenzyme M reductase was assayed for methane formation from methyl-coenzyme M and coenzyme B at 65 °C as described previously *(24)*.

2.2.7 Activation Assay for Methyl-Coenzyme M Reductase

The production of methane by MCR from methyl-coenzyme M and coenzyme B was followed in calibrated and stoppered 10 ml vials containing 95% N_2/5% H_2 as gas phase. The liquid phase, with a total volume of 300 μl, contained 50 mM Tris-HCl, pH 7.6, 10 mM methyl-coenzyme M, 1 mM coenzyme B, 0.3 mM aquocobalamine, A2, A3a, 30 mM titanium(III) citrate and an appropriate amount of purified inactive methyl-coenzyme M reductase. Air-stable components were added to the reaction vials first, followed by the addition of Ti(III) citrate to remove any remaining oxygen. The reaction was started by increasing the temperature from 4 °C to 60 °C and it was stopped

after 40 min by decreasing the temperature back to 4 °C. A 0.1 ml sample from the gas phase was withdrawn and analyzed by gas chromatography with flame ionized detection (GC-FID) for the presence of methane. For calibration of the peak area two standards were used containing either 1.0% or 0.5% methane.

2.2.8 Construction of Expression Vector for A2

The plasmid used in the studies was pET24b$^+$. The pET expression system is under control of the T7 promoter and *lac* operator. The T7 promoter is not recognized by *E. coli* RNA polymerase and only a minimum expression of the target gene is achieved without T7 RNA polymerase. The expression of T7 RNA polymerase is under the control of the *lac* promoter. The gene of interest was inserted under control of the T7 RNA polymerase promoter with 6-histidine tag at C-terminus. For selection purposes, the pET plasmid encodes a kanamycin resistance gene.

The A2 gene from *M. thermoautotrophicus* was amplified by PCR with Easy-A^{TM} High-Fidelity PCR Cloning Enzyme (Stratagene; Amsterdam, Netherlands) using genomic DNA of *M. thermoautotrophicus* as template. The following primers were used: 5´-GCT AGC ATG TCT TTC ATA AAA CTG GAA AAT -3´ (sense; *NheI* restriction site is underlined) and 5´-CTC GAG TTA CTC CCT GAA CAT CTT ACT CTT-3´ (antisense; *XhoI* restriction site is underlined) or 5´-CTC GAG CTC CCT GAA CAT CTT ACT CTT-3´ (antisense; *XhoI* restriction site is underlined; the antisense primer did not include the stop codon in order to place a His$_6$-tag at the C-terminus of the protein).

After insertion of A2 into pET 24b$^+$ (Novagen, Germany), *E. coli* Rosetta^{TM}2(DE3) Singles^{TM} Competent Cells (Novagen, Germany) were transformed with the plasmid for expression via standard heat-shock protocol. Briefly, cells were incubated with the target plasmid on ice for 30 minutes. Then the mixture was heat-shocked at 42 °C for 45 seconds, followed by quenching on ice for 2 minutes. Cells were allowed to recover for 1 hour at 37 °C in SOC broth with gentle agitation. After recovering, cells were plated on SOC plates supplemented with kanamycin (34 mg/l) and chloramphenicol (100 mg/l).

2.2.9 Expression of A2 Protein

E. coli strain Rosetta^{TM}2(DE3) Singles^{TM} Competent Cell was used to express the A2 protein studied in this dissertation. The designation "DE3" indicates that the strain is a λDE3 phage lysogen. It contains a chromosomal copy of the gene for T7 RNA polymerase under the control of the *lac* UV5 promoter. If there is no lactose or lactose analog present, *lac* repressor binds to the *lac* promoter to block the transcription so that no T7 RNA polymerase is expressed. As a result, no target protein could be expressed either. But when lactose or an appropriate lactose analog is present, the *lac* repressor dissociates from the *lac* promoter and T7 RNA polymerase will be induced, which then induced the target gene. In our A2 expression studies, IPTG (isopropyl-β-D-thiogalactopyranoside) was used as a lactose analog.

First, *E. coli* strain Rosetta^{TM}2(DE3) Singles^{TM} Competent Cells were transformed with pET plasmid derivative containing the gene for A2-histidine as described above. Cells were isolated on SOC plate with kanamycin (34 mg/l) and chloramphenicol (100 mg/l). A single colony of the cell containing our expression plasmid was picked to

inoculate 2 mL SOC medium containing kanamycin and chloramphenicol and it was incubated overnight for about 15 hours at 37 ºC. A 1.5% inoculum was used to inoculate 100 mL medium that was incubated for eight hours at 37 ºC, and used to inoculate two 1 L-size flasks of the same medium. Inducer IPTG (isopropyl-β-D-thiogalactopyranoside) was added to a final concentration of 0.1 mM when the OD_{600} reached 0.4-0.5. Then the incubation was continued for 6 hours and cells (OD ~4.0) were harvested by centrifugation at 5000 g x 20 min and stored at -80 ºC.

2.2.10 Purification of A2 Protein

The purification of the A2 protein was performed in the anaerobic chamber. The cell pellet from 2 L growth was resuspended in 80 ml 50 mM Tris-HCl buffer with 100 mM NaCl, pH 7.6 (buffer A). Cell lysis was conducted by sonification followed by centrifugation at 160,000 g x 30 min at 4 ºC. The supernatant containing the A2 protein was filtered using a 0.22 μm filter unit. The A2 protein was then purified by immobilized metal affinity chromatography using a Ni-His Trap column connected to a Pharmacia fast protein liquid chromatography (FPLC) system. The column was washed with buffer A before the filtered supernatant was loaded. The protein was then eluted using a linear imidazole gradient from 0% to 100% buffer B (50 mM Tris-HCl (pH 7.6), 100 mM NaCl, and 500 mM imidazole). The fractions containing the pure A2 protein determined by sodium dodecyl sulfate-polyacrylamide gel electrophoresis (SDS-PAGE) were pooled and stored at 4°C. The protein concentration of A2 protein was determined using the Bradford method as described in **2.2.6.**

2.2.11 Purification of A3a Protein

A3a protein was purified from cell extract of *M. marburgensis* following the steps for cell growing and harvesting described in **2.2.2** under strictly anaerobic condition. The purification steps were performed in the anaerobic chamber as previously described (*35*) with additional modifications. After ultracentrifugation, the cell pellet was resuspended in 80 mL 50 mM Tris-HCl, pH 7.6 (Buffer C) and then loaded on a DEAE-cellulose column to separate soluble proteins from lipid vesicles which did not bind to the resin. After washing the column with Buffer C, the same buffer containing 1 M NaCl was applied and all dark-colored eluate was collected and concentrated using a centricon ultrafiltration unit with a 100 kDa cut-off. Concentrated eluate was subsequently loaded on a S-300 Sephacryl gel filtration column equilibrated with Buffer C containing 0.1 M NaCl and fractions were combined in three different pools after isocratic elution with Buffer C containing 0.1 M NaCl. The high-molecular weight pool (crude A3a protein) was applied on a Phenyl-Sepharose column, followed by elution with a decreasing salt gradient from 1 M NaCl to 0 M NaCl in Buffer C. Fractions were pooled, concentrated and characterized by SDS-PAGE and native gel.

2.2.12 Reconstitution of A3a Protein

Reconstitution of the iron-sulfur cluster was performed in the anaerobic chamber using a procedure described previously (*109*). Dithiothreitol in 50 mM Tris-HCl (pH 7.6) was added to the protein to a final concentration of 5 mM. $FeCl_3$ and Na_2S (dissolved in anaerobic H_2O) in at least a five-fold molar excess with respect to the protein concentration were added to the solution. After 3 hours, the mixture was centrifuged at

4500 rpm for 5 minutes and desalted on a PD-10 column equilibrated with 50 mM Tris-HCl (pH 7.6). The reconstituted protein was stored at 4°C.

2.2.13 EPR Experiments

EPR spectra at X-band (9.38 GHz) were obtained with a Bruker EMX-6/1 EPR spectrometer composed of the EMX 1/3 console, ER 041 X6 bridge with built-in ER-0410-116 microwave frequency counter, ER-0706 inch magnet with 60 mm air gap, and ER-4119-HS, high sensitivity perpendicular-mode cavity. All spectra were recorded with a field modulation frequency of 100 kHz. Cooling of the sample was either performed with an Oxford Instruments ESR 900 cryostat with an ITC4 temperature controller or with a liquid nitrogen finger dewar at 77 K. Data acquisition was supplied with the software by Bruker (WINEPR Acquisition program, May 1, 1997, version 2.3.1.), data manipulation (determination of g-values, subtraction, baselining, integration and conversion to ASCII files for use with Origin) was done with the WINEPR program version 2.11. EPR tubes (Wilmad, 714-PQ-8) were 4 mm outer diameter (0.38 mm wall thickness) and 13.5 cm length, high purity quartz tubes. The samples were stored in the dark and immersed in liquid nitrogen. To facilitate handling, the EPR probes were linked with a pierced rubber tubing to polystyrene sticks with a label. Spin quantitations were carried out under nonsaturating conditions using 10 mM copper perchlorate as the standard (10 mM $CuSO_4$; 2 M $NaClO_4$; 10 mM HCl). Double integration of the signals and comparison to the signal of the standard were performed. The programs of S.P.J. Albracht were used for computer simulations of the EPR signals (*110*).

68

2．3 RESULTS

2.3.1 Synthesis and Purification of MCR Substrates

Methyl-coenzyme M (CH$_3$-S-CoM, 2- (methylthio) ethanesulfonate) and coenzyme B (HS-CoB, N-7-mercaptoheptanoyl-O-phospho-L-threonine), were both synthesized (for structures see Figure 1.4). CH$_3$-S-CoM was synthesized from coenzyme M (HS-CoM, 2-mercaptoethanesulfonate) by methylation with methyl iodide (CH$_3$I) and was purified on a Q-sepharose column. A dry white powder (1.8 g) was obtained at the end. Purity was judged by NMR spectrometry (Figure 2.3).

Synthesis of coenzyme B (HS-CoB, N-7-Mercaptoheptanoyl-O-phospho-L-threonine) involved four steps including synthesis of: 7,7'-Dithioheptanoic acid; 7,7'-dithiobis(succinimido-oxyheptanoate); (+)-N,N'-(7,7'-Dithio-diheptanyl) bis (O-phospho-L-threonine) and N-7-Mercaptoheptanoyl-O-phospho-L-threonin (*106*). After the detection of the product by Ellman's reagent, the combined fractions were lyophilized to powder and ~17 mg coenzyme B was obtained. Purity was judged by NMR spectrometry. Most of work on coenzyme B synthesis was contributed by Mi Wang and the results of purified coenzyme B are available in his dissertation.
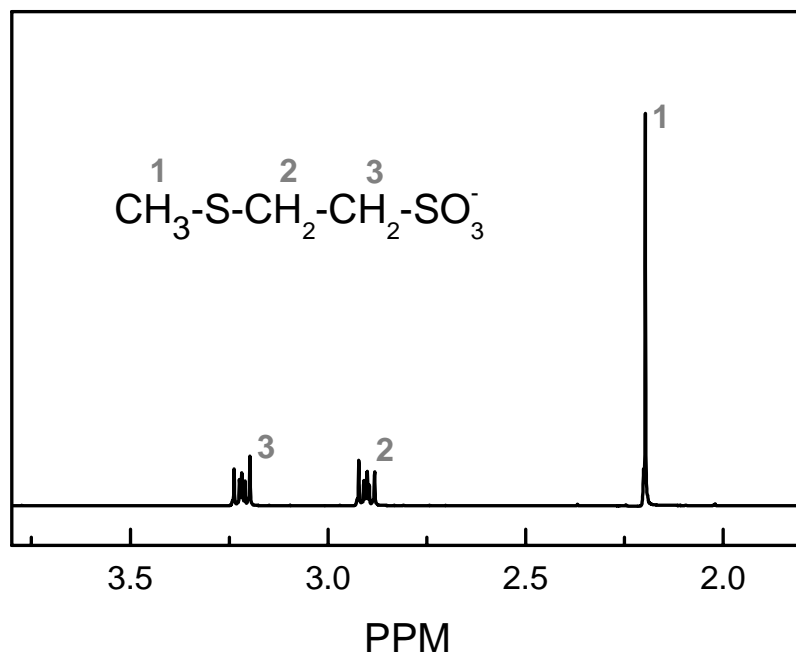
Figure 2.3. NMR spectra of synthesized and purified methyl-coenzyme M.

2.3.2 Purification of MCR in the Silent State

M. marburgensis was grown at an optimal temperature of 65 °C in a 13 L glass fermenter containing 10 L medium as described in the Methods section. The growth curve is shown in Figure 2.4. Cells were harvested at a ΔOD_{578} of ~4.5. To obtain MCR in the MCR-silent state, the gas phase was not changed before harvesting. The cell culture was cooled down to ~10 °C. The cells were harvested anaerobically using a flow-through centrifuge. Although strict exclusion of molecular oxygen is not necessary in this case, the rest of the purification procedure was performed in an anaerobic chamber. The cells were resuspended in 10 mM Tris-HCl buffer, pH 7.6. No additional coenzymes were added to the buffers in this procedure. Cell extract was subjected to fractionation by subsequent 70% and 100% ammonium sulfate precipitation steps. After resuspension of the precipitated MCR in low salt buffer, anion-exchange chromatography was performed on a Q-Sepharose column, using a step gradient. MCR eluted at a concentration of 0.52 M NaCl. Fractions were pooled together and concentrated using an Amicon concentration device with a 30 kDa cut-off filter (Millipore) to an enzyme concentration of ~200 μM. The purity of MCRsilent was judged by SDS-PAGE and the concentration was determined by both the method of Bradford and measuring the absorbance at 420 nm. The SDS-PAGE is shown in Figure 2.5. The gel shows the increase in purity during the different steps of the purification procedure. Purified MCR shows three clear bands, implicating the presence of three subunits: α, β, and γ. By judging from SDS-PAGE, the purity of MCR was at least 90%.
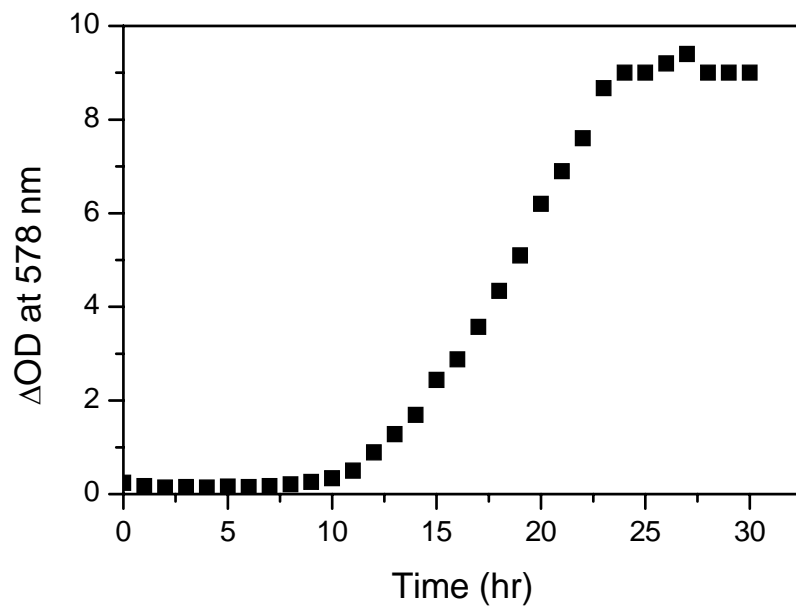
Figure 2.4. Growth curve of *Methanothermobacter marburgensis* growing in a 13 L fermenter at 65°C. For growth conditions see the text.
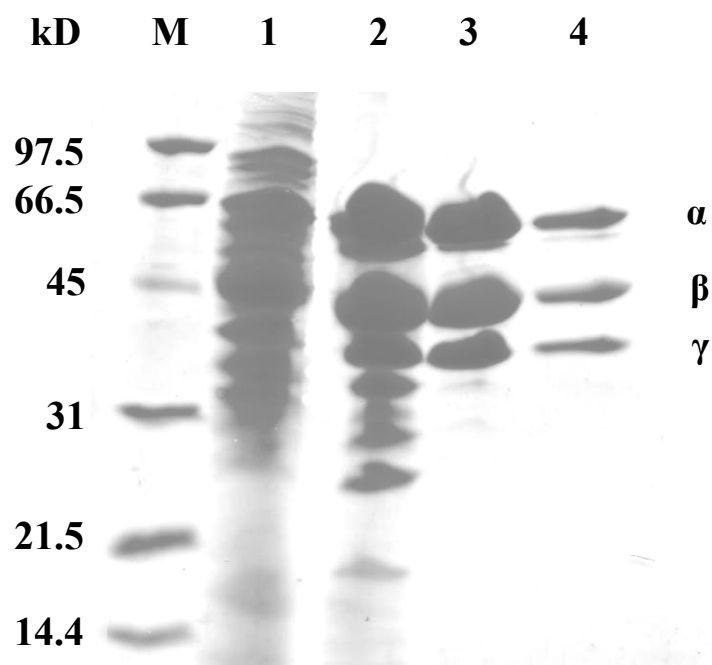
Figure 2.5. SDS-PAGE of MCR in different stages of the purification.

Lane M: Molecular weight marker; Lane 1: Cell lysate; Lane 2: Sample from 100% ammonium sulfate precipitation; Lane 3: Sample after Q-sepharose column; Lane 4: Sample from Amicon Centrifugal Filter (30 kD cut-off).

The purified enzyme was mainly in the MCRsilent form, as determined by absorption and EPR spectroscopy, but always contained traces of MCRox1 or even MCRred1. With low amounts of MCRox1 or MCRred1 present, the activation assays would show background levels of methane production since MCRred1 is the active form and MCRox1 is converted to MCRred1 in the presence of Ti(III) citrate (*23*). The presence of MCRred1 will result in a linear background formation of methane. The presence of MCRox1, however, would result in an exponential increase of methane. As long as these levels of methane formation are relatively low they should not interfere with our measurements. However, when only low levels of activation are achieved there is a chance that we may not be able to observe the activation effect. In order to lower the amount of MCRred1 as much as possible, an equimolar amount of ferricyanide was added to oxidize the Ni-porphinoid from the +1 oxidation state (MCRed1) to the +2 oxidation state (MCRsilent). The ferricyanide was removed before the enzyme preparation was used in the activation experiments. MCRox1 can be removed by incubating the samples at 65°C for 10-15 min. The MCRox1 will convert into MCRred1, but in the absence of stabilizing components like Ti(III) citrate and methyl-coenzyme M the red1 form is not stable and is subsequently converted into the silent form.

2.3.3 Expression and Purification of A2 Protein

The A2 gene was cloned into the T7 RNA polymerase-controlled expression vector pET 24b$^+$ by Bärbel Buchenau at the Max-Planck-Institute for Terrestrial Microbiology in Marburg, Germany. The overexpression was performed at Auburn University. The protein was expressed in *E. coli* strain Rosetta^{TM}2(DE3) Singles^{TM} Competent Cells. Different growth conditions and IPTG concentrations were tested. The optimal growth temperature was 27 °C. The optimal concentration of the inducer IPTG was 0.1 M. Normally, 2 L of cell culture was grown till a ΔOD_{600} of ~4.0 was obtained. The cells were harvested and broken by sonication. After centrifugation the cell extract was loaded on a Ni-his-tag column. The SDS-PAGE in Figure 2.6, showed that after this step the purity of the A2 protein was at least 90%. The purified protein was only stable for a couple of days. Concentration of purified protein using a centricon ultrafiltration unit normally resulted in irreversible precipitation. Different conditions such as different pH conditions were tested to improve the stability of purified protein. The addition of 5 mM ATP to the protein solution extended the half-life time of the protein to 2 weeks.
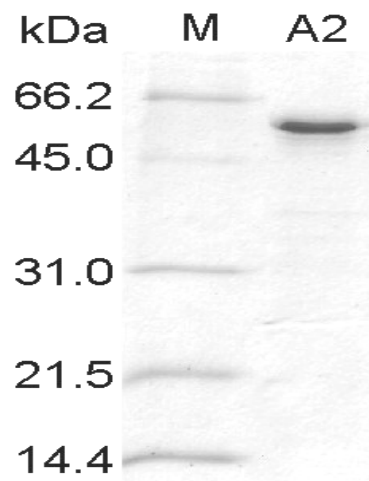
Figure 2.6. SDS-PAGE of purified A2 protein. The size of the molecular weight markers (M) is indicated.

2.3.4 Effects of Coenzyme B and Heterodisulfide on the Activation Assay

The assay mixture that was used for the activation studies contained the following compounds: buffer, methyl-coenzyme M, coenzyme B, aquocobalamine, A2, ATP, Mg^{2+} A3a (crude fractions), Ti(III) citrate and MCR. Methyl-coenzyme M is important for the stabilization of the formed MCRred1 form. Ti(III) citrate is the source of electrons for the activation of MCR and it is assumed that the electrons are first donated to the A3a protein and then to MCR. The A3a protein needs ATP, donated from the A2 protein and Mg^{2+} to create a very low potential electron.

Aquocobalamine was added to remove the formed heterodisulfide from the reaction mixture. Heterodisulfide is an inhibitor of MCR. The effect of heterodisulfide on MCRred1 is shown in Figure 2.7. With increasing concentrations of heterodisulfide, the active MCRred1 signal is gradually converted into the MCRsilent form. The MCRred1 sample contained a little MCRox1 which seemed not to be affected by heterodisulfide. The aquocobalamine splits the heterodisulfide into coenzyme M and coenzyme B. The coenzyme B can again serve as a substrate. The presence of coenzyme B in the activation assay mixture seems logical since this compound is a substrate. Still we have some evidence that it may also inhibit the activation of MCR. This is based on parallel studies involving the 'spontaneous' activation of the MCRox1 form (Figure 2.8). This effect was first observed by Dr. Duin during the purification of MCRox1. After the 100% ammonium sulfate precipitation step and resuspension of the protein pellet, it was found that MCR in the MCRox1 form would spontaneously convert into the active MCRred1 form in a timely course. This spontaneous activation is not observed after the enzyme
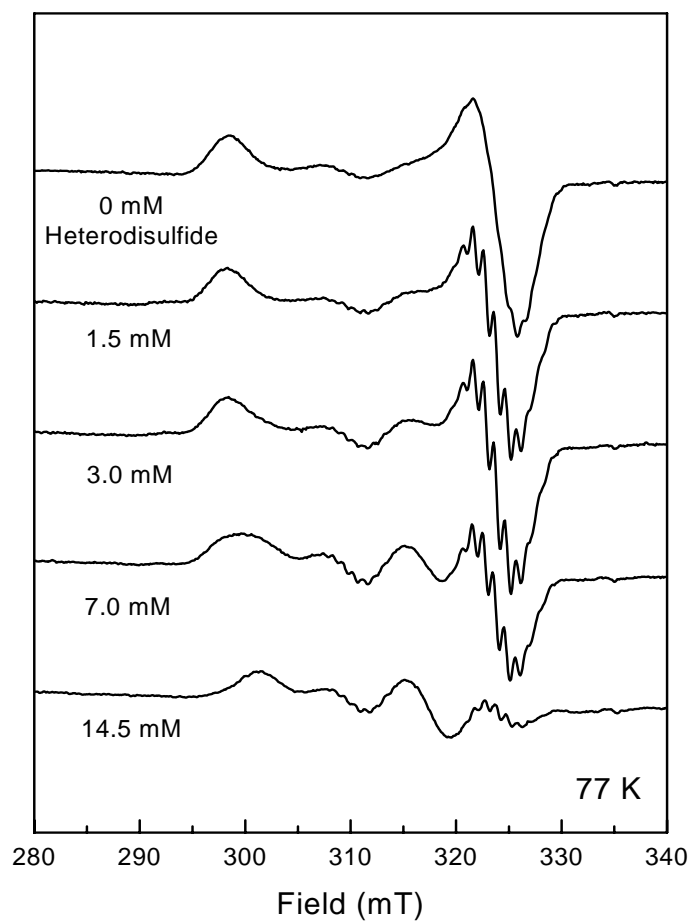
Figure 2.7. Effect of heterodisulfide on MCRred1.

is further purified on the Q-sepharose column. This experiment was repeated here at Auburn in an attempt to find which compound could help with the activation. In the presence of methyl-coenzyme M a higher conversion of MCRox1 into MCRred1 is observed over a period of 56 h at RT (Figure 2.8). Increasing the temperature to 65 °C speeds up this process (data not shown). This effect does not seem to depend on ATP (data not shown). This might be a different system from the one of MCRsilent while the possibility that these systems are correlated to each other or involve the same activating components could not be ruled out. Surprisingly, it was found that coenzyme B had an inhibitory effect on the spontaneous activation of MCRox1 (Figure 2.9). Further work on the spontaneous activation of MCRox1 was not successful and will not be further discussed. However, this work provided us with some clue about the potential inhibitory effect of coenzyme B. The fact that only a very low level of activation of the MCRsilent form has been observed may be due to a similar inhibitory effect of coenzyme B. We were not able to prove this point since in our system we did not see coenzyme B dependent activation.
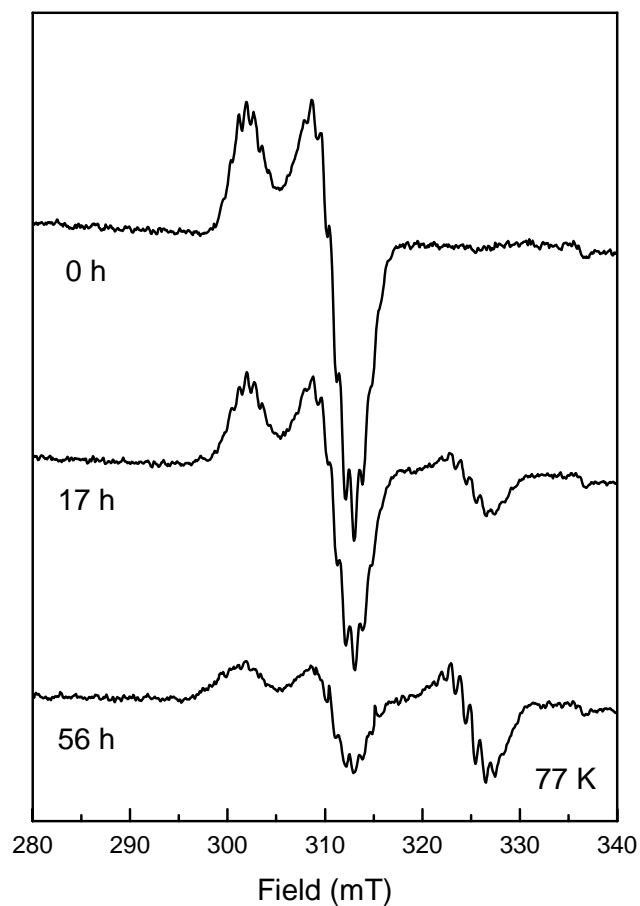
Figure 2.8. Spontaneous activation of the inactive MCRox1 form into the active MCRred1 form observed in the resuspended MCR preparation after the 100% ammonium sulfate precipitation step. The protein incubated at RT in the presence of 10 mM methyl-coenzyme M.
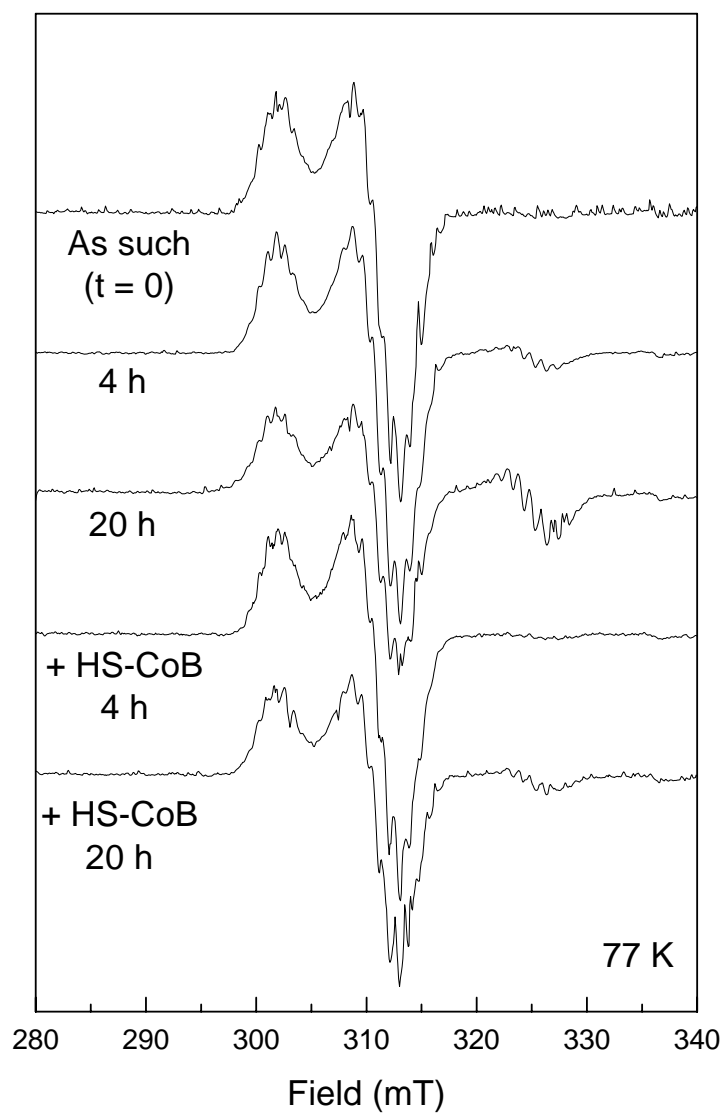
Figure 2.9. Spontaneous activation observed in semi-pure fractions and inhibition effect of HS-CoB (5 mM) on activation. Samples were incubated at RT.

2.3.5 Purification of A3a Protein Using the Activation Assay

The simplified reconstitution system containing component A2, MCRsilent and the reductant Ti(III) citrate was used to detect A3a in the fractions of the different purifications steps. Each vial contained 300 μl reaction mixture including: 50 mM Tris-HCl (pH 7.6), 2 μmol methyl-coenzyme M, 1.25 μmol coenzyme B, 0.1 μmol aquocobalamine, 4 μmol Mg^{2+}, 2 μmol ATP, 4 μmol titanium (III) citrate, 55 μg A2, 1.2 mg MCRsilent and the different fractions from the purification procedure. Air-stable components were added to the reaction vials first, followed by the addition of Ti (III) citrate to remove the oxygen. The reaction was started by incubation at 60°C and the amount of produced CH_4 was measured by GC-FID after 40 min. The various pooled fractions from different steps of the A3a purification were assayed for reconstitution of the ATP-dependent activation system. Table 2.1 shows the data for the cell extraction and S-300 Sephacryl gel filtration chromatography step. For comparison, Figure 2.12 shows an overlay of the purification profile and that of a separate calibration run with proteins with known molecular weights. The different pooled fractions were named Seph-I (fractions 18 to 22), Seph-II (fractions 23 to 28), Seph-III (fractions 29 to 33) and Seph-IV (fractions 34 to 38) respectively (Figure 2.10).

Two kinds of MCRsilent preparations were used in the activation assays. Table 2.1(a) shows the data for the heat-treated MCRsilent form. Table 2.1(b) shows the data for the ferricyanide-treated MCRsilent form. The tables show that in both cases there is still background formation of methane for both types of preparations. The background levels were similar and very small in both cases and did not influence the observation.
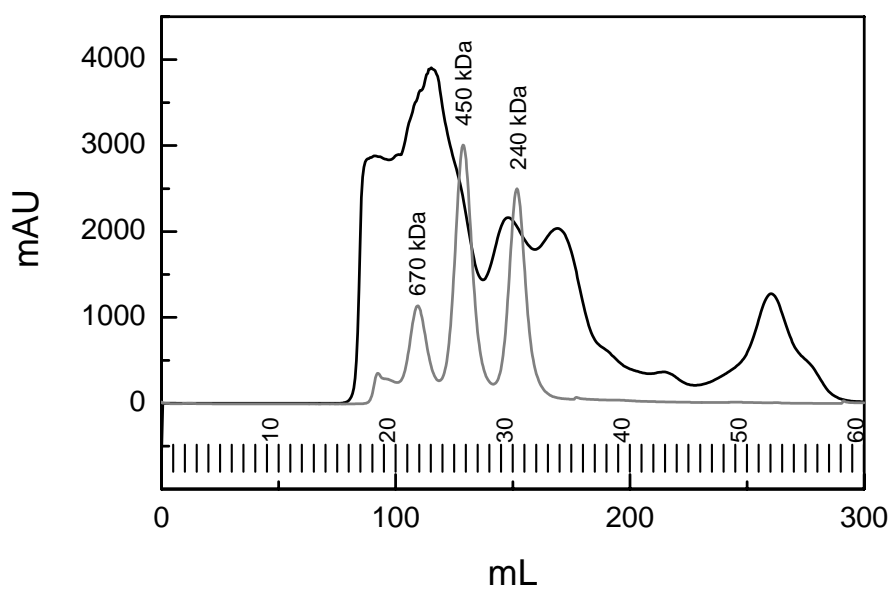
Figure 2.10. FPLC profile of Sephacryl gel filtration chromatography step.

Pooled fractions: Seph-I (fractions 18-22), Seph-II (fractions 23-28), Seph-III (fractions 29-33), Seph-IV (fractions 34-38).

Table 2.1(a)

Vial no	Fraction	MCR (heat)	A_2	CH_4 (nmol/min)	Corrected CH_4 (nmol/min)
1	-	+	-	5.8	-
2	CE	-	-	124.6	-
3	Seph-III	-	-	12.9	-
4	CE	+	+	129.5	-0.9
5	Seph-I	+	+	11.4	5.6
6	Seph-II	+	+	14.3	8.5
7	Seph-III	+	+	21.0	2.3
8	Seph-IV	+	+	10.5	4.7

Table 2.1(b)

Vial no	Fraction	MCR (ferricyanide)	A_2	CH_4 (nmol/min)	Corrected CH_4 (nmol/min)
1	-	+	-	2.1	-
2	CE	-	-	124.6	-
3	Seph-III	-	-	12.9	-
4	CE	+	+	112.1	-14.6
5	Seph-I	+	+	8.3	6.2
6	Seph-II	+	+	15.9	13.8
7	Seph-III	+	+	18.0	3.0
8	Seph-IV	+	+	4.0	1.9

Table 2.1. Activation assay with Ti(III) citrate as electron donor. Cell extracts (CE) and pooled fractions from the Sephacryl gel filtration step (Seph-I through IV) were assayed. All assays were performed as described in the text. The last colums, 'corrected CH_4', contains the amounts of CH_4 produced after subtraction of the background values from the MCR used, MCR present in cell extract or MCR present in the Seph-III fraction. (a) Heat-treated MCRsilent was used. (b) Ferricyanide-treated MCRsilent was used.

The two tables showed that cell extract by itself could be activated. Since the cell extract was not treated with heat or ferricyanide, as not to damage the A3a protein, this is attributed to small amounts of MCRred1 and MCRox1 present in the extract. After the Sephacryl column step, much lower levels of methane production were detected. Based on the calibration curve it is expected that the A3a protein (~500 kDa) is present in Seph-I and/or Seph-II. Seph-III shows relatively high levels of methane production due to the presence of MCR in the pool. This was expected from the calibration curve and further confirmed by SDS-PAGE (not shown). Seph-II shows a relative high level of methane formation and, according to the calibration curve, should contain protein with the appropriate size for A3a component. Thus, Seph-II was further purified on a Phenyl-sepharose column (Figure 2.11). Different fractions were pooled together: Øseph-I: fractions 3 to 8, Øseph-II: fractions 15 to 25, and Øseph-III: fractions 40 to 49. When these were tested in the activation assay no significant activity was found (not shown). The Ø-fractions were checked with UV-vis spectra and fraction Øseph-II showed an absorption band at 420 nm, indicative for the presence of an iron-sulfur cluster-containing protein. So this crude sample from the phenyl-sepharose chromatography step was investigated by both SDS-PAGE and native gels (Figure 2.12). The fraction seems to contain a large protein with a molecular weight around 500 kDa and it is possible a pentameric enzyme of αβ protomers with one subunit being 58 kDa and the other being 42 kDa.
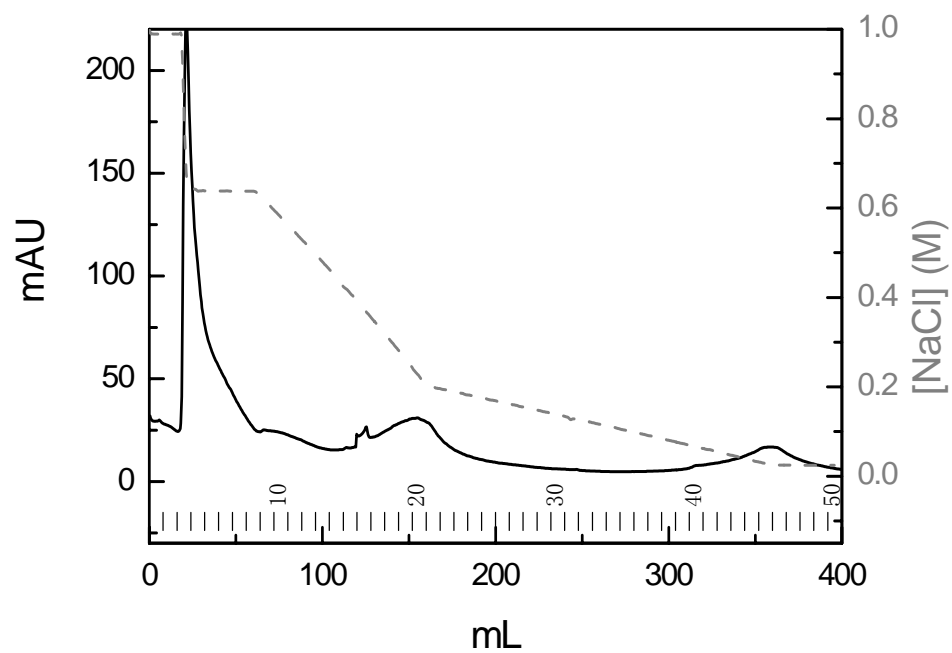
Figure 2.11. FPLC Profile for the phenyl-sepharose chromatography step.

Pooled fractions: Øseph-I: fractions 3 to 8, Øseph-II: fractions 15 to 25,

and Øseph-III: fractions 40 to 49.
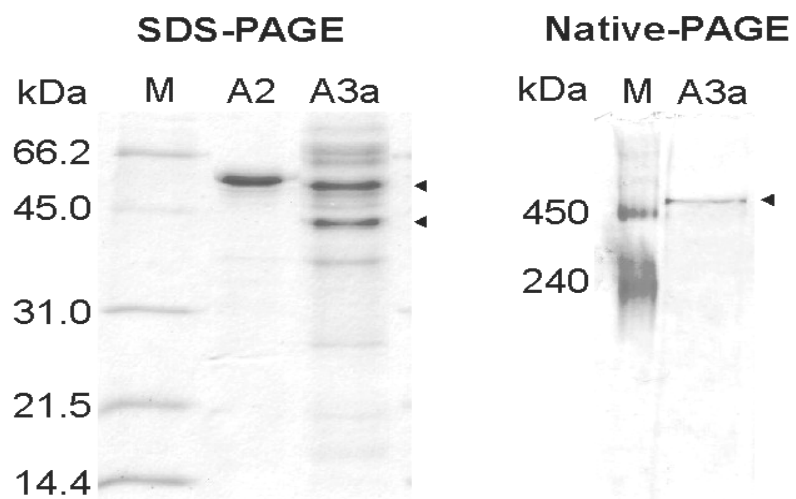
Figure 2.12. SDS-PAGE and native gels of the ØSephII Fraction. The size of the molecular weight markers (M) is indicated.

2.3.6 EPR Characterization of A3a Protein

According to the literature, the A3a protein is an oxygen-labile, iron-containing component, assumed to function like an electron carrier (*35*). Characterization of the Øseph-II fraction, showed that it contains a protein with properties very similar as those published for A3a from *M. thermoautotrophicus* (*35*) : an apparent molecular weight of 500 kDa and an absorption band at 420 nm. EPR spectroscopy was carried out to further characterize the sample. About 300 μl of protein sample reduced by dithionite was frozen in liquid nitrogen and measured at 9 K in the EPR spectrometer. Figure 2.13 shows the EPR spectrum, with contains a typical signal for [4Fe-4S] $^{2+/+}$ clusters with g_{xyz} = 1.88, 1.93, and 2.04. The two sharp features around g = 2.00 are two radical species probably due to the dithionite and other components in the fraction. If we assume that the cluster belongs to the major protein component (which we assume to be A3a), it can be concluded that the cluster content is very low. From the double integral of the EPR signal and the protein concentration of the sample, it was estimated that about 5% of the protein contained an intact cluster. This might be the reason that it does not function properly in the activation assay. Of course we cannot exclude that the iron-sulfur cluster belongs to another protein in the crude protein fraction.
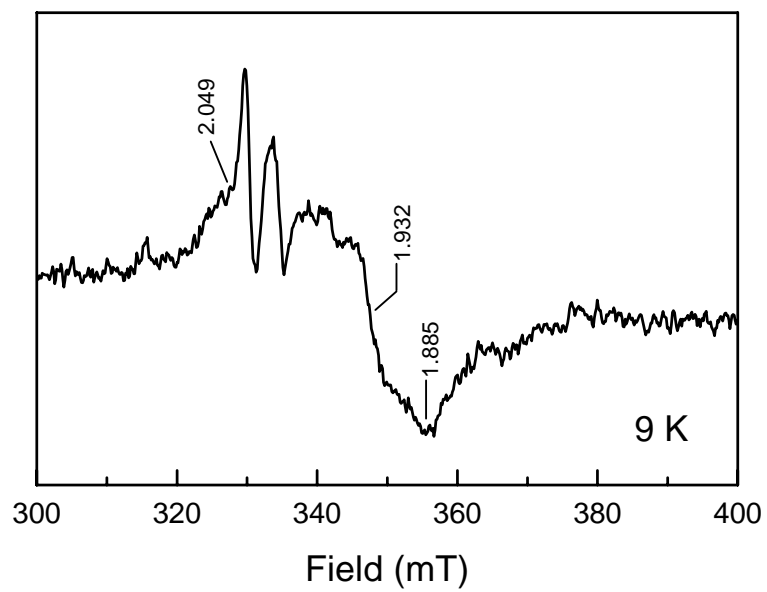
Figure 2.13. EPR spectra of purified A3a after reduction with dithionite.

2.3.7 Activation Assay with Cluster-reconstituted Fractions

Based on the estimated low cluster content it can be hypothesized that the A3a protein might need a full cluster content to function properly in the activation assay. Therefore, we attempted to reconstitute the cluster by incubating the protein fractions for three hours in the presence of Na_2S, $FeCl_3$, and dithiothreitol. The reconstituted samples were directly used in the activation assay. Removal of salt and other compounds by running the samples over a desalting column might remove the cluster too. This also prevented the confirmation of cluster reconstitution by EPR spectroscopy. It should be noted, however, that this method was used successfully in reconstituting the 4Fe cluster in the YfgB protein studied in our laboratory. The cluster reconstitution procedures were applied to each of the pooled fractions from the Sephacryl chromatography step and the Phenyl-sepharose chromatography step for a complete set of data. The simplified reconstitution system driven by Ti (III) citrate was used to test for A3a presence after the cluster-reconstitution. The method setup was the same as before. The reaction was started by incubation the samples at 60 °C for 40 min. A 0.1-ml sample of the gas phase was taken and injected into the gas chromatograph fitted with an FID. The methane peak area was measured and the rate of CH_4 formation was calculated. Table 2.2 gives an overview of the data obtained for all the samples. No significant increased levels of methane were detected.

Table 2.2 (a)

Vial No	Fraction	MCR (heat)	A_2	CH_4 (nmol/min)	Corrected CH_4 (nmol/min)
1	-	+	-	4.4	-
2	Seph-I*	+	+	6.3	1.9
3	Seph-II*	+	+	12.0	7.6
4	Seph-III*	+	+	26.1	21.7

Table 2.2 (b)

Vial No	Fraction	MCR (ferricyanide)	A_2	CH_4 (nmol/min)	Corrected CH_4 (nmol/min)
1	-	+	-	2.1	-
2	Øseph-I	+	+	2.9	0.8
3	Øseph-II	+	+	2.8	0.7
4	Øseph-III	+	+	2.5	0.4
5	Øseph-I*	+	+	3.1	1.0
6	Øseph-II*	+	+	3.5	1.4
7	Øseph-III*	+	+	3.2	1.1

Table 2.2. Results of the activation assay with Ti(III) citrate as electron donor. Pooled fractions from the different purification steps and reconstituted fractions were assayed. All assays were performed as described in the text. (a): Pooled fractions from the Sephacryl gel filtration chromatography step that underwent the cluster reconstitution procedure (b): Pooled fractions from the Phenyl-Sepharose chromatography step. '✱' indicates the fractions that underwent the cluster-reconstitution procedure.

2. 4 DISCUSSION

The first point that has to be addressed is the use of the A2 component from *Methanothermobacter thermoautotrophicus* in our activity assays. *Methanothermobacter thermoautotrophicus* was first named *Methanobacterium thermoautotrophicum*, after its discovery. Due to the similarities in energy conservation, the same impressive biosynthetic capacity, and similar but limited genetic information, a similar species that was isolated from a waste water treatment facility in Marburg, Germany, was named *Methanobacterium thermoautotrophicum*, strain Marburg. The original species was named strain ΔH. In 1981, the DNA relatedness between the two strains was investigated by DNA-DNA hybridization and it was brought to attention that these two organisms should be classified into two different species due to the relatively low degree of DNA homology. In addition, it was found that the membrane fraction of the ΔH strain exhibited high ATPase activity, which could not be detected in the Marburg strain (*111*). This notion that these strains should be reclassified was supported by the investigation of their genome organizations with more advanced techniques ten years later by which the maps of the chromosomes could be established. The study indicated again that the ΔH and Marburg strains, despite their similarity in phenotype, were genetically heterogeneous (*112*). Thus the proposals to create a new genus for *Methanobacterium thermoautotrophicum* were put forward and were accepted. Now the ΔH and Marburg strains belong to different species, *Methanothermobacter thermoautotrophicus* and *Methanothermobacter marburgensis* respectively.

Comparison of the sequences of MCR from both species shows that these are genetically almost identical. The α-subunits, for example differ only in five amino acids.

92

Although this comparison was not possible for the A2 component (the genome of the *M. marburgensis* is not available) it seems safe to assume that the A2 proteins from both species are very similar. Despite the fact that we did not detect activation of MCR we assume that this is not due to the use of the A2 protein from a different species.

For MCR from *M. thermoautotrophicus*, only low amounts of activation (2-5%) were obtained with the simplified three-component system containing A2, A3a and Ti(III) citrate. Our goal was to reproduce the simplified three-component system in *M. marburgensis* and further improve the activation rate by the full purification of component A3a. In addition, the inhibitory effect of coenzyme B would be tested. The purification procedure was a challenging and difficult process that involved not only cross-testing different fractions in the enzymatic assay but also stabilization of each component in an active state so that meaningful assays could be performed. In our study, It has been shown that with at least 90% pure A2 and perhaps 70% pure A3a we were not able to generate active MCRred1 from MCRsilent. The assay with reconstituted A3a also did not show increased activity either.

Component A2 was purified to 90% purity. According to the amino acid sequence analysis, it has two ATP-binding domains and is postulated to be a provider of ATP in the activation assay (*34*). The A2 component was expressed in *E. coli*. with a six-histidine tag on its C-terminus, which greatly facilitated the purification through affinity chromatography on a nickel chelate column. From SDS-PAGE the purity of the A2 protein was estimated to be at least 90% (Figure 2.6). With the introduction of histidine tags to the N-terminal or C-terminal of proteins, many fusion enzymes are functionally as active as the natural types. However, some tagged ones reveal lower

activities due to the formation of insoluble inclusion bodies or soluble, but presumably misfolded conformations when expressed in *E. coli.* (*113-116*). This might explain the instability of the A2 protein and could be one of the reasons why the activation of MCR did not work. In future work, an A2 protein without a histidine tag could be purified by affinity chromatography using an ATP-agarose column or a dye-ligand column. This protein has to be tested in the activation assay as described above.

In the first stage, the potential A3a-protein-containing fractions were tested as such and no significant activity was observed after the phenyl sepharose column step (not shown). Further characterization of the three main peaks (pooled fractions I, II and III) showed that fraction ØSephII, contained a protein with a size of approximately 500 kDa and a purity of 70% (Figure 2.12). A spectrum was detected for this sample in EPR spectroscopy that was characteristic for a $[4Fe-4S]^{+/2+}$ cluster (Figure 2.10). Due to the low amount of detectable cluster in comparison with the total protein content we proposed that the 500 kDa protein was the A3a protein and that the iron-sulfur cluster was only partially present and needed to be reconstituted. There is an equal chance, however, that the cluster belonged to a different protein with a much lower concentration. Unfortunately, even after cluster-reconstitution of variant fractions, the amount of methane formed in the activation assays was still negligible (Table 2.2).

It has been proposed that A3a was the likely site for ATP hydrolysis. There is also a study that showed upon the addition of Mg^{2+}/ATP and CH_3-S-CoM to cell extracts of *M. thermoautotrophicus*, a shift in *g*-value of an iron-sulfur center was detected. However it was not clear if the effect was a consequence of activation by ATP since ATP and

CH$_3$-S-CoM were not studied independently (*35, 117*). We tested the effect of ATP on reduced A3a and no change in the EPR signal was detected (data not shown).

2. 5 CONCLUSION

To study the activation of MCRsilent in *M. marburgensis*, we mimicked the reconstitution system characterized in *M. thermoautotrophicus*. There is a minimum of two required components, A2 and A3a. In the presence of these components and the reductant Ti(III) citrate, MCR from *M. thermoautotrophicus* was activated, however, only 2-5% activation was detected in comparison with the *in vivo* specific activity of MCR. MCRsilent and component A2 were purified to high purity. The presence of A3a in crude fractions should lead to complementation of the activation system but no significant activation was detected. Following a purification method from the literature we purified a protein to 70% purity that we assume was the A3a component. This protein may contain low level (< 5%) of an iron-sulfur cluster. Attempts to increase the cluster content of the A3a protein did not result in higher activation levels of MCR. There are several possible explanations for the absence of any activation of MCR. Firstly, the A2 and A3a proteins might not be sufficient for MCRsilent activation and an additional component is still missing. Due to the very low activation in *M. thermoautotrophicus* it is also possible that they are not true activating components of MCR, but the effect is due to a side reaction. Alternatively, the his$_6$-tag on the A2 protein might be interfering with either ATP-binding or ATP transfer. It is also possible that the A2 protein from *M. thermoautotrophicus* is not able to interact with the A3a protein from *M. marburgenis*.

CHAPTER THREE

SPECTROSCOPIC STUDIES ON A NICKEL-METHYL SPECIES FORMED IN

METHYL-COENZYME M REDUCTASE

3．1 INTRODUCTION

It has been elaborated on in previous chapters that Methyl-coenzyme M reductase

(MCR) catalyzes the reaction of methyl-coenzyme M (CH_3-S-CoM) and coenzyme B

(HS-CoB) to form methane (CH_4) and the heterodisulfide of coenzyme M and coenzyme

B (CoM-S-S-CoB), which is the important final step in methanogenesis. Overproduction

of methane is not good for the global climate and environment because methane is a

significant green-house gas that escapes to the atmosphere as a result of human activities.

We are interested in elucidating a practical way to control this methane formation and the

development of a novel class of F_{430}-based biocatalysts to catalyze methane activation,

which would be of great interest for the petrochemical industry. These topics continue to

attract world-wide attention in academic circles. Investigation of the mechanism of MCR

and the components involved in MCR activation would be the first items on the 'to do

list'. In this chapter, we present a possible intermediate in the reaction cycle. Currently

there are two hypothetical reaction mechanisms that differ in essential steps that have

been proposed for MCR. A schematic overview of both models is presented in Figure.3.1.
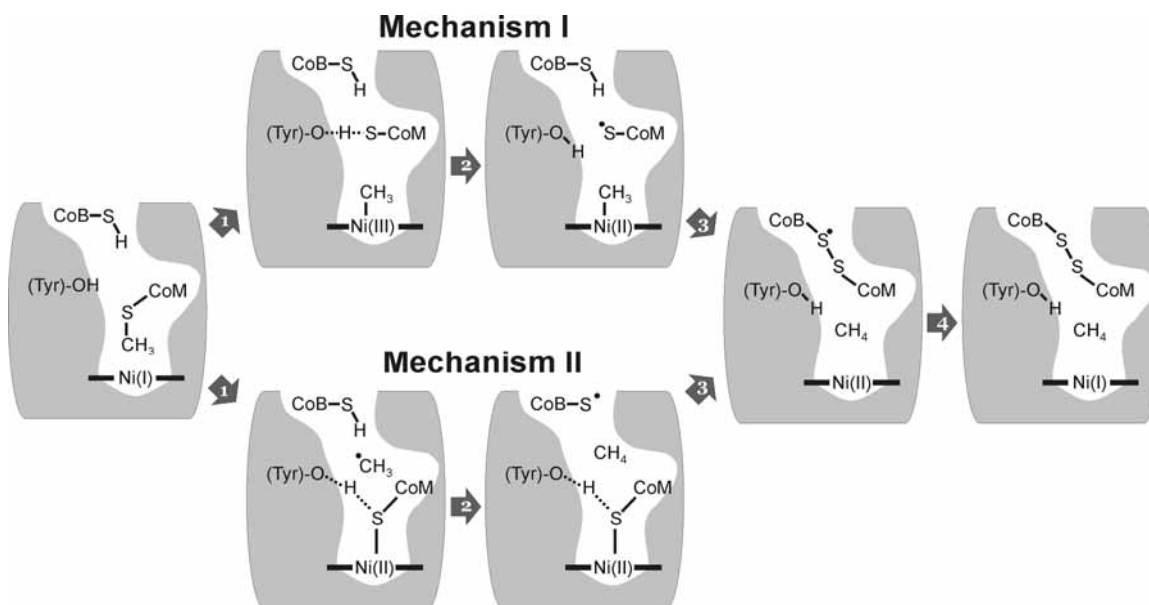
Figure 3.1. Schematic overview of the two hypothetical reaction mechanisms for methane formation by MCR (see text for details).

In the first model, the key intermediate is a nickel-methyl species, CH_3-Ni(III)-F_{430}, generated by the attack of the Ni(I) from MCRred1 on the methyl group in the first step of the mechanism. The highly reactive CH_3-Ni(III)-F_{430} species immediately oxidizes coenzyme M (HS-CoM) forming a coenzyme M thiyl radical and CH_3-Ni(II)-F_{430}. In the next step the thiyl species reacts with coenzyme B forming a heterodisulfide anion radical. At the same time, protonation of the nickel-methyl species results in the formation of CH_4 and Ni(II)-F_{430}. Subsequently the Ni(II)-F_{430} is reduced back to Ni(I)-F_{430} by the heterodisulfide anion radical. With respect to model II, the key difference from model I is the attack of Ni(I) at the thioether sulfur instead of the methyl group of methyl-coenzyme M in the first step, yielding a Ni(II)-thiolate and a methyl radical. Unfortunately no direct evidence is available regarding the reaction mechanism. Therefore substrate analogs and inhibitors have been used and it was found that a nickel-thiol bond can be formed with coenzyme M with the nickel in the 1+, 2+, 3+ states (*17, 21, 27, 29, 46*). Up to now, a nickel-methyl species has only been observed in free Ni(I)-F_{430}M (penta methylated form of F_{430}). The formation of a nickel-alkyl species in MCR was first observed between the nickel (formally 3+) and 3-bromopropane sulfonate (BPS), a potent inhibitor of MCR (*40*) and similar results were observed using bromo-alkyl sulfonate compounds with longer carbon chains (*118*). In this chapter, we show the observation and spectroscopic studies of a nickel-methyl species formed when active MCRred1 was incubated with bromomethane (BrMe). The new species is therefore dubbed: MCR_{BrMe}. The formation of this species is of great significance since it will help with the detection of such a species in the reaction cycle.

Related to this is the intriguing discovery of high concentrations of MCR in methanotrophic archaea, which strongly implies that this enzyme catalyzes the first step in the anaerobic oxidation of methane (AOM) by working in the reverse direction (*16*). Here we show that the incubation of the nickel-methyl species with the substrate analog coenzyme M results in conversion into methyl-coenzyme M, a first look inside a possible reversal of the methane production mechanism.

3．2 MATERIALS AND METHODS

3.2.1 Biochemical and Chemical Reagents

Tris base, Taps, sodium dithionite, potassium permanganate, ammonium acetate, methyl iodide, and ^{13}C-labled bromomethane and coenzyme were purchased from Sigma-Aldrich (St. Louis, MO). Potassium phosphate (monobasic anhydrous and dibasic anhydrous), 2-propanol, absolute ethanol, glycerol, magnesium sulfate, magnesium chloride, ammonium chloride, sodium chloride, and ammonium sulfate were from Fisher Biotech (Pittsburgh, PA). Q-sepharose, and PD-10 columns were purchased from Amersham Biosciences (Piscataway, NJ). Centricon ultrafiltration units were from Millipore (Bedford, MA).

Standard anaerobic buffers were used for all purifications and experiments. The buffers were filtered (0.22 μm) and subsequently boiled under nitrogen gas flow. They were stirred under vacuum for a period of 1-2 h. The buffers could then be used or stored under nitrogen with 0.3 atmospheric overpressure applied to the head space of the bottle.

3.2.2 Purification of MCR in the Red1 State

M. marburgensis cells were grown as described in section **2.2.5**, using 80% H_2/20% CO_2/0.1% H_2S as a growth gas. The gas phase was switched to 100% H_2 for a period of 30 min before harvesting to induce the MCRred1 and MCRred2 forms in the cells. The cells were cooled over a 10 min period to 10 °C under continuous gas flow and were then harvested anaerobically by centrifugation using a flow-through centrifuge (Hettich, contifuge 17 RS). Approximately 50 g of wet cells were obtained. All the

following steps were performed in an anaerobic chamber (Coy Instruments) filled with 95% N_2/5% H_2, as described in section **2.2.5**.

MCRred1 was purified from 100% H_2 gassed cells in the presence of 10 mM coenzyme M (*24*). The MCRred2 signal was lost during purification due to removal of coenzyme B. This method generally yielded 150 mg MCRred1c (in 120 ml) with 0.5–0.9 spins per nickel (red1*c* indicates red1 state with *c*oenzyme M present). The specific activity of the purified enzyme was 10–30 U per mg protein calculated for one spin per mol F_{430} (*24*). Methyl-coenzyme M reductase activity was determined as previously described (*24*).

3.2.3   Preparation of MCR_{BrMe} Samples

For this experiment, the coenzyme M was removed from the sample by extensive washing with 50 mM Tris/HCl pH 7.6 by ultrafiltration with an Amicon Ultra Centrifugal Filter Device with a 100 kDa cut off (Millipore). MCRred1 was incubated with increasing amounts of BrMe (added as a saturated solution of 14 mg/ml at 25ºC in 50 mM Tris/HCl pH 7.6). Conversion of the MCRred1 signal into the MCR_{BrMe} signal could be followed in either absorption spectroscopy or EPR spectroscopy. An MCR_{BrMe} sample was prepared for ENDOR measurements by incubation of 0.8 mM MCR in 50 mM Tris/HCl pH 7.6 with a 50 fold excess of BrMe.

3.2.4   EPR Experiment

The continuous wave EPR experiments in our lab were carried out as described in section **2.2.12**. The pulse EPR experiments were carried out in the laboratory of Dr.

Jeffrey Harmer at X-band (9.73 GHz) and W-band (94.234 GHz) on a Bruker E680 spectrometer equipped with a helium gas-flow cryostat from Oxford Inc. The W-band (94.234 GHz) echo-detected EPR spectra were measured at 25 K by integrating over the echoes created with the mw pulse sequence $\pi/2$-τ-π-τ-echo, with mw pulse lenths $t_{\pi/2} = 32$ ns, $t_{\pi} = 64$ ns, and an inter-pulse delay of $\tau = 300$ ns, 400 ns, and 500 ns. The first derivative of this spectrum was calculated numerically. The field was calibrated using the two central lines from a CaO sample containing manganese ions.

3.2.5   Pulse ENDOR and HYSCORE Experiment

In addition to EPR spectroscopy, pulse electron nuclear double resonance (ENDOR) and hyperfine sublevel correlation (HYSCORE) spectroscopy were applied to characterize the electronic and geometric structure of MCR_{BrMe} in detail (*119*). The X-band Davies-ENDOR spectra were measured at 25 K with the mw pulse sequence π-T-$\pi/2$-τ-π-τ-echo, with mw pulses of lenth $t_{\pi/2} = 28$ ns and $t_{\pi} = 56$ ns, and a $\tau = 142$ns. A radio-frequency pulse of length 4 µs and variable frequency ν_{ENDOR} was applied during time T. The Q-band (34.76 GHz) Davies-ENDOR spectra were measured on a home-built spectrometer in the Harmer Laboratory at 20 K with the mw pulse sequence π-T-$\pi/2$-τ-π-τ-echo, with mw pulses of length $t_{\pi/2} = 32$ ns and $t_{\pi} = 64$ ns, and a $\tau = 200$ ns. A radio-frequency pulse of length 9 µs and variable frequency ν_{ENDOR} was applied during time T. HYSCORE experiments employed the pulse sequence $\pi/2$-τ-$\pi/2$-t_1-π-t_2-$\pi/2$-τ-echo. Measurements were made at 25 K using the following parameters: mw pulses of lengths $t_{\pi/2} = t_{\pi} = 16$ ns, starting times 96 ns for t_1 and t_2, and

time increments Δt = 16 ns (data matrix 256 × 256), and a τ = 132 ns. An eight-step phase cycle was used to remove unwanted echoes. The HYSCORE data were processed with MATLAB 7.0 (The MathWorks, Inc.). The time traces were baseline corrected with an exponential, apodized with a Gaussian window and zero filled. After a two-dimensional Fourier transformation absolute-value spectra were calculated. The EPR and Davies-ENDOR spectra were simulated with the program EasySpin (*120*) and the HYSCORE spectra with a program written in-house (J. Harmer) (*121*). The orientation selection of all the X-band spectra, needed to simulated the ENDOR and HYSCORE spectra, was calculated with the g-values given and a Gaussian linewidth of 150 MHz (this simplified spin Hamiltonian accurately describes the shape of the X-band CW EPR spectrum).

3.2.6   HYEND Experiment

The HYEND (hyperfine correlated ENDOR) experiment correlates ENDOR frequencies with their corresponding hyperfine couplings. The pulse sequence is shown in Scheme 3.1. The nuclear frequency dimension is obtained by varying the frequency of the two selective $\pi/2$ r.f. pulses, and the hyperfine dimension by the FT of the echo modulations recorded as a function of the time T. The states attained during the experiment for an S = ½, I = ½ spin system are shown in Scheme S1. The experiment is easily understood qualitatively. We assume that the first m.w. pulse is on resonance with the allowed EPR transition (1, 3) and the r.f. pulse has the frequency ω_α and is thus resonant with the nuclear transition (1, 2). The first m.w. pulse inverts the polarization of transition (1, 3), and the selective r.f. pulse transfers the polarization of transition (1, 2) to
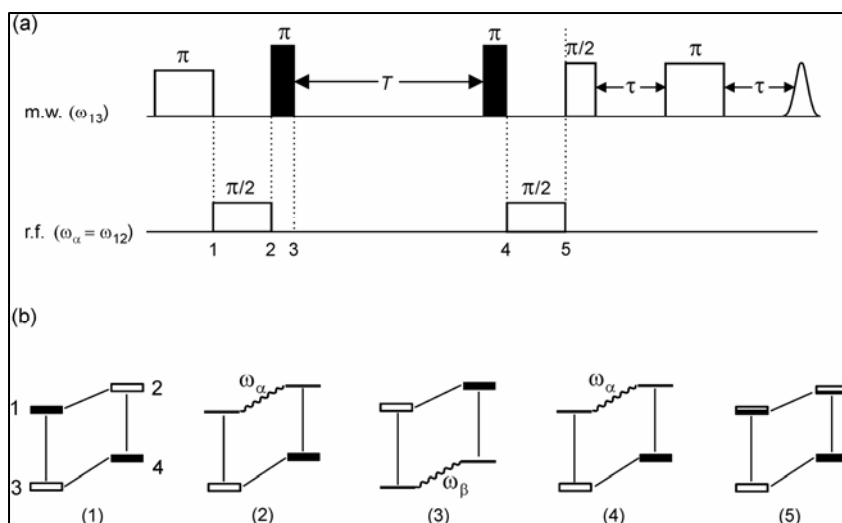
Scheme 3.1. HYEND experiment. (a) Pulse sequence. (b) Four level energy diagrams for an $S = \frac{1}{2}$, $I = \frac{1}{2}$ spin system illustrating the different states obtained during the experiment.

nuclear coherence (wavy line). This coherence is immediately transferred by a non -selective m.w. π pulse to the β electron spin manifold, where it evolves with the nuclear frequency ω_β for a time T. The second non-selective m.w. π pulse transfer the nuclear coherence back to the α manifold, where the second r.f. pulse transfers the nuclear coherence back to electron polarization, which is detected with the m.w. primary echo sequence. The two r.f. pulses must remain coherent during the sequence, and then the polarization created by the second r.f. pulse is dependent upon the phase accumulated by the nuclear coherence during the time T in the β manifold with respect to the phase of the r.f field. This phase is given by $(\omega_\alpha + \omega_\beta) T$ (weak coupling) or $(\omega_\alpha - \omega_\beta) T$ (strong coupling). The HYEND signal as a function of T, for an isotropic hyperfine interaction with the r.f. pulses resonant with a nuclear transition, is given by $V_{\alpha/\beta}(T) = \pm sign\ (2\omega_I + A)\cos(\omega_- T)$ with $\omega_- = \omega_\alpha - \omega_\beta = A_S$. HYEND (*122*) experiments were carried out by using the pulse sequence π-$\pi/2_{rf}$-π_t-T-π_t-$\pi/2_{rf}$-$\pi/2$-$\pi/2$-τ-π-echo, with mw pulse lengths of t_π = 40 ns for the preparation pulses, and $t_{\pi t}$ = 16 ns for the coherence transfer pulses. A selective radio frequency pulse $(\pi/2_{rf})$ of length 2 μs and variable frequency was applied with a four-step phase cycle of the radio frequency pulse [(x,x)-(-x,x)-(x,-x)-(-x,-x)]. Time T was varied with a starting time T_0 = 100 ns and an increment of ΔT = 12 ns. Fourier transformation along this dimension gives the hyperfine axis $\nu_{HYPERFINE}$.

3.2.7   UV-visible Spectroscopy

UV-vis spectra were recorded on a HP-8453 or HP-8452 diode-array spectrophotometer equipped with 1 cm cells and a Brinkman Lauda RM6 thermostated

water bath to maintain the temperature at $25.0 \pm 0.1\ ^\circ$C. A concentration of approximately 20 μM MCRred1 was used in the experiments.

3.2.8   NMR Spectroscopy

^{1}H NMR spectra were applied to identify the product of the reaction. ^{1}H NMR spectra were obtained on a multi-pulse Bruker AV 400 spectrometer.

3. 3 RESULTS

3.3.1 EPR Studies of the Nickel-methyl Species

Figure 3.2 shows CW EPR recorded at W-band for the sample preparation MCRred1a, MCR$_{BrMe}$ and simulation, and simulations using known g values for MCRox1 (*123*) , and MCR$_{BPS}$ (*40*). The impurity marked with '+' in the BrMe spectrum, which has g-values of 2.130, 2.139, and 2.224, amounts to c.a. 2% of the signal, and is an ox3 species (*21*). The figure shows that upon addition of either BPS or BrMe there is a significant change in the g values in comparison to MCRred1. The g values of the different species can be found in Table 3.1. The W-band spectra were recorded by Dr. Jeffrey Harmer.

The dependence of conversion of the MCRred1 signal into the MCR$_{BrMe}$ signal on the BrMe concentration was studied by titrating MCR in the MCRred1 form with increasing amounts of BrMe (added as a saturated solution in 50 mM Tris-HCl, pH 7.6). For each BrMe concentration an EPR sample was prepared by freezing the enzyme solution in an EPR tube in liquid nitrogen after 1 min of incubation time. Figure 3.3 shows the results of the titration. MCRred1 used was 0.1 mM. With increasing concentration of BrMe more MCRred1 was converted into a new EPR signal, MCR$_{BrMe}$. Figure 3.4 shows the increase of the signal intensity of the MCR$_{BrMe}$ EPR signal as a function of the BrMe concentration. A 50% conversion from MCRred1 to MCR$_{BrMe}$ was achieved at a concentration of 8mM BrMe.
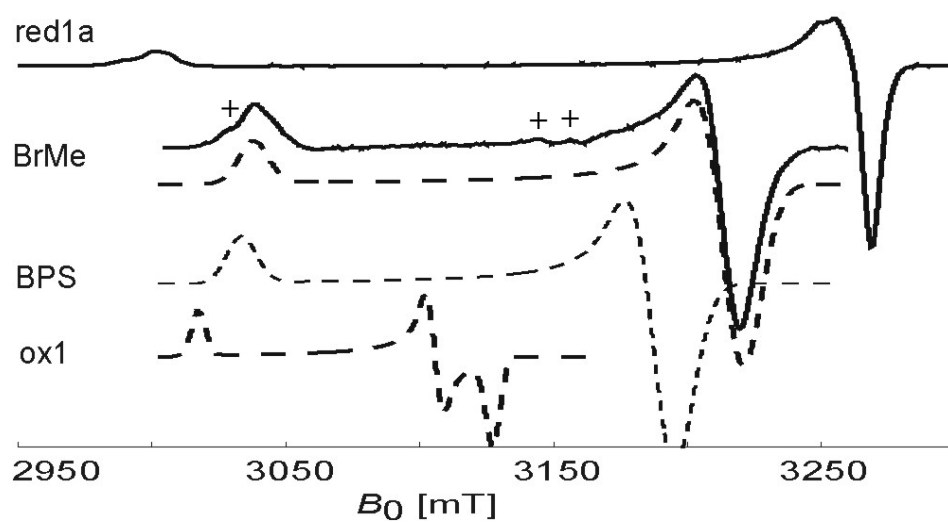
Figure 3.2. W-band (94.234 GHz) EPR spectra for the species: (a) MCR_{red1a}, (b) MCR_{BrMe} and simulation (dotted line), and simulations for using known g-values determined at W-band for (c) MCR_{ox1} and (d) MCR_{BPS}. The impurity marked with + in the BrMe spectrum is an ox3 species. Figure prepared by Dr. Jeffrey Harmer.

Complex	g_1	g_2	g_3
MCRred1a	2.061	2.070	2.250
MCRox1	2.153	2.168	2.231
MCR$_{BPS}$	2.108	2.112	2.219
MCR$_{BrMe}$	2.093	2.093	2.216

Table 3.1. *g*-values for MCR$_{BrMe}$ and several relevant MCR species.
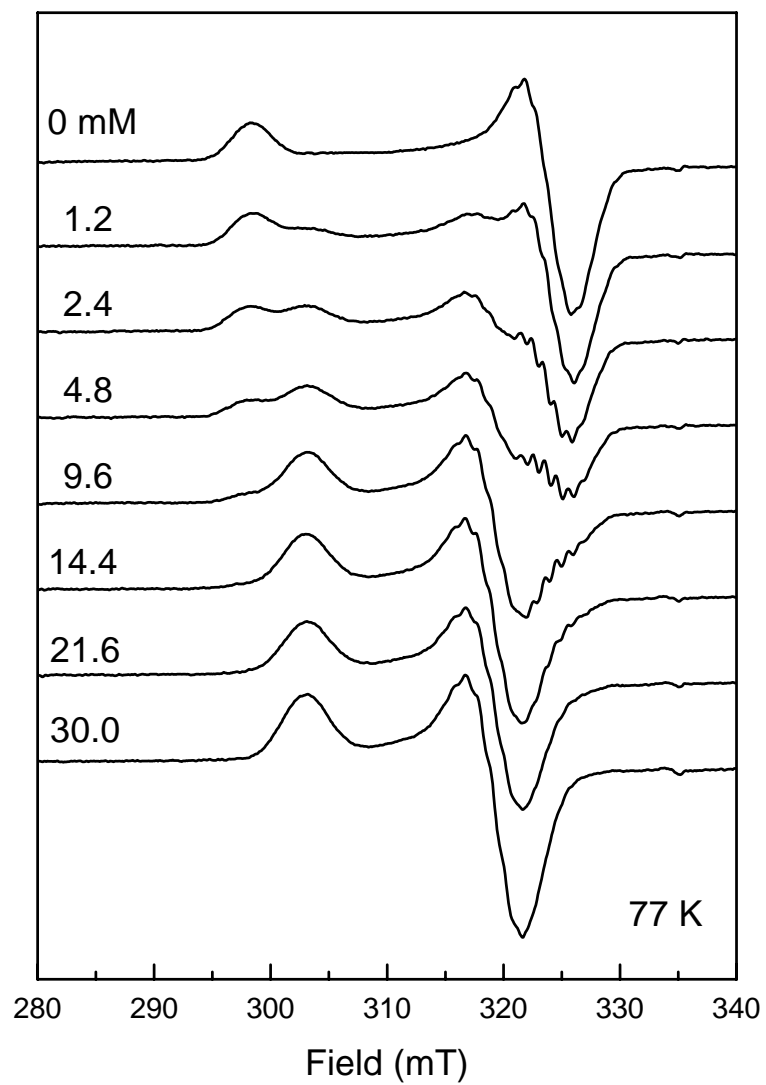
Figure 3.3. EPR spectra following the BrMe-dependent conversion of MCRred1 into MCR_BrMe.
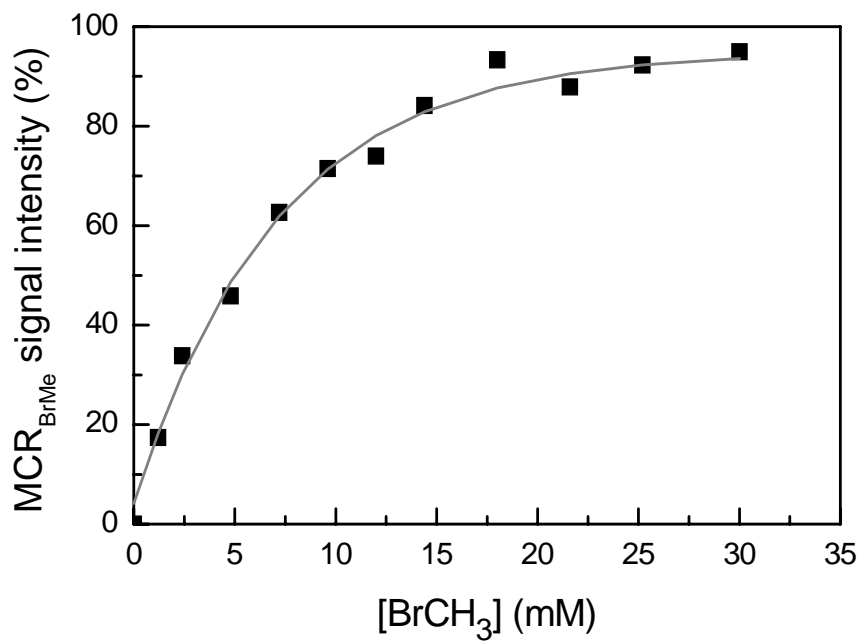
Figure 3.4. Titration curve showing the increase of the intensity of the MCR_{BrMe} EPR signal as a function of the BrMe concentration.

3.3.2 Stability Study of the Nickel-methyl Species

The formed MCR_{BrMe} signal is relatively unstable compared with the MCR_{BPS} signal which has a half-life of ~8 h at pH 7.6 under anaerobic conditions (*118*). MCR_{BrMe} decays with a half-life of ~20 min at pH 7.6 (Figure 3.5). UV-visible absorption was applied *in situ* to monitor the stability in parallel to the EPR study. The UV-visible absorption spectra of MCR_{BrMe} resemble the spectra of MCR_{BPS}, MCRsilent and MCRox1 with a maximal absorbance at 423nm while the MCRred1 form has a maximal absorbance at 388 nm and a weaker broad band at 715nm (Figure 3.6). Both studies show that the most of the MCR_{BrMe} signal decayed to a MCRsilent form after 45 min.

To see if the pH had an influence on the signal stability, the experiment was repeated at pH 9.0 and similar result were obtained (data not shown). To test if the excess BrMe would react with the nickel-methyl species, excess BrMe was removed by addition of KCN. No change in stability was observed (data not shown). When the experiments were performed in stoppered bottles, examination of samples of the gas phase using a gas chromatograph did not indicate the presence of ethane. 1% and 0.5% samples of ethane in N_2 were used as standards for both elution time and peak intensity.
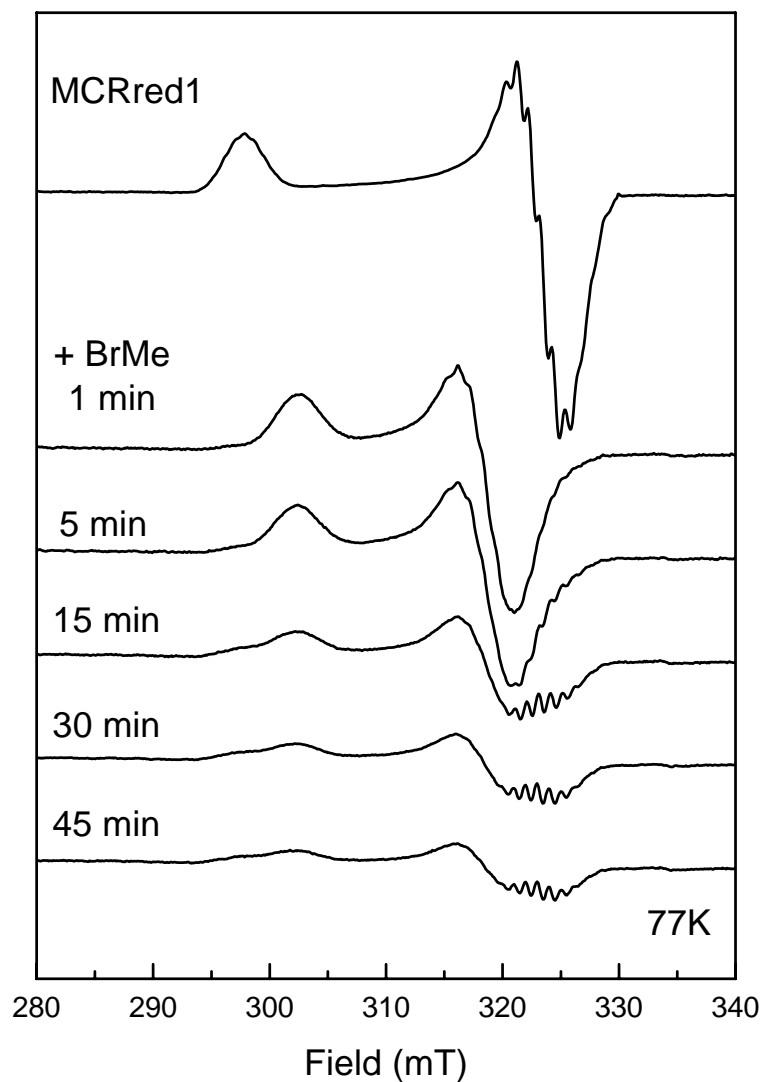
Figure 3.5. EPR spectra, following the conversion of the MCRred1 signal into the MCR$_{BrMe}$ signal and the subsequent decrease of the MCR$_{BrMe}$ signal over time. The BrMe concentration was 5 mM, The MCR concentration was 20 μM, and no coenzyme M was present. Buffer: 50 mM TrisHCl, pH 7.6.

113
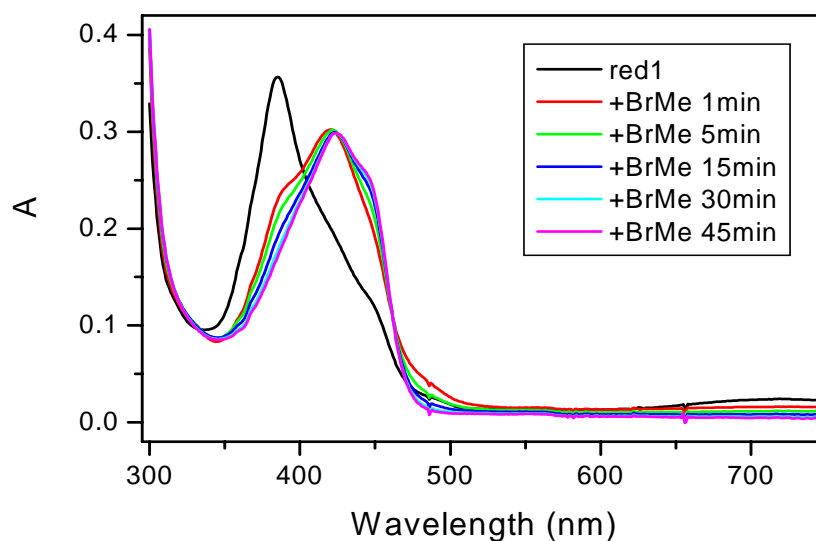
Figure 3.6. UV-visible spectra, following the conversion of the MCRred1 signal into the MCR$_{BrMe}$ signal and the subsequent decrease of the MCR$_{BrMe}$ signal over time. The BrMe concentration was 5 mM. The MCR concentration was 20 μM. No coenzyme M was present. Buffer: 50 mM TrisHCl, pH 7.6.

3.3.3 ENDOR Evidence for the Formation of the Nickel-methyl Species

The detailed electronic and geometric structure of MCR_{BrMe} was characterized by Dr. Jeffrey Harmer using ENDOR and HYSCORE spectroscopy with the help of isotopic labeling of the BrMe with ^{13}C. An X-band Davies ENDOR spectrum recorded at g_3 is shown in Figure 3.7, together with the simulations for ^{1}H and ^{14}N signals, and a ^{13}C signal with the two carbon peaks being given by $\nu_{rf} \sim \left| A_3/2 \pm \nu_{13C} \right|$, where $A_3 = 44$ MHz and $\nu_{13C} = 3.3$ MHz. The nitrogen signals in Fig. 3.7 are assigned to the four pyrrole nitrogens of F_{430} with hyperfine couplings in the range c.a. 25-35 MHz which are typical values for F_{430} when the unpaired electron is in a nickel orbital with a high d_{x2-y2} character. Figure 3.8 gives the X-band Davies ENDOR spectra measured at 25 K at different field positions with a short π pulse to attenuate small couplings signals from protons.

A HYEND experiment which correlates ENDOR frequencies ν_{rf} directly against their hyperfine couplings $\nu_{hyperfine}$ was recorded at $g_{1,2}$ as shown in Figure 3.9 (*119*). In this plot the ^{13}C signals are resolved from proton signals and the nitrogen signals that are suppressed below detection. This allows the ^{13}C hyperfine couplings to be read directly from the graph, $A_{1/2} = 18$ MHz. These data are supported by X-band HYSCORE measurements (figure not shown). From these spectra, the large ^{13}C hyperfine coupling indicates unambiguously that the methyl group from BrMe is directly coordinated to the nickel ion.

Furthermore, it is expected that the three proton hyperfine couplings of the coordinated methyl group should have large anisotropic hyperfine couplings as they are close to spin density, which is supported by the data from Q-band Davies ENDOR

115

spectra (Figure 3.10) and X-band HYSCORE spectra measured at the proton region (Figure not shown). They both feature proton ridges that could be simulated with hyperfine couplings that range from -6 to +13 MHz (Table 3.2) and the hyperfine orientation of methyl carbon and one methyl proton is described in Figure 3.11.
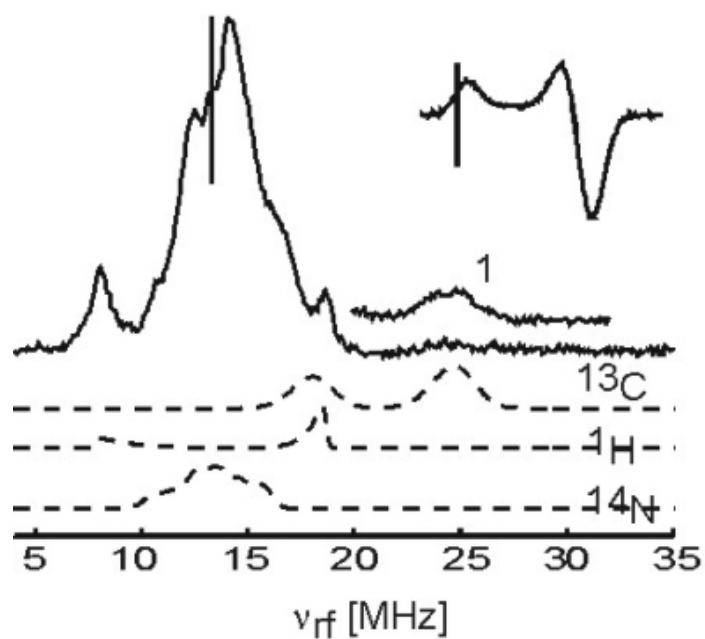
Figure 3.7 X-band Davies ENDOR spectrum measured at g_3 field position (see inset for low field end). Dotted lines indicate simulations for the methyl ^{13}C, ^{1}H and pyrrole ^{14}N nuclei. "**1**" shows the measurement of the high frequency feature of the ^{13}C signal with a higher S/N. Figure prepared by Dr. Jeffrey Harmer.
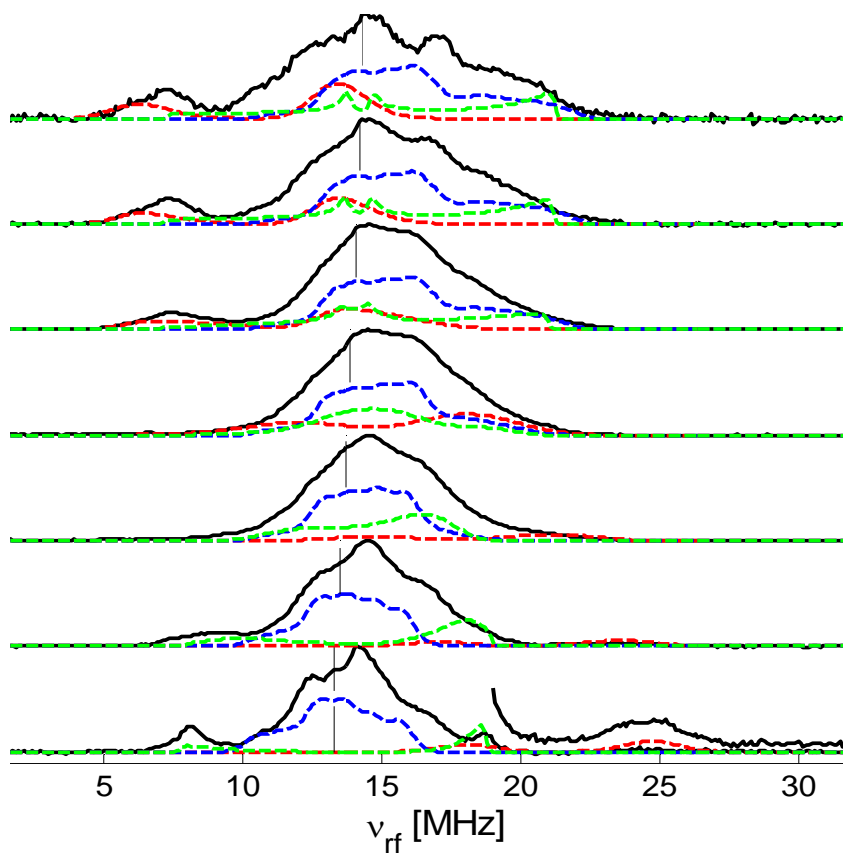
Figure 3.8. X-band (9.726 GHz) Davies ENDOR spectra measured at 25 K with a short π pulse of length 56 ns to attenuate signals from protons with small couplings. Field positions from bottom to top are 312.1, 316.6, 321.1, 325.6, 330.1, 333.6, 335.6 mT. Simulations: green - methyl ^{1}H, red line – methyl ^{13}C, and blue line – pyrrole ^{14}N. Figure prepared by Dr. Jeffrey Harmer.
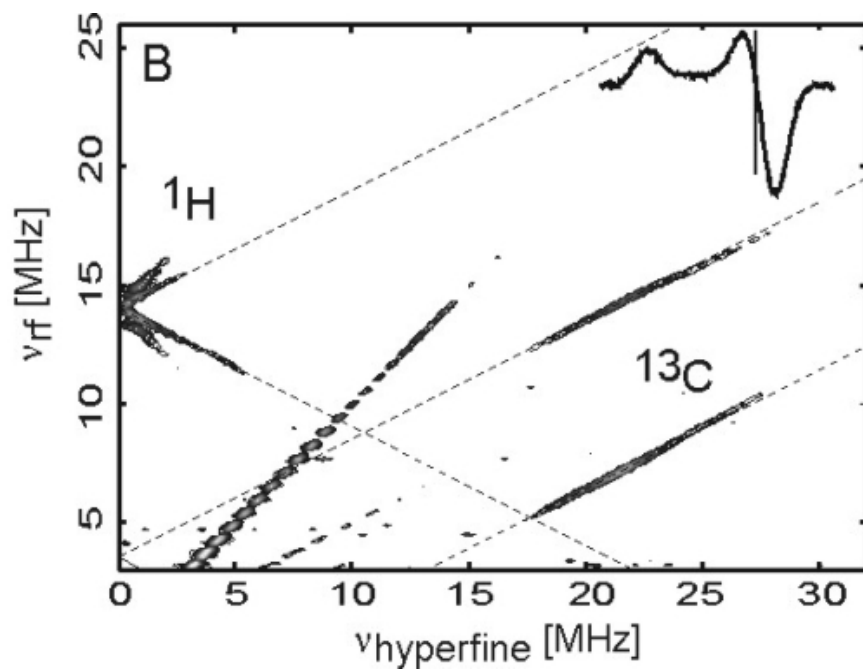
Figure 3.9. X-band HYEND spectrum measured at the field position of $g_{1,2}$ (see inset for high field end). Protons ($A_{max} \sim 7$ MHz) and a strongly coupled ^{13}C nucleus are indicated. Figure prepared by Dr. Jeffrey Harmer.
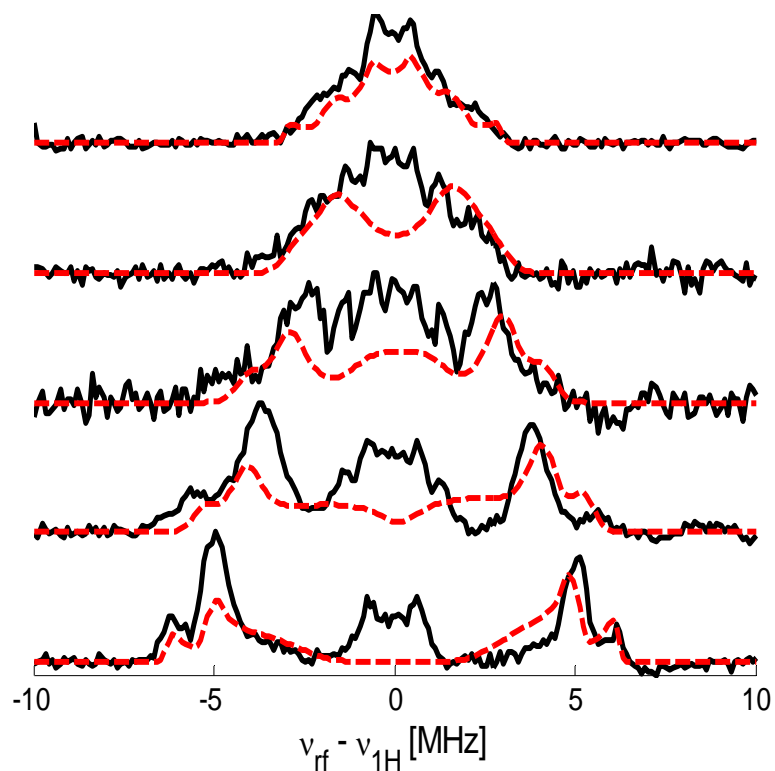
Figure 3.10. Q-band (34.76 GHz) Davies ENDOR spectra measured at 20 K. Solid black line: experimental, red dotted line: simulation. Field positions from bottom to top are 1126 mT, 1140.3 mT, 1154 mT, 1169 mT, 1183 mT. Simulations include the three methyl protons with the EPR parameters given in Table 3.2. Figure prepared by Dr. Jeffrey Harmer.

	g_1	g_2	g_3	g_{iso}
MCR$_{BrMe}$	2.093	2.093	2.216	2.134
	A_1[MHz]	A_2[MHz]	A_3[MHz]	A_{iso}[MHz]
^{13}CMe	18.0±2	-18±2	-44.0±2	-26±2
^{1}HMe	-4.0	3.0	12.5	3.8
	-6.0	1.0	10.5	1.8
	-6.0	1.0	10.0	1.7

Table 3.2 Experimental g-values, methyl^{13}C and ^{1}H hyperfine couplings for MCR$_{BrMe}$. Signs are based on DFT calculations (*124*).
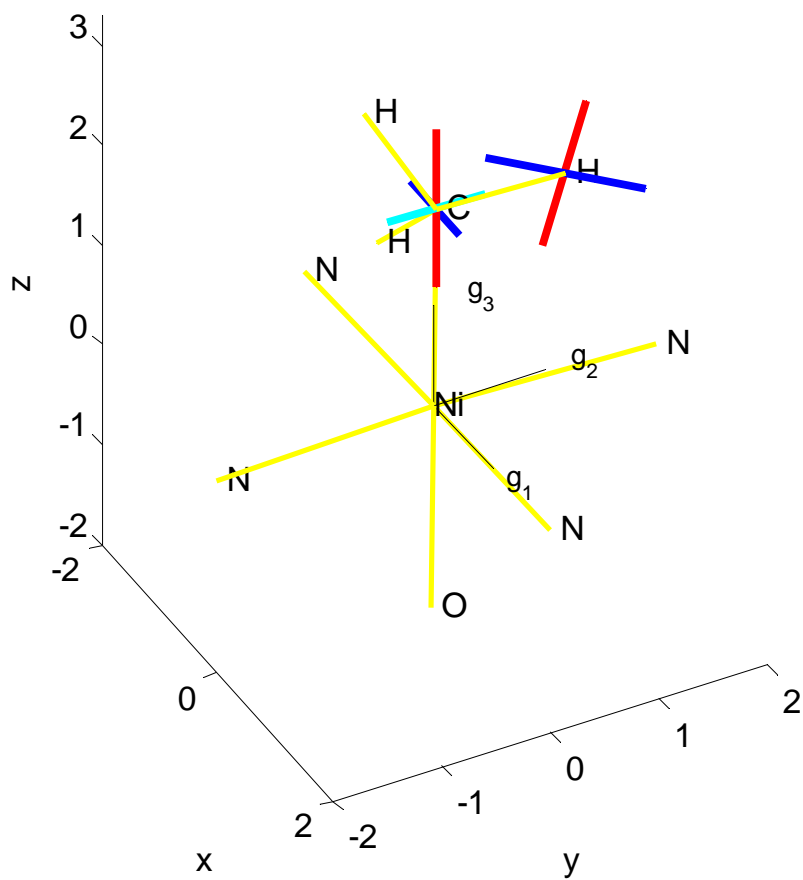
Figure 3.11. Orientation of the hyperfine axes of the methyl carbon and one methyl proton in the *g*-matrix reference frame: axis A_1 – blue, axis A_2 – cyan, axis A_3 – red. Figure prepared by Dr. Jeffrey Harmer.

3.3.4 'Back Reaction' from MCR$_{BrMe}$ to MCRred1

The results demonstrate the formation of nickel methyl species in the MCR active site. Ni(I) of MCRred1 conducts a nucleophilic attack on BrMe to form MCR$_{BrMe}$ and releases bromide. It adds plausibility to proposed mechanism models that proceed via such catalytic intermediates with the natural substrates. Since Ni(III) species are highly oxidative, species like CH$_3$-Ni(III) F$_{430}$ may be crucial for the reverse reaction of MCR, the anaerobic oxidation of methane. It is expected that MCR$_{BrMe}$ could react with HS-CoM to convert MCR$_{BrMe}$ back to MCRred1 and form CH$_3$-S-CoM. EPR spectroscopy was conducted to monitor the conversion. MCRred1 was first washed extensively with 10 mM Taps pH 10.0 by ultrafiltration with Amicon Ultra Centrifugal Filter Units with a 100 kDa cut-off to make sure that all coenzyme M is removed. The MCR$_{BrMe}$ signal was immediately induced by addition of 50 mM BrMe. The MCRred1 EPR signal reappeared in part after addition of 20 mM HS-CoM. At least 50% conversion occurred and the remaining MCR$_{BrMe}$ probably decayed into an MCRsilent form (Figure 3.12).

3.3.5 NMR Evidence for the Formation of Methyl-coenzyme M from MCR$_{BrMe}$

If MCR$_{BrMe}$ is a catalytic intermediate in anaerobic methane oxidation, it should be able to interact with thiolate coenzyme M (HS-CoM) to form methyl-coenzyme M (CH$_3$-S-CoM) which could be identified by NMR. After the MCR$_{BrMe}$ signal was induced, the Ni(III)-CH$_3$ species was incubated with 20mM coenzyme M. An EPR sample was taken to confirm the full conversion of the MCR$_{BrMe}$ signal back into the MCRred1 signal.
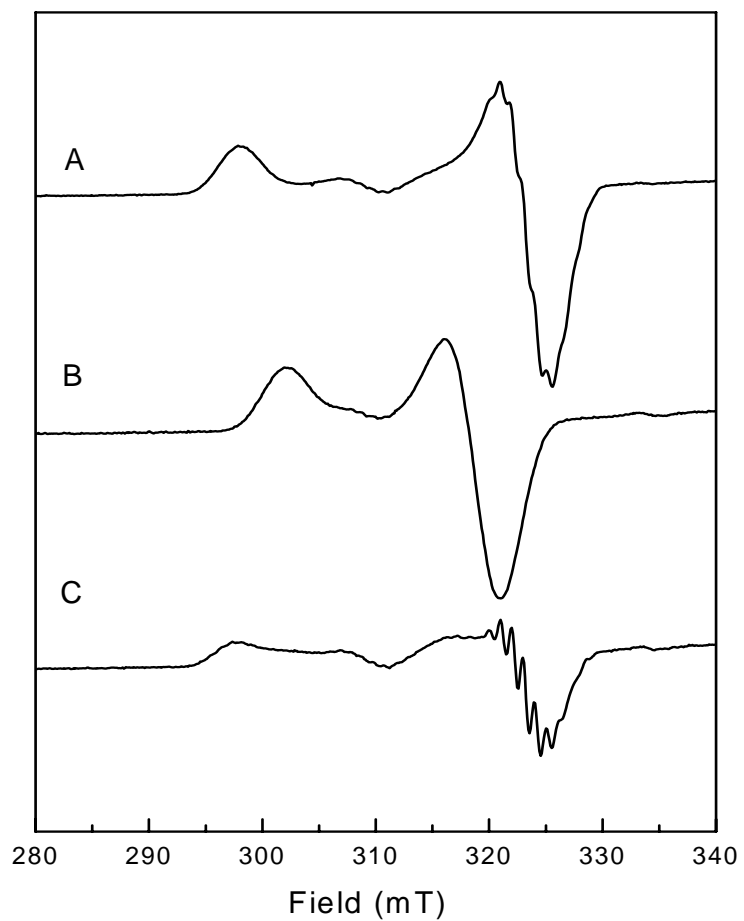
Figure 3.12. EPR spectra of the conversion of MCRred1 (**A**) into MCR$_{BrMe}$ (**B**) with the addition of 50 mM BrMe. The MCR$_{BrMe}$ signal is partly converted back into the MCRred1 form (**C**) by addition of 20 mM coenzyme M.
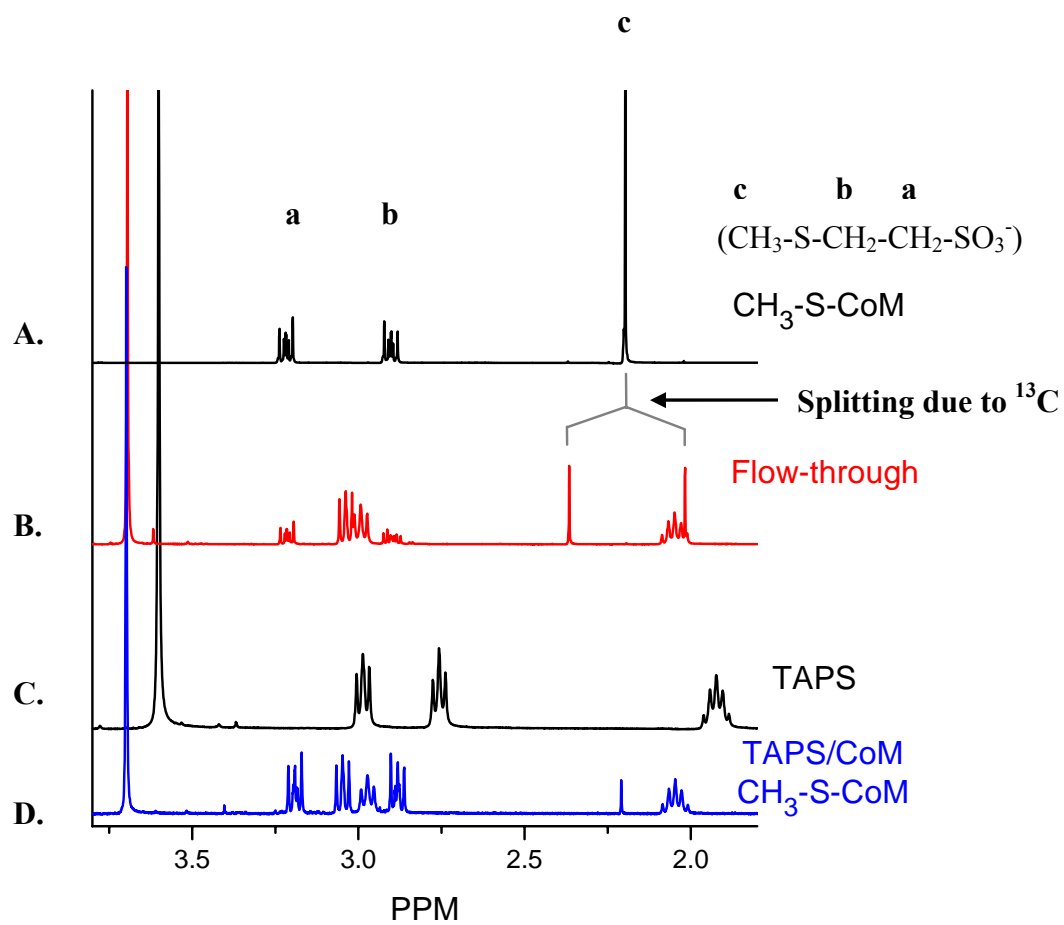
Figure 3.13. ^1H NMR spectra of: A) CH_3-S-CoM, B) the flow-thru sample after back reaction, C) TAPS, D) Mixture of TAPS, HS-CoM and CH_3-S-CoM.

Subsequently the protein solution was concentrated in an Amicon concentration unit using a filter with a 30 kDa cutoff. The flow-through was concentrated, lyophilized and dissolved in D_2O. The NMR spectra of this sample showed the presence of methyl-coenzyme M in the flow-through sample (Figure 3.13). The equal splitting of the methyl proton peak is due to the labeled carbon from BrMe. This is the first evidence for a partial back reaction. It also implies the important role the Ni(III)-CH_3 species could play in the reversible reaction.

3. 4 DISCUSSION

The formation of a nickel-alkyl species in MCR was first proven by reaction of MCR in the Ni(I) F_{430} state with 3-bromopropane sulfonate (BPS), which is a potent inhibitor of MCR with an apparent K_i of 50 nM (*33*). With the help of isotopic labeling of the C-3 carbon of this compound with ^{13}C it was shown that upon incubation with BPS, a bond was formed between the nickel (formally 3+) and the C-3 carbon (*40*). Similar results were obtained with bromo-alkyl sulfonate compounds with longer carbon chains (*118*). When MCRred1 is incubated with BrMe, a new EPR signal designated MCR$_{BrMe}$ with *g*-values of 2.216 and 2.093 is induced. The signal is similar to that of MCR$_{BPS}$ (Figure 3.14). Upon addition of either BPS or BrMe there is a significant change in the *g* values in comparison with MCRred1a (Table 3.1). But for BES (bromoethanesulfate), another inhibitor based on methyl-coenzyme M structure (K_i = 8 μM) (*105*), the reaction quenched the MCRred1 EPR signal (*125*) by oxidizing Ni(I) to Ni(II), as showed in Figure 3.13. The species has been studied by Mi Wang in the Duin laboratory. MCR$_{BPS}$ is described as a Ni(III)-propylsulfonate or a high spin Ni(II) with an alkylsulfonate radical based on EPR studies (*125*). MCR$_{BrMe}$ was assigned as a Ni(III) form because of its close identity to the MCR$_{BPS}$ spectrum (Figure 3.2). This was confonfirmed by DFT calculations (*124*). The undetectable hyperfine splitting from the bromide (I=3/2) of BrMe or BPS displays that the bromide is not close to the paramagnetic center, which strongly indicates the elimination of the bromide before or during the formation of a nickel-methyl species. The bromide formation was confirmed in a specific assay performed by Mi Wang and will be published elsewhere.
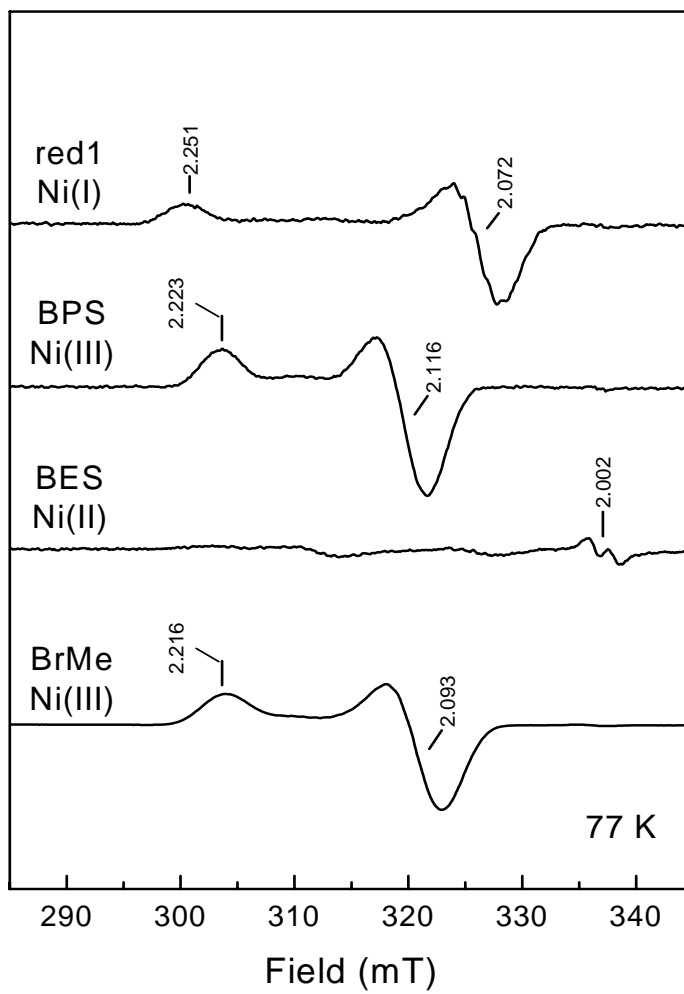
Figure 3.14. EPR spectra for MCR_BrMe compared with MCR_BPS, MCR_BES

To confirm the formation of a Ni(III)-$^{13}CH_3$ species in MCR, ENDOR was applied to detect the hyperfine coupling due to the ^{13}C isotope, and it was proven unambiguously that the methyl group from BrMe is directly coordinated to the nickel ion (*124*).

Complete conversion of the MCRred1 signal into the MCR_{BrMe} signal was achieved by incubation of MCRred1 with approximately 50 fold excess of BrMe in 50 mM Tris-HCl pH 7.6. The formed MCR_{BrMe} signal was not as stable as the MCR_{BPS} signal. The MCR_{BrMe} decayed to an EPR-silent Ni(II) state with a half-life of ~20 min at pH 7.6. It was considered that the instability of the methyl-nickel complex may be due to a homolytic cleavage of the nickel-carbon bond at low pH. The rate of the decay, however, was similar at pH 10.0. Formation of ethane was also not observed, possibly due to the reaction of BrMe with the Ni(III)-CH_3 species. Thus, we concluded that the nickel-methyl species was inherently unstable.

Although a methyl-nickel species has not yet been detected in MCR with native substrate, it has been described that methane is formed from the reaction of Ni(I)-derivatives of $F_{430}M$ and activated methyl donors (*126*). Further, alkyl-Ni(III) species have been shown to undergo reactions to the alkyl-Ni(II) followed by protonolysis to yield alkane (*127*), which resembles the intermediate steps proposed in model I. Our work is the first time that a nickel-methyl species has been observed in MCR. It supports the possible intermediacy of a nickel-methyl species in a hypothetical MCR mechanism. Caution needs to be taken to propose more than that since there is no real connection between this reaction and the physiological mechanism of MCR. Bromomethane and native substrate methyl-coenzyme M are physically and chemically very different. Bromide is an excellent leaving group. Its conjugated acid HBr is a strong

acid with pKa ~9. In contrast to bromide, either the methyl group (CH_3^-) or the mercaptoalkylsulfonate group (CoM-S^-) of methyl-coenzyme M is a very poor leaving group with pKa of 50 for CH_4 or 8 for CoM-HS. According to this, the elimination of bromide in the ionic reaction of MCRred1 and BrMe is reasonable whereas the feasibility that MCRred1 interacts with methyl-coenzyme M to eliminate a $^-$S-CoM is pretty slim (*128, 129*). Theoretical studies indicate that the cleavage of a strong C-S bond in methyl-S-CoM to form a weak methyl-nickel bond is thermodynamically unfavorable (*44*). A new DFT-based mechanism has been proposed by Duin and McKee that circumvents this problem by first having a protonation of F_{430}, either on the nickel or on a N ligand to the nickel. This makes the formation of a nickel-methyl species later in the reaction energetically feasible.

The intriguing discovery of the high concentrations of MCR in methanotrophic archaea strongly implies that this enzyme catalyzes the first step in the anaerobic oxidation of methane (AOM) (*16*) by working in the reverse way. This hypothesis is supported by the observation that the Ni(III)-CH_3 species in MCR reacts with coenzyme M resulting in the formation of methyl-coenzyme M. It is predicted that methyl-coenzyme M is formed in the presence of heterodisulfide, the product of MCR reaction, and this study is under way.

3. 5 CONCLUSION

This chapter describes that methyl-coenzyme M can react with BrMe with the formation of a methyl-Ni(III) species showing that methyl-Ni(III) could be an intermediate which was disputed. The results do not show that methyl-Ni(III) is an intermediate in methane formation from methyl-coenzyme M but do support the intermediacy of the methyl-nickel species in methane formation. The EPR signal of methyl-nickel species detected in our study was not stable and it decayed within one hour. In addition, it was determined that the incubation of the nickel-methyl species with the substrate analog coenzyme M resulted in the regeneration of methyl-coenzyme M, which supported the working hypothesis that MCR was involved in the first step of the anaerobic methane oxidation.

CHAPTER FOUR

PURIFICATION OF A NEW HYDROXYLAMINE OXIDOREDUCTASE FROM

METHYLOMICROBIUM ALBUM ATCC 33003

4．1 INTRODUCTION

The oxidation of ammonia to nitrite is a universal process in the biological nitrogen cycle. The nitrifying bacterium *Nitrosomonas europaea,* a well-studied autotrophic microorganism, derives energy from this oxidation pathway, consisting of two enzymes: ammonia monooxygenase (AMO) and hydroxylamine oxidoreductase (HAO). AMO catalyzes the first step reaction to convert ammonia to hydroxylamine: $NH_3 + O_2 + 2e^- + 2H^+ \rightarrow NH_2OH + H_2O$. HAO, a central player in electron transfer in this organism, is responsible for the second step of the reaction, the oxidation of hydroxylamine to nitrite: $NH_2OH + H_2O \rightarrow HNO_2 + 4e^- + 4H^+$ (*68, 69, 130*). HAO is found in the periplasmic region of the bacterium and it is one of the most complex hemoproteins known containing seven *c*-hemes (*131, 132*) as well as an unusual heme present in the active site, designated as P460 (*133-136*).

The oxidation of hydroxylamine to nitrite is an energy-gaining step generating four electrons in autotrophic nitrifying bacteria. Two of the electrons are used by AMO for the oxidation of ammonium, while the other two electrons flow into a respiratory electron transport chain involving cytochrome c_{554}, cytochrome c_{552} and a terminal cytochrome c

oxidase (*137*). In contrast, heterotrophic nitrifying bacteria are incapable of utilizing the energy derived from hydroxylamine oxidation for growth (*138-140*) with one exception (*141*). The periplasmic hydroxylamine oxidase, purified from heterotrophic nitrifiers, do not contain heme *c* or heme P460 (*138, 139, 141*)

It is shown that methanotrophs and ammonia-oxidizing bacteria have a number of similarities in physiological and biochemical aspects (*73*). The ability of methanotrophic bacteria to oxidize ammonia to nitrite has been known for over 30 years (*142*). Surprisingly, the oxidation of ammonia to hydroxylamine is catalyzed by the methane monooxygenases (mMO) enzyme (*142*). Based on genetic studies it has been proposed that the oxidation of hydroxylamine to nitrite is catalyzed by either a small cytochrome P460 enzyme or a P460-containing HAO (*143, 144*). Since no physiological information on *in vivo* activities of these proteins is available, it remains unknown how methanotrophs catalyze hydroxylamine oxidation and how the electron flow is mediated within the pathway. Most recently, an HAO-like gene was sequenced from the Type I methanotroph, *Methylomicrobium album* ATCC 33003 (*78*). Here we purified and characterized the gene product and demonstrated its function in hydroxylamine oxidation.

4. 2 MATERIALS AND METHODS

4.2.1 Biochemical and Chemical Reagents

Magnesium sulfate heptahydrate, potassium nitrate, calcium chloride dihydrate, iron(II) sulfate heptahydrate, zinc sulfate heptahydrate, manganese chloride tetrahydrate, cobalt chloride hexahydrate, nickel chloride hexahydrate, boric acid, folic acid, sodium molybdate, thiamine hydrochloride, pantothenic acid hemicalcium salt, vitamin B_{12}, riboflavin, nicotinamide, biotin, EDTA iron(III) sodium salt, copper sulfate, sodium dithionite, sodium phosphate dibasic, methylthiazolyltetrazolium bromide (MTT), phenazine methosulfate (PMS), hydroxylamine, TAPS, and MOPS were purchased from Sigma-Aldrich (St. Louis, MO). Potassium phosphate (monobasic anhydrous), 2-propanol, absolute ethanol, sodium chloride, and Tris-base were from Fisher Biotech (Pittsburgh, PA). Q-sepharose, Superdex-200, and Mono-Q columns were purchased from Amersham Biosciences (Piscataway, NJ). Centricon ultrafiltration units were from Millipore (Bedford, MA).

Standard anaerobic buffers were used for all purifications and experiments. Standard buffers contain 50 mM Tris-HCl (pH 8.0) or 50 mM TAPS/MOPS (pH 6.0~9.0). The buffers were filtered (0.22 μm) and subsequently boiled under nitrogen gas flow. They were stirred under vacuum for a period of 1-2 h. The buffers could then be used or stored under nitrogen with 0.3 atmospheric overpressure applied to the head space of the bottle.

134

4.2.2 Preparation of Nitrate Mineral Salts (NMS) Medium

1 L 10× stock NMS solution was prepared containing 40.6 mM $MgSO_4$, 99.0 mM KNO_3, and 15.5 mM $CaCl_2$ in 900 mL tap distilled water. A 100× stock Whittenbury trace element solution including $FeSO_4$, $ZnSO_4$, $MnCl_2$, $CoCl_2$, $NiCl_2$, H_3BO_3 and Na_2EDTA was added and followed by addition of 0.1% sodium molybdate, 3.5% FeEDTA and 100 mM copper sulfate solution. Then the solution was brought up to total volume of 1000 mL. 100× phosphate stock solution and 1000× vitamin stock solution for NMS were prepared separately. Phosphate stock solution with KH_2PO_4 and Na_2HPO_4 was autoclaved or filter sterilized. Vitamin stock solution with biotin, folic acid, thiamin-HCl, calcium pantothenate, vitamin B_{12}, riboflavin and nicotinamide was filter sterilized. A 1 L NMS medium was prepared by adding 900 mL tap distilled water to 100 mL 10× NMS solution and autoclaved (for agar plates, 16-19 g Difco agar was added per liter). The final NMS medium was prepared by mixing 1 L sterilized NMS with 10 mL phosphate stock solution and 10 mL vitamin stock solution.

For NMS medium preparation, tap distilled water is used since most methanotrophs grow poorly in water that is too pure.

4.2.3 Cell Growth

Methylomicrobium album ATCC 33003 plated on agar/NMS medium grew under a 50% methane/50% air atmosphere at RT in an airtight jar. Colonies formed in approximately 1 week and were stored at 4 °C for a couple of weeks.

Cells were grown in serum bottles in NMS medium. A 2 ml culture (OD 0.3) was used to inoculate a 100 ml culture grown in a 1 L bottle, and 15 mL from the 100 mL

culture was used to inoculate a 1 L culture grown in a 2 L bottle. The cells were harvested when an OD of 0.2-0.3 was reached after 3 days, by centrifugation at 5000 x g for 20 min. The harvested cells were stored in -80 °C. A 1 L culture produced approximate 1.5 g (wet weight) cells in three days. Purity was tested regularly by plating the cells on trypton-yeast extract agar plates or by observing culture homogeneity under a microscope.

4.2.4 Purification of HAO

The preparation of the cell-free extract and the purification were performed at room temperature. The columns used for purification were fitted to an FPLC. Protein was detected by measuring the absorbance at 280 nm. Cells from the enriched Anammox culture (~10 g wet weight) were first resuspended in 40 ml 10 mM Tris-HCl, pH 8.0 (buffer A). Subsequently, the cell suspension was sonicated 3 times for 7 min each at full power. Whole cells and cell debris were removed by centrifugation at 160,000 x g for 30 min. The supernatant was loaded on a Q-sepharose (weak anion-exchange chromatography) column equilibrated with buffer A. A linear gradient of 0-0.5 M NaCl in buffer A was applied at 4 mL/min. Active fractions were pooled, washed and concentrated to ~ 10 mL with centricon ultrafiltration units with a 10 kDa cut-off. Further purification was achieved by strong anion-exchange chromatography on a Mono-Q column. Proteins were eluted in a 0-0.5 M NaCl gradient in buffer A at a rate of 2 mL/min. Active fractions were pooled and concentrated using a with a centricon ultrafiltration unit with a 30 kDa cut-off. The concentrated enzyme solution was finally purified by gel filtration on a prepacked Superdex 200 HR 10/30 column. The gel

filtration column was preequilibrated with buffer A containing 0.1 M NaCl at a rate of 0.5 mL/min. Active fractions were stored in 4 °C.

4.2.5 Protein Determination

The protein concentration was determined by using the method of Bradford (*108*) with bovine serum albumin (Serva) as standard.

4.2.6 Enzyme Activity Assay

The activity assay for HAO was performed under anaerobic conditions at 25 º C by following the reduction of MTT (ε_{578} = 13.0 mM^{-1}·cm^{-1}) via PMS using an UV/vis HP 8453 spectrophotometer equipped with a thermostatic cell holder. One unit of activity is defined as 1nmol of MTT reduced/min. The reaction mixture (1 mL) contained 50 µmol of Tris-HCl (pH 8.0), 20 nmol of PMS, 0.4 µmol of MTT, and 1 µmol of hydroxylamine. The reaction was started by the addition of an appropriate amount of enzyme. The standard assays were performed in 1.5 mL cuvettes sealed with butyl-rubber stoppers and were made anaerobic with argon.

4.2.7 UV-visible Spectroscopy

Spectra of HAO in 50 mM Tris-HCl (pH 8.0) at room temperature were recorded on an UV/vis HP 8453 spectrophotometer. The spectral bandwidth was 1 nm. HAO-reduced spectra were obtained by adding hydroxylamine with different final concentrations, or dithionite.

4. 3 RESULTS

4.3.1 Purification of HAO

The HAO from *Methylomicrobium album* ATCC 33003 was purified from the soluble fraction by different chromatography steps. Sequential anion-exchange chromatography steps (Q-Sepharose and Mono-Q) were used for the initial purification. The proteins with hydroxylamine oxidoreductase activity eluted from these columns at ~0.2 M NaCl (Figure 4.1 and 4.2). Finally, the fractions with the highest specific activity were collected, subsequently concentrated, and applied to a Superdex 200 gel filtration column (Figure 4.3). After size-exclusion chromatography, the fractions with activity were judged on SDS-PAGE (Figure 4.4). Fraction 14 with most activity has an intense band at 60 kDa and a weak band around 10 kDa. Fraction 15 apparently has another band at 40 kDa which was assigned to a heme protein observed in the sample using UV-visible spectroscopy. Totally, a 6-fold purification was obtained, indicating that the HAO content of the total cell-free extract was about 18% (Table 4.1). The preparation contained more than 90% HAO, as indicated by the symmetrical peak on the Superdex 200 at 280 nm wavelength and clear bands shown on SDS-PAGE.
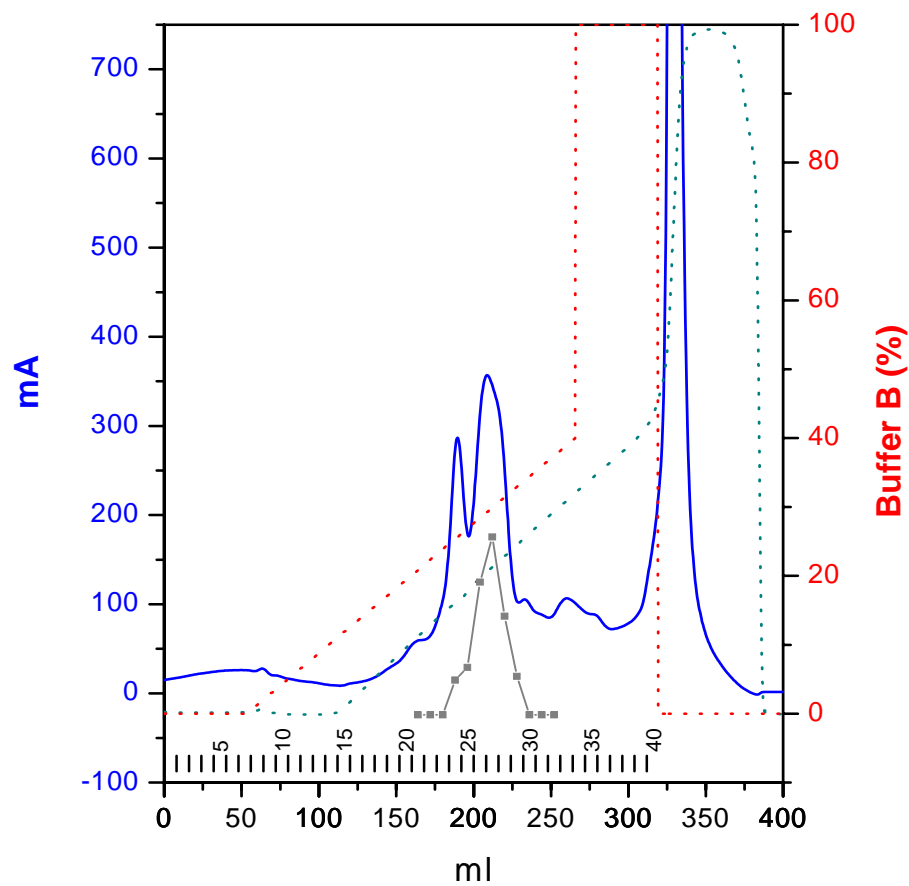
Figure 4.1. FPLC profile of the Q-Sepharose chromatography step. The red dashed lines represent the % concentration of buffer B. The blue-green dotted lines represent the conductivity. The gray dots and lines represent the relative HAO activity in the resepctive fractions.
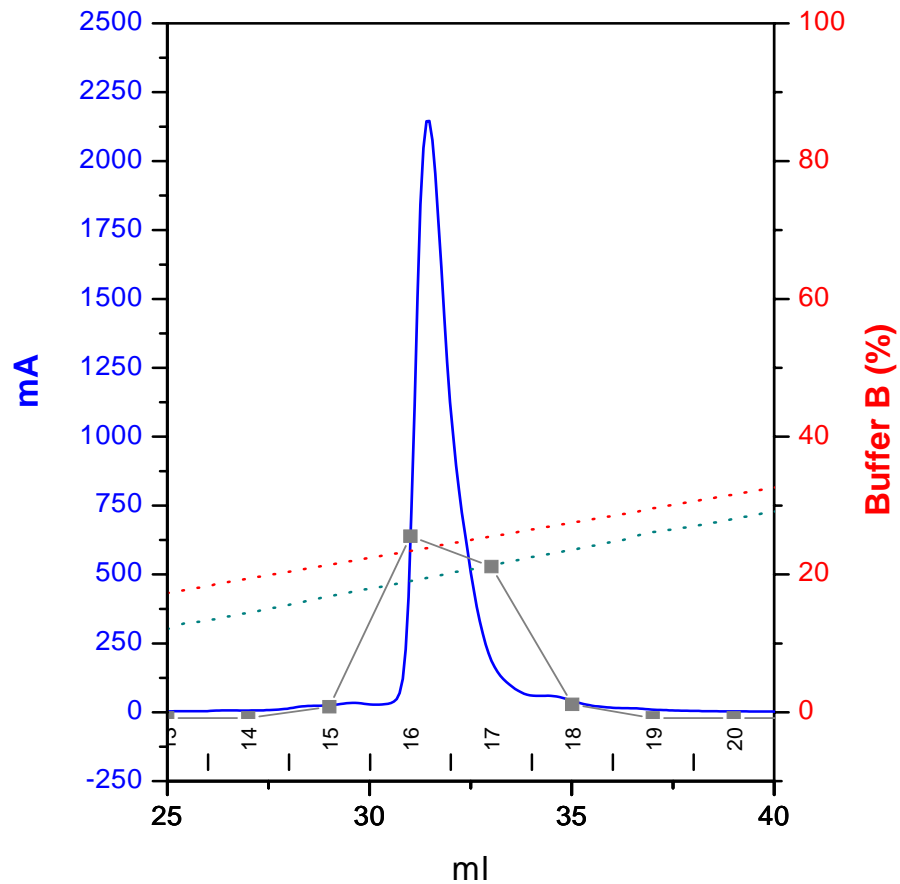
Figure 4.2. FPLC profile of Mono-Q chromatography step. The red dashed lines represent the % concentration of buffer B. The blue-green dotted lines represent the conductivity. And the gray dots and lines represent the relative HAO activity in the resepctive fractions.
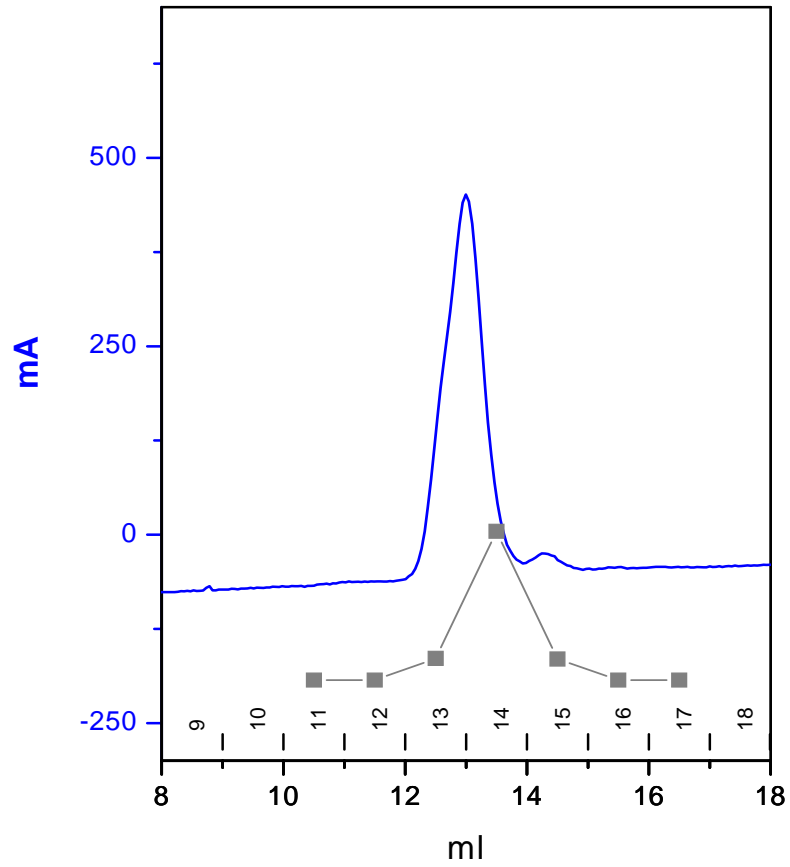
Figure 4.3. FPLC profile of the Superdex-200 chromatography step. The gray dots and lines represent the relative HAO activity in the resepctive fractions.

Purification step	Total protein (mg)	Total activity (units)	Specific activity (units/mg)	Purification (x-fold)
Cell extract	46.8	552.5	11.8	1.0
Q-Sepharose	4.0	220.9	55.8	4.7
Mono-Q	1.6	97.8	59.8	5.1
Superdex-200	0.4	26.2	65.5	5.6

Table 4.1. Purification of hydroxylamine oxidoreductase (HAO) from *Methylomicrobium album* ATCC 33003.
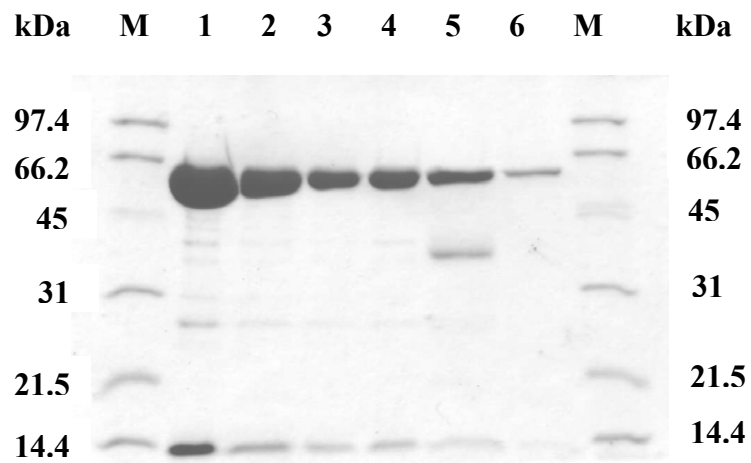
Figure 4.4. SDS-PAGE of fractions from the Superdex-200 chromatography step. Lane M: Low range of molecular weight marker; Lanes 1-4: Fraction 14 in different concentrations; Lane 5: Fraction 15. This fraction contains an additional band that is assigned to a heme-containing protein; Lane 6: Fraction with copper protein from different purification (see below).

Initially there was doubt about the purity of the protein. Part of this had to do with the detection of a copper-containing protein which seemed to elute together with the HAO protein (see below). Therefore the purification procedure was repeated. In this procedure, however, the Mono Q chromatography step was performed using different pH values: pH 6.0, 7.0, 8.0 and 9.0. To prevent buffer effects the same buffer mixture of 50 mM MOPS/50 mM TAPS was used for all four different pH values. Figure 4.5 shows the different profiles obtained at the different pH values. At pH 9.0 the major protein band elutes as a single peak. At both pH 8.0 and pH 7.0 there seem to be two major protein bands that elute very closely together. At pH 6.0, we get a broad band that elutes even before the salt gradient is applied and a sharper band at a higher salt concentration. SDS-PAGE of all the major protein fractions show the same major components, a 60 kDa and and a 10 kDa band. Figure 4.6 shows the SDS-PAGE for the chromatography step at pH 6.0. The first lane is the broad band that comes down first. The third lane is the sharp band that comes later. Both bands seem to contain the same protein. From this study it can be concluded that the HAO is pure and is a heterodimer. The different bands that we see in the purification procedure on the Mono Q chromatography step are due to the same protein with different charges. The fact that at pH 6.0, part of the HAO comes down before the salt gradient starts and the remaining part does early in the salt gradient indicates that the pI of HAO is very close to pH 6.0. This was confirmed by isoelectric focusing that indicated a pI of 6.0~6.5 (data not shown).
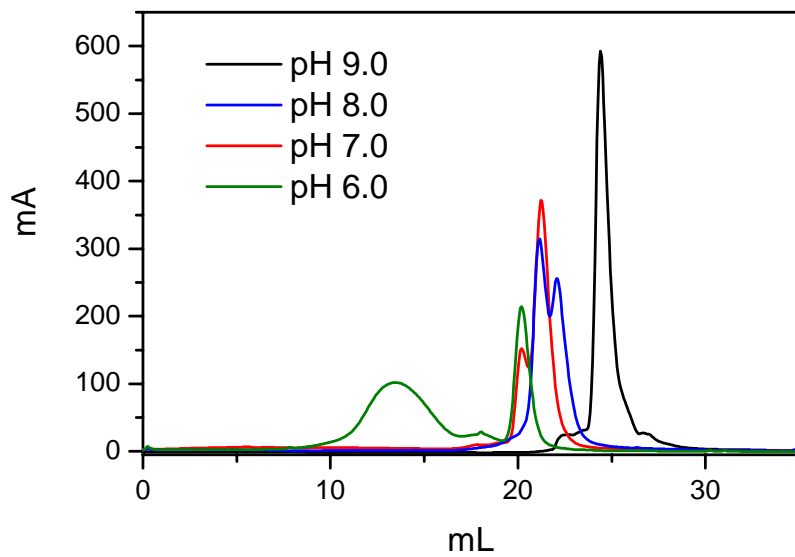
Figure 4.5. FPLC profiles of the Mono-Q chromatography step under different pH conditions. Fraction size was 1 mL.
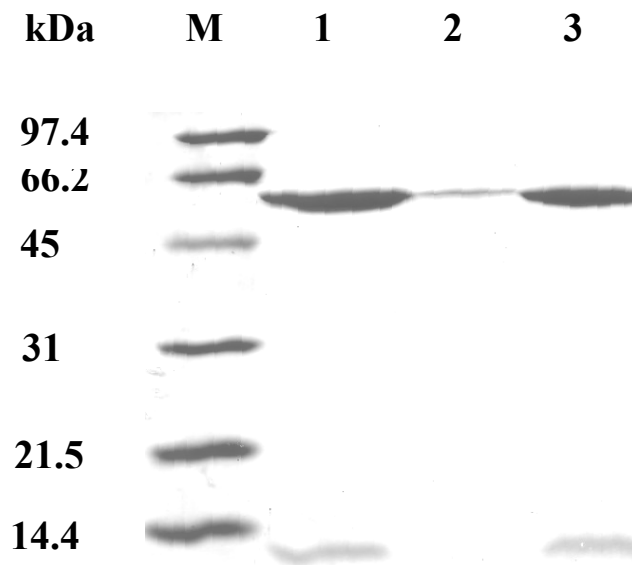
Figure 4.6. SDS-PAGE of the samples from Mono-Q chromatography step at pH 6.0. Lane M: Low range of molecular weight marker; Lane 1: Pooled fractions fractions 10-17 (see Figure 4.5). Lane 2: Pooled fractions 18-19. Lane 3: Pooled fractions 20-22.

4.3.2 UV-visible Absorption Spectrum of Purified HAO

Figure 4.7 shows a typical absorption spectrum for the HAO protein. The spectrum has a shoulder at 300 nm and two resolved bands at 350 nm and 420 nm.

4.3.3 A Heme-containing Protein with HAO Activity

Since HAO from *N. europaea* is a heme-containing protein every fraction was checked for the presence of heme by absorption spectroscopy. Fraction 17 from the Mono-Q chromatography step and fraction 15 from the Superdex 200 chromatography step display typical heme spectra with absorption maxima at 420 nm (Soret band), 524 nm (β-band), and 552 nm (α-band). The unusual absorption peak at 468 nm typical for the P460 containing enzyme from *N. europaea* was not observed. The separation of the HAO protein and the heme-containing protein by size-exclusion chromatography shows that these two proteins are not related.

Figure 4.8, however, shows that the heme-containing protein also has HAO activity. The protein shows a heme spectrum typical for reduced heme. The additional shoulder at 400 nm is probably due to the presence of the HAO protein. The addition of 1.2 mM hydroxylamine did not interact with the protein as isolated since the heme is already reduced (data not shown). To test if the oxidized heme can interact with hydroxylamine, the oxidant ferricyanide was added to oxidize the heme first. When ferricyanide was added, the bands at 524 nm and 552 nm were replaced with a broad band at 540 nm, and the band at 420 nm shifted to 410 nm. Upon the sequential addition of hydroxylamine both the ferricyanide and the heme-containing protein were reduced. Figure 4.9 shows the data for the heme-containing protein were the ferricyanide spectrum has been subtracted

from the overall spectrum. Comparison of the hydroxylamine-reduced protein and dithionite-reduced protein shows that an almost full reduction is achived with the hydroxylamine (Figure 4.8). In a control experiment we incubated ferricyanide with different amount of hydroxylamine. No reduction of ferricyanide was detected. From these experiments it can be concluded that the heme-containing protein can be reduced by hydroxylamine. However, since the sample stil contains the other HAO protein it can not be excluded that the HAO is actually reducing both the ferricyanide and the heme-containing protein. This would be an interesting result since that would make the heme-containing protein a candidate for the natural electron acceptor for HAO. Further purification of the heme-containing protein is needed to discern between these two possibilities.
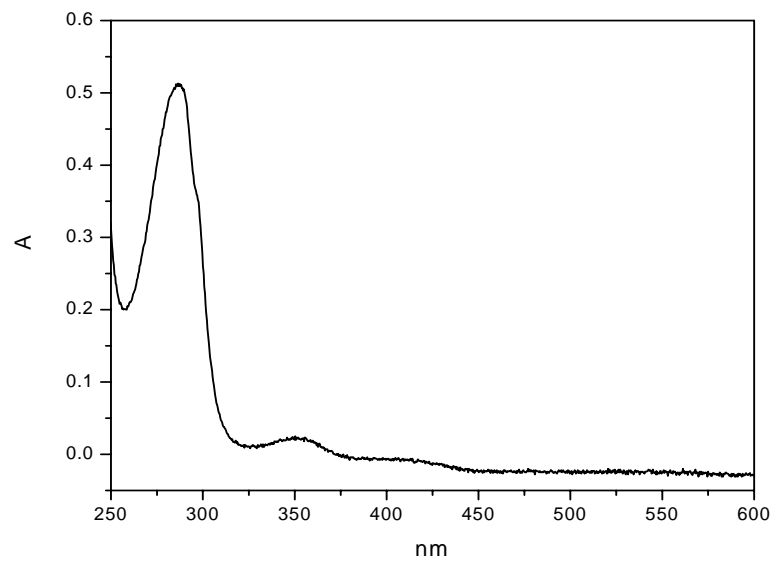
Figure 4.7. UV-visible absorption spectrum of purified HAO
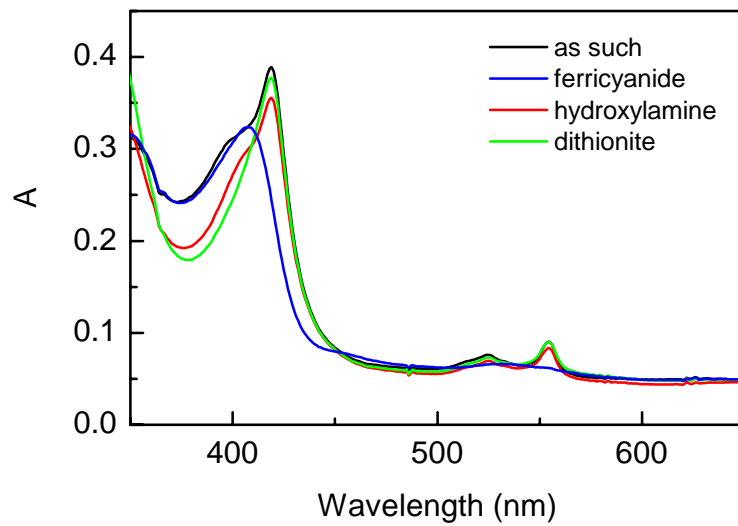
Figure 4.8. UV-visible absorption spectra of Fraction 15
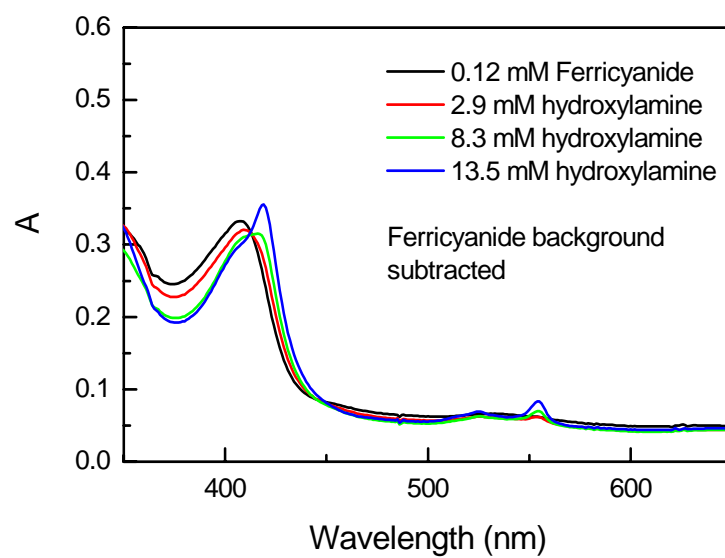
Figure 4.9. UV-visible spectra of Fraction 15.

4.3.4 Purification of HAO with EDTA

Since most HAO are periplasmic enzymes and potentially membrane associated, various conditions were tested including high salt, high pH and EDTA for the extraction of the protein. Cells were broken as described before. Subsequently the membrane/cytosol preparation was split into four different samples. One sample was incubated on ice. To the second sample, NaCl was added to a concentration of 1 M. To a third sample EDTA was added to a concentraion of 5 mM. For the fourth, the pH was adjusted to pH 9.0. All samples were incubated for 30 min on ice. The membranes were removed from the individual sample by ultra centrifugation. Subsequently the activity in the supernatant was tested. It was found that the activity of cell extracts with EDTA increased significatantly compared to the activity with other conditions (Figure 4.10). The purification profiles of the sample with the added EDTA were very similar to those shown in Figures 4.1 and 4.2. Like in Figure 4.1 the Q-sepharose chromatography step showed two major peaks. In this case however, the fractions of this first peak showed a clear blue color. These fractions also seem to contain significant activity. The protein seems to be very similar to HAO in size as judged by SDS-PAGE (Figure 4.4). Both the 60 kDa and 10 kDa bands seem to be present. It shows the typical Cu^{2+} EPR spectra (Figure 4.11). This protein has not been further purified but its identity need to be clarified.
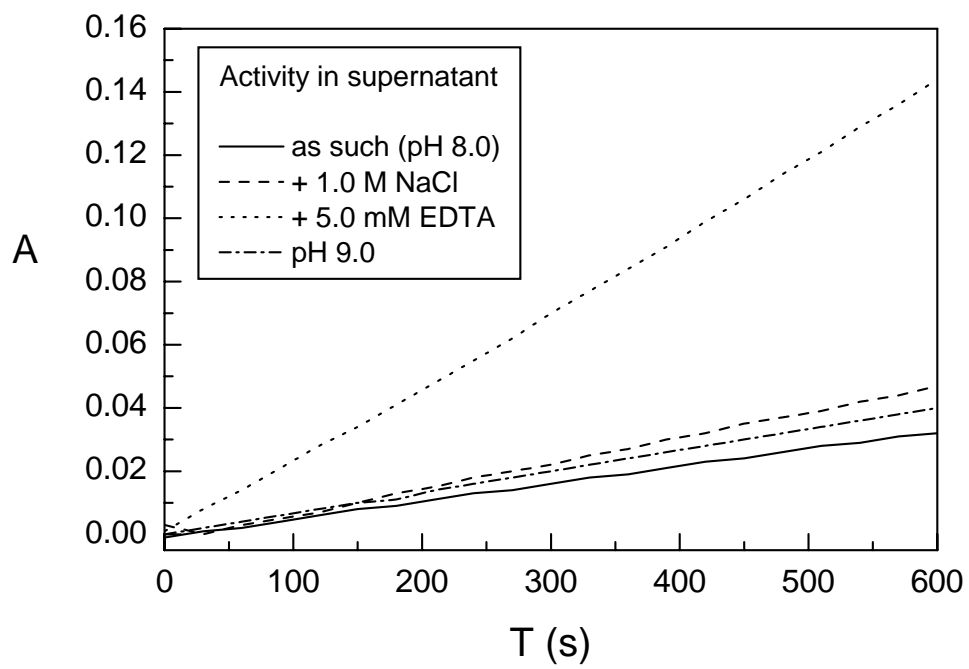
Figure 4.10. HAO activity in cell extracts with different conditions.
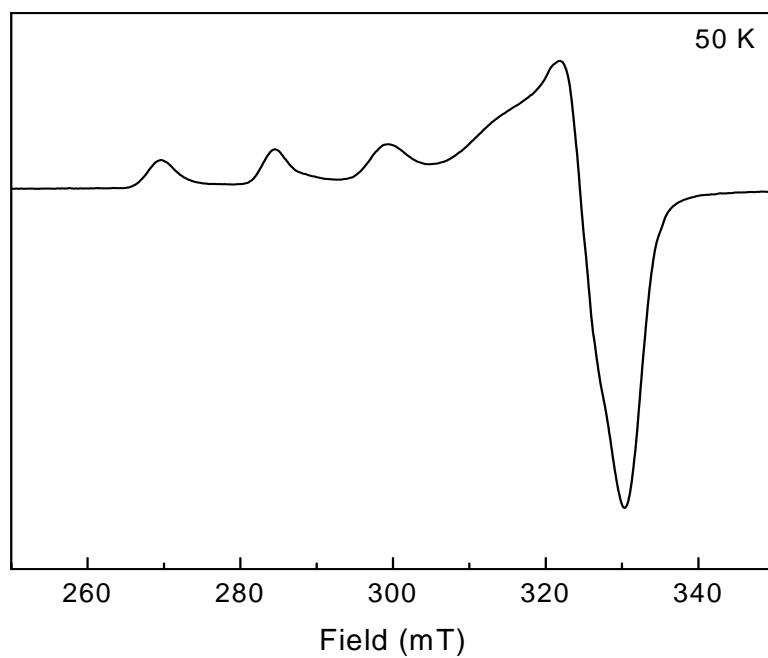
Figure 4.11. EPR spectrum of the copper containing protein

4．4 DISCUSSION AND CONCLUSION

This chapter reports on a novel hydroxylamine oxidoreductase isolated from *Methylomicrobium album* ATCC 33003. The properties of this enzyme were compared with known HAO from the other type of methanotroph as well as nitrifying bacteria (Table 4.2). Our protein seems to be a heterodimer and does not contain a heme prosthetic group or iron-sulfur cluster. EPR data did not show any signal in either dithionite reduced or ferricyanide oxidized protein. The protein, however, might contain labile non-heme iron as has been proposed for the *Pseudomonas* HAO (*141*).

The only other methanothroph investigated for the presence of HAO is *Methylococcus capsulatus* Bath, a Type II methanothroph. It contains an enzyme similar to cytochrome P-460 with a 16 kDa subunit. The enzyme was proposed to have both copper and iron in equimolar levels and it was the first time to identify a P-460-like enzyme that is capable of oxidation of hydroxylamine by a methanotroph (*143*). This enzyme apparently has different features from the one that we are currently studying. The microorganism currently being studied is a Type I methanotroph. All the physiological data showed this bacterium is capable of conversion of NH_2OH to NO_2. A HAO-like gene has been sequenced but no P-460 gene has been found (*78*). In fact, a P-460 gene has never been found with a DNA probe in Type I methanotroph (*145*). To have a better comparison of HAO from *M. album* with the other HAO enzymes more studies are underway, including the determination of the K_m and V_{max}, amino acid sequence and reaction product analysis.

During purification of HAO from *M. album*, it was interesting to find a heme protein that co-purified with the HAO protein on the ion-exchange column at pH 8.0.

(This was not the case at the other pH values). The absorption maximum at 550 nm (Figure 4.8) is typical for c-type cytochromes. When the heme was first oxized by ferricyanide it was partially reduced by hydroxylamine. Since the protein sample still contained traces of the other HAO it can not be excluded that this effect is due to the HAO protein. This would indicate that this heme protein acts like the cytochrome c_{554} or c_{552} that can accept electrons from HAO.

Another interesting finding is that with the treatment of EDTA during the purification, the HAO activity in the cell extracts increased significantly. A copper-containg protein eluted from the Q-sepharose column with very similar propeties as the HAO protein (Figure 4.4). The EPR spectrum is typical for a Cu^{2+} (Figure 4.11). The copper concentration in the fraction directly from the Q-sepharose column was very high: 1.7 mM. This protein needs further characterization. It could be similar in function as azurin, the blue-copper protein in respiratory nitrite-reducing systems or involves in the electron transfer of electron from the HAO reaction.

	Nitrosomonas europaea	*Thiosphaera pantotropha*	*Pseudomonas PB16*	*M. capsulatus*	*Methylomicrobium album*
mol mass (kDa)	189	20	132	183	70?
Mr subunit (kDa)	63	20	68	39/16.4	60/10?
composition	α_3	α	α_2	$\alpha\beta$	$\alpha\beta$?
heme c	24	none	none	1	none
heme type	P-460			P-460	
pI	5.3	ND	ND	6.98	6.0
Vmax (units/mg)	28	0.13	0.45	56.4	ND
Km (μM)	10	33	37	NR	ND
e-acceptor	PMS MTT Cyt$_{554}$	Cyt C K$_3$Fe(CN)$_6$ Cyt$_{551}$	K$_3$Fe(CN)$_6$	PMS	PMS+ MTT
localization	periplasm	periplasm	ND	NR	periplasm
Reference	(*67*)	(*138*)	(*141*)	(*143*)	this chapter

Table 4.2. Comparison of hydroxylamine oxidoreductase (HAO) from various microorganisms. NR, not reported; ND, not determined (yet).

REFERENCES

1. Thauer, R. K., and Bonacker, L. G. (1994) Biosynthesis of coenzyme F_{430}, a nickel porphinoid involved in methanogenesis, *Ciba Found.Symp. 180*, 210-227.

2. Thauer, R. K. (1985) Nickelenzyme im Stoffwechsel von methanogenen Bakterien, *Biol.Chem.Hoppe-Seyler 366*, 103-112.

3. Friedmann, H. C., Klein, A., and Thauer, R. K. (1991) Biochemistry of coenzyme F_{430}, a nickel porphinoid involved in methanogenesis, *New Comprehensive Biochemistry 19*, 139-154.

4. Eschenmoser, A. (1986) Chemistry of corphinoids, *Annals of the New York Academy of Sciences 471*, 108-129.

5. Duin, E. C., Warren, M. J., and Smith, A. (2007) Role of coenzyme F_{430} in methanogenesis, in *Tetrapyrroles: their birth, life and death*, p. Online, Landes Bioscience, Georgetown.

6. Pfaltz, A., Livingston, D. A., Jaun, B., Diekert, G., Thauer, R. K., and Eschenmoser, A. (1985) Zur Kenntnis des Faktors F_{430} aus methanogenen Bakterien: Über die Natur der Isolierungsartefakte von F_{430}, ein Beitrag zur Chemie von F_{430} und zur konformationellen Stereochemie der Ligandperipherie

von hydroporphinoiden Nickel(II)-Komplexen, *Helvetica Chimica Acta 68*, 1338-1358.

7.   Wondimagegn, T., and Ghosh, A. (2000) A first-principles quantum chemical study of coenzyme F_{430}: Interplay of skeletal stereoisomerism and conformation in the stabikization of nickel(I), *Journal of the American Chemical Society 122*, 6375-6381.

8.   Thauer, R. K. (1998) Biochemistry of methanogenesis: a tribute to Marjory Stephenson, *Microbiology 144*, 2377-2406.

9.   Hanson, R. S., and Hanson, T. E. (1996) Methanotrophic bacteria, *Microbiological Reviews 60*, 439-471.

10.   Jaun, B. a. T., R.K. (2007) Methyl-coenzyme M Reductase and Its Nickel Corphin Coenzyme F_{430} in Methanogenic Archaea, *Met. Ions Life Sci. 2*, 323-356.

11.   Smith, D. R., Doucette-Stamm, L. A., Deloughery, C., Lee, H., Dubois, J., Aldredge, T., Bashirzadeh, R., Blakely, D., Cook, R., Gilbert, K., Harrison, D., Hoang, L., Keagle, P., Lumm, W., Pothier, B., Qiu, D., Spadafora, R., Vicaire, R., Wang, Y., Wierzbowski, J., Gibson, R., Jiwani, N., Caruso, A., Bush, D., Safer, H., Patwell, D., Prabhakar, S., McDougall, S., Shimer, G., Goyal, A., Pietrokovski, S., Church, G. M., Daniels, C. J., Mao, J. I., Rice, P., Nölling, J., and Reeve, J. N. (1997) Complete genome sequence of Methanobacterium thermoautotrophicum D H: Functional analysis and comparative genomics, *Journal of Bacteriology 179*, 7135-7155.

12.   Diekert, G., Gilles, H. H., Jaenchen, R., and Thauer, R. K. (1980) Incorporation of 8 succinate per mol nickel into factors F_{430} by Methanobacterium thermoautotrophicum *Archives of Microbiology 128*, 256-262.

13.   Ellefson, W. L., Whitman, W. B., and Wolfe, R. S. (1982) Nickel-containing factor F_{430}: Chromophore of the methylreductase of Methanobacterium *Proceedings of the National Academy of Sciences of the United States of America 79*, 3707-3710.

14.   Hoehler, T. M., Alperin, M. J., Lidstrom, M. E., and Tabita, F. R. (1996) Anaerobic methane oxidation by a methanogen-sulfate reducer consortium: geochemical evidence and biochemical considerations, in *Microbiol growth on C1 compounds*, pp 326-333, Kluwer Academic Publishers, Dordrecht.

15.   Valentine, D. L., and Reeburgh, W. S. (2000) New perspectives on anaerobic methane oxidation, *Environmental Microbiology 2*, 477-484.

16.   Shima, S., and Thauer, R. K. (2005) Methyl-coenzyme M reductase and the anaerobic oxidation of methane in methanotrophic Archaea, *Current Opinion in Microbiology 8*, 643-648.

17.   Ermler, U., Grabarse, W., Shima, S., Goubeaud, M., and Thauer, R. K. (1997) Crystal structure of a 300 kDa methyl-coenzyme M reductase, the key enzyme of biological methane formation, at 1.45 Å resolution, *Science 278*, 1457-1462.

18.   Jaun, B. (1990) Coenzyme F_{430} from methanogenic bacteria: Oxidation of F_{430} pentamethyl ester to the Ni(III) form, *Helvetica Chimica Acta 73*, 2209-2217.

19. Jaun, B., and Pfaltz, A. (1986) Coenzyme F_{430} from methanogenic bacteria: Reversible one-electron reduction of F_{430} pentamethyl ester to the nickel(I) form, *Journal of the Chemical Society,Chemical Transactions*, 1327-1329.

20. Holliger, C., Pierik, A. J., Reijerse, E. J., and Hagen, W. R. (1993) A spectroelectrochemical study of factor F 430 nickel(II/I) from methanogenic bacteria in aqueous solution, *Journal of the American Chemical Society 115*, 5651-5656.

21. Duin, E. C., Signor, L., Piskorski, R., Mahlert, F., Clay, M. D., Goenrich, M., Thauer, R. K., Jaun, B., and Johnson, M. K. (2004) Spectroscopic investigation of the nickel-containing porphinoid cofactor F_{430}. Comparison of the free cofactor in the +1, +2 and +3 oxidation states with the cofactor bound to methyl-coenzyme M reductase in the silent, red and ox forms, *Journal of Biological Inorganic Chemistry 9*, 563-576.

22. Rospert, S., Böcher, R., Albracht, S. P. J., and Thauer, R. K. (1991) Methyl-coenzyme M reductase preparations with high specific activity from H_2-preincubated cells of Methanobacterium thermoautotrophicum *FEBS Letters 291*, 371-375.

23. Goubeaud, M., Schreiner, G., and Thauer, R. K. (1997) Purified methyl-coenzyme-M reductase is activated when the enzyme-bound coenzyme F_{430} is reduced to the nickel(I) oxidation state by titanium(III) citrate, *European Journal of Biochemistry 243*, 110-114.

24. Mahlert, F., Grabarse, W., Kahnt, J., Thauer, R. K., and Duin, E. C. (2002) The nickel enzyme methyl-coenzyme M reductase from methanogenic archaea: in

vitro interconversions among the EPR detectable MCR-red1 and MCR-red2 states, *Journal of Biological Inorganic Chemistry 7*, 101-112.

25.   Telser, J., Horng, Y. C., Becker, D. F., Hoffman, B. M., and Ragsdale, S. W. (2000) On the assignment of nickel oxidation states of the ox1, ox2 forms of methyl-coenzyme M reductase, *Journal of the American Chemical Society 122*, 182-183.

26.   Jaun, B., Sigel, H., and Sigel, A. (1993) Methane formation by methanogenic bacteria: Redox chemistry of coenzyme F_{430}, in *Metal ions in biological systems*, pp 287-337, Marcel Dekker Inc., New York.

27.   Telser, J., Davydov, R., Horng, Y. C., Ragsdale, S. W., and Hoffman, B. M. (2001) Cryoreduction of methyl-coenzyme M reductase: EPR characterization of forms, MCR ox1 and MCR red1 *Journal of the American Chemical Society 123*, 5853-5860.

28.   Duin, E. C., Cosper, N. J., Mahlert, F., Thauer, R. K., and Scott, R. A. (2003) Coordination and geometry of the nickel atom in active methyl-coenzyme M reductase from Methanothermobacter marburgensis as detected by X-ray absorption spectroscopy, *Journal of Biological Inorganic Chemistry 8*, 141-148.

29.   Craft, J. L., Horng, Y. C., Ragsdale, S. W., and Brunold, T. C. (2004) Spectroscopic and computational characterization of the nickel-containing F_{430} cofactor of methyl-coenzyme M reductase, *Journal of Biological Inorganic Chemistry 9*, 77-89.

30.   Craft, J. L., Horng, Y. C., Ragsdale, S. W., and Brunold, T. C. (2004) Nickel oxidation states of F_{430} cofactor in methyl-coenzyme M reductase, *Journal of the American Chemical Society 126*, 4068-4069.

31.   Mahlert, F., Bauer, C., Jaun, B., Thauer, R. K., and Duin, E. C. (2002) The nickel enzyme methyl-coenzyme M reductase from methanogenic archaea: in vitro induction of the nickel-based MCR-ox EPR signals from MCR-red2, *Journal of Biological Inorganic Chemistry 7*, 500-513.

32.   Ankel-Fuchs, D., and Thauer, R. K. (1986) Methane formation from methyl-coenzyme M in a sytem containing methyl-coenzyme M reductase, component B and reduced cobalamin, *European Journal of Biochemistry 156*, 171-177.

33.   Ellermann, J., Rospert, S., Thauer, R. K., Bokranz, M., Klein, A., Voges, M., and Berkessel, A. (1989) Methyl-coenzyme-M reductase from Methanobacterium thermoautotrophicum (strain Marburg), *European Journal of Biochemistry 184*, 63-68.

34.   Kuhner, C. H., Lindenbach, B. D., and Wolfe, R. S. (1993) Component A2 of methylcoenzyme M reductase system from Methanobacterium thermoautrophicum D H: Nucleotide sequence and functional expression by Escherichia coli *Journal of Bacteriology 175*, 3195-3203.

35.   Rouviere, P. E., and Wolfe, R. S. (1989) Component A3 of the methylcoenzyme M methylreductase system of Methanobacterium thermoautotrophicum ΔH: Resolution into two components, *Journal of Bacteriology 171*, 4556-4562.

36. Hartzell, P. L., Donnelly, M. I., and Wolfe, R. S. (1987) Incorporation of coenzyme M into component C of methylcoenzyme M methylreductase during in vitro methanogenesis, *Journal of Biological Chemistry 262*, 5581-5586.

37. Ragsdale, S. W., Kadish, K. M., Smith, K. M., and Guilard, R. (2003) Biochemistry of methyl-CoM reductase and coenzyme F_{430}, in *Porphyrin Handbook*, pp 205-228, Elsevier Science, San Diego.

38. Ermler, U. (2005) On the mechanism of methyl-coenzyme M reductase, *Dalton Trans.*, 3451-3458.

39. Ahn, Y., Krzycki, J. A., and Floss, H. G. (1991) Steric course of the reduction of ethyl coenzyme M to ethane catalyzed by methyl coenzyme M reductase from Methanosarcina barkeri *Journal of the American Chemical Society 113*, 4700-4701.

40. Hinderberger, D., Piskorski, R., Goenrich, M., Thauer, R. K., Schweiger, A., Harmer, J., and Jaun, B. (2006) A nickel-alkyl bond in an inactivated state of the enzyme catalyzing methane formation, *Angewandte Chemie 45*, 3602-3607.

41. Jaun, B., and Pfaltz, A. (1988) Coenzyme F_{430} from methanogenic bacteria: Methane formation by reductive carbon-sulphur bond cleavage of methyl sulphonium ions catalysed by F_{430} pentamethyl ester, *Journal of the Chemical Society, Chemical Transactions*, 293-294.

42. Lin, S. K., and Jaun, B. (1991) Coenzyme F_{430} from methanogenic bacteria: Detection of a paramagnetic methylnickel(II) derivative of the pentamethyl ester by ^{2}H-NMR spectroscopy, *Helvetica Chimica Acta 74*, 1725-1738.

43.   Goenrich, M., Duin, E. C., Mahlert, F., and Thauer, R. K. (2005) Temperature dependence of methyl-coenzyme M reductase activity and of the formation of the methyl-coenzyme M reductase red2 state induced by coenzyme B, *Journal of Biological Inorganic Chemistry 10*, 333-342.

44.   Pelmenschikov, V., Blomberg, M. R. A., Siegbahn, P. E. M., and Crabtree, R. H. (2002) A mechanism from quantum chemical studies for methane formation in methanogenesis, *Journal of the American Chemical Society 124*, 4039-4049.

45.   Pelmenschikov, V., and Siegbahn, P. E. M. (2003) Catalysis by methyl-coenzyme M reductase: A theoretical study for heterodisulfide product formation, *Journal of Biological Inorganic Chemistry 8*, 653-662.

46.   Finazzo, C., Harmer, J., Bauer, C., Jaun, B., Duin, E. C., Mahlert, F., Goenrich, M., Thauer, R. K., Van Doorslaer, S., and Schweiger, A. (2003) Coenzyme B induced coordination of coenzyme M via its thiol group to Ni(I) of F_{430} in active methyl-coenzyme M reductase, *Journal of the American Chemical Society 125*, 4988-4989.

47.   Krüger, M., Meyerdierks, A., Glöckner, F. O., Amann, R., Widdel, F., Kube, M., Reinhardt, R., Kahnt, J., Böcher, R., Thauer, R. K., and Shima, S. (2003) A conspicuous nickel protein in microbial mats that oxidize methane anaerobically, *Nature 426*, 878-881.

48.   Moran, J. J., e. a. (2004) *Archaea 1*, 303-309.

49.   Shilov, A. E., e. a. (1999) *Dokl. Akad. Nauk 367*, 557-559.

50.   Gong, W., e. a. (1998) Structure of a biological sensor: A new mechanism for heme-driven signal transduction, *Proc. Natl. Acad. Sci. USA 95*, 15177-15182.

51.   Lanzilotta, W. N., e. a. (2000) Structure of the CO sensing transcription factor CooA, *Nat. Struct. Biol. 7*, 876-880.

52.   Paoli, M. e. a. (2002) Structure-function relationships in heme-proteins, *DNA and Cell Biology 21*, 271-280.

53.   Bredt, D. S., and Snyder, S. (1994) Nitric oxide - A physiological messenter molecule, *Annu. Rev. Biochem. 63*, 175-261.

54.   Schultz, H., e. a. (1998) prototype of a heme chaperone essential for cytochrome *c* maturation, *Science 281*, 1197-1200.

55.   Hou, S., e. a. (2000) Myoglobin-like aerotaxis transducers in Archea and Bacteria, *Nature 403*, 540-544.

56.   Mogi, T., Saiki, K., and Anraku, Y. (1994) Biosynthesis and functional role of heme O and heme A, *Molecular Microbiology 14*, 391-398.

57.   Keilin, D. (1927) The cytochrome, an intracellular respiratory pigment common to micro.ovrddot.organisms, plants and animals, *Comptes Rendus des Seances de la Societe de Biologie et de Ses Filiales 97*, Appendix 39-70.

58.   Slater, E. C. (2003) Keilin, cytochrome, and the respiratory chain, *Journal of Biological Chemistry 278*, 16455-16461.

59.   Mowat, C. G., and Chapman, S. K. (2005) Multi-heme cytochromes--new structures, new chemistry, *Dalton Transactions*, 3381-3389.

60.   Stevens, J. M., Daltrop, O., Allen, J. W. A., and Ferguson, S. J. (2004) C-type cytochrome formation: Chemical and biological enigmas, *Accounts of Chemical Research 37*, 999-1007.

61. Moore, G. R. a. p., G. W. (1990) *Cytochromes c: evolutionary, structural, and physicochemical aspects*, Springer-Verlag, New York.

62. Barker, P. D., and Ferguson, S. J. (1999) Still a puzzle: why is haem covalently attached in c-type cytochromes?, *Structure FIELD Full Journal Title:Structure (London, England : 1993) 7*, R281-290.

63. Martinez, S. E., Huang, D., Szczepaniak, A., Cramer, W. A., and Smith, J. L. (1994) Crystal structure of chloroplast cytochrome f reveals a novel cytochrome fold and unexpected heme ligation, *Structure (Cambridge, MA, United States) 2*, 95-105.

64. Haser, R., Pierrot, M., Frey, M., Payan, F., Astier, J. P., Bruschi, M., and Le Gall, J. (1979) Structure and sequence of the multiheme cytochrome c3, *Nature (London, United Kingdom) 282*, 806-810.

65. Iverson, T. M., Arciero, D. M., Hsu, B. T., Logan, M. S. P., Hooper, A. B., and Rees, D. C. (1998) Heme packing motifs revealed by the crystal structure of the tetra-heme cytochrome c_{554} from Nitrosomonas europaea, *Nature Structural Biology 5*, 1005-1012.

66. Igarashi, N., Moriyama, H., Fujiwara, T., Fukumori, Y., and Tanaka, N. (1997) The 2.8 Å structure of hydroxylamine oxidoreductase from a nitrifying chemoautotrophic bacterium, Nitrosomonas europaea, *Nat Struct Biol FIELD Full Journal Title:Nature structural biology 4*, 276-284.

67. Arciero, D. M., and Hooper, A. B. (1993) Hydroxylamine oxidoreductase from Nitrosomonas europaea is a multimer of an octa-heme subunit, *Journal of Biological Chemistry 268*, 14645-14654.

68. Hooper, A. B., and Nason, A. (1965) Characterization of hydroxylamine-cytochrome c reductase from the chemoautotrophs Nitrosomonas europaea and Nitrosocystis oceanus, *J Biol Chem FIELD Full Journal Title:The Journal of biological chemistry 240*, 4044-4057.

69. Hendrich, M. P., Petasis, D., Arciero, D. M., and Hooper, A. B. (2001) Correlations of Structure and Electronic Properties from EPR Spectroscopy of Hydroxylamine Oxidoreductase, *Journal of the American Chemical Society 123*, 2997-3005.

70. Andersson, K. K., Kent, T. A., Lipscomb, J. D., Hooper, A. B., and Munck, E. (1984) Mossbauer, EPR, and optical studies of the P-460 center of hydroxylamine oxidoreductase from Nitrosomonas. A ferrous heme with an unusually large quadrupole splitting, *J Biol Chem FIELD Full Journal Title: The Journal of biological chemistry 259*, 6833-6840.

71. Hooper, A. B., Debey, P., Andersson, K. K., and Balny, C. (1983) Heme P460 of hydroxylamine oxidoreductase of Nitrosomonas. Reaction with CO and H2O2, *Eur J Biochem FIELD Full Journal Title: European journal of biochemistry / FEBS 134*, 83-87.

72. Collins, M. J., Arciero, D. M., and Hooper, A. B. (1993) Optical spectropotentiometric resolution of the hemes of hydroxylamine oxidoreductase. Heme quantitation and pH dependence of Em, *J Biol Chem FIELD Full Journal Title: The Journal of biological chemistry 268*, 14655-14662.

73. Bedard, C., and Knowles, R. (1989) Physiology, biochemistry, and specific inhibitors of methane, ammonia, and carbon monoxide oxidation by methanotrophs and nitrifiers, *Microbiological Reviews 53*, 68-84.

74. Colby, J., Stirling, D. I., and Dalton, H. (1977) The soluble methane monooxygenase of Methylococcus capsulatus (Bath). Its ability to oxygenate n-alkanes, n-alkenes, ethers, and alicyclic, aromatic and heterocyclic compounds, *Biochemical Journal 165*, 395-402.

75. Dalton, H. (1977) Ammonia oxidation by the methane oxidizing bacterium Methylococcus capsulatus strain Bath, *Archives of Microbiology 114*, 273-279.

76. Bergmann, D. J., Zahn, J. A., Hooper, A. B., and DiSpirito, A. A. (1998) Cytochrome P460 genes from the methanotroph *Methylococcus capsulatus* Bath, *J. Bacteriol. 180*, 6440-6445.

77. Bergmann, D. J., Hooper, A. B., and Klotz, M. G. (2005) Structure and sequence conservation of *hao* cluster genes of autotrophic ammonia-oxidizing bacteria: Evidence for their evolutionary history, *Appl. Environ. Microbiol. 71*, 5371-5382.

78. Nyerges, G., and Stein, L. Y. (2007) Expression of hydroxylamine oxidoreductase in the methanotrophic bacterium, *Methylomicrobium album*, *In preparation*.

79. Palmer, G., and Que, L., Jr. (2002) Electron Paramagnetic Resonance of Metalloproteins, in *Physical Methods in Bioinorganic Chemistry*, p 121, University Science Books, Sausalito, California.

80. Brudvig, G. W. (1995) Electron Paramagnetic Resonance Spectroscopy, in *Methods in Enzymology*.

81. Pilbrow, J. R., and Hanson, G. R. (1993) Electron Paramagnetic Resonance, *Methods in Enzymology 227*, 330-352.

82. Hoff, A. J. a. E., Ed. (1989) *Advanced EPR: Aplications in Biology and Biochemistry*, Amsterdam.

83. Carrington, A. e. a. (1967) *Introduction to Magnetic Resonance*, New York.

84. Weil, J. A., Bolton, J. R., and Wertz, J. E. (1995) *Electron Paramagnetic Resonance: elementary theory and practical applications*, John Wiley & sons, inc., New York / Wertz, J.E., Bolton, J.R. (1972) Chapman and Hall, New York.

85. Gordy, W. *e. a.* (1980) *Theory and Applications of Electron Spin Resonance*, New York.

86. Feher, G. (1956) *Phys. Rev. 103*, 834-835.

87. Eisenberger, P. a. p., P. S. (1967) *J. Chem. Phys. 47*, 3327-3334.

88. Derose, V. J. a. H., B.M. (1995) Protein Structure and Mechanism Studied by Electron Nuclear Double Resonance Specroscopy, *Methods in Enzymology 246*, 554-589.

89. Hoffman, B. M. (1991) Electron nuclear double resonance (ENDOR) of metalloenzymes, *Accounts of Chemical Research 24*, 164-170.

90. Kurreck, H., e. a. (2003) ENDOR Spectroscopy - A Promising Technique for Investigating the Structure of Organic Radicals, *Angewandte Chemie International Edition in English 23*, 173-194.

91. Swartz, H. M., et al., (1972) *Biological Applications of Electron Spin Resonance*, Wiley-Interscience, New York.

92. Atherton, N. M. (1973) *Electron Spin Resonance*, Wiley, New York.

93.   Dorio, M. M. a. F., J. H. (1979) *Multiple Electron Resonance Spectroscopy*, Plenum, New York.

94.   Schweiger, A. (1982) *Structure and Bonding*, Vol. 51.

95.   Abragam, A. a. P., M. H. L. (1951) *Proc. R. Soc. Lond. A 205*, 135-153.

96.   Lowe, D. J. (1992) ENDOR and EPR of metalloproteins, *Prog.Biophys.Molec.Biol 57*, 1-22.

97.   Van Doorslaer, S., and Vinck, E. (2007) The strength of EPR and ENDOR techniques in revealing structure-function relationships in metalloproteins, *Physical Chemistry Chemical Physics 9*, 4620-4638.

98.   Conrad, R. (1996) Soil microorganisms as controllers of atmospheric trace gases (H 2 , CO, CH 4 , OCS, N 2 O and NO), *Microbiological Reviews 60*, 609-640.

99.   Ungerfeld, E. M., Rust, S. R., Boone, D. R., and Liu, Y. (2004) Effects of several inhibitors on pure cultures of ruminal methanogens, *Journal of Applied Microbiology 97*, 520-526.

100.   Rouviere, P. E., Escalante-Semerena, J. C., and Wolfe, R. S. (1985) Component A2 of the methylcoenzyme M methylreductase system from Methanobacterium thermoautotrophicum *Journal of Bacteriology 162*, 61-66.

101.   Blaut, M., Müler, V., and Gottschalk, G. (1992) Energetics of methanogenesis studied in vesicular systems, *Journal of Bioenergetics and Biomembranes 24*, 529-546.

102.   Blaut, M. (1994) Metabolism of methanogens, *Antonie van Leeuwenhoek 66*, 187-208.

103. Rouviere, P. E., Bobik, T. A., and Wolfe, R. S. (1988) Reductive activation of the methyl coenzyme M methylreductase system of Methanobacterium thermoautotrophicum D H, *Journal of Bacteriology 170*, 3946-3952.

104. Sauer, K. a. T., R. K. (1999) Methanol: coenzyme M methyltransferase from *Methanosarcina barker*i-substitution of corrinoid harboring subunit MtaC by free Co(I)balamine, *Eur. J. Biochem 261*, 674-681.

105. Gunsalus, R. P., Romesser, J. A., and Wolfe, R. S. (1978) Preparation of coenzyme M analogues and their activity in the methyl coenzyme M reductase system of Methanobacterium thermoautotrophicum *Biochemistry 17*, 2374-2377.

106. Noll, K. M., Donnelly, M. I., and Wolfe, R. S. (1987) Synthesis of 7-mercaptoheptanoylthreonine phosphate and its activity in the methylcoenzyme M methylreductase system, *Journal of Biological Chemistry 262*, 513-515.

107. Schönheit, P., Moll, J., and Thauer, R. K. (1980) Growth parameters (K_S, μ_{max}, Y_S) of methanobacterium thermoautotrophicum *Archives of Microbiology 127*, 59-65.

108. Bradford, M. M. (1976) *Analytical Biochemistry 72*, 248-254.

109. Fish, W. W. (1988) Rapid colorimetric micromethod for the quantitation of complexed iron in biological sample, *Methods in Enzymology 158*, 357-364.

110. Beinert, H., and Albracht, S. P. J. (1982) New insights, ideas and unanswered questions concerning iron-sulfur clusters in mitochondria, *Biochimica et Biophysica Acta 683*, 245-277.

111. Brandis, A., Thauer, R. K., and Stetter, K. O. (1981) Relatedness of strains DH and Marburg of Methanobacterium thermoautotrophicum, *Zentralblatt fuer*

Bakteriologie, Mikrobiologie und Hygiene, Abt. 1, Originale C: Allgemeine, Angewandte und Oekologische Mikrobiologie 2, 311-317.

112.   Stettler, R., and Leisinger, T. (1992) Physical map of the Methanobacterium thermoautotrophicum Marburg chromosome, *Journal of Bacteriology 174*, 7227-7234.

113.   Woestenenk, E. A., Hammarstroem, M., van den Berg, S., Haerd, T., and Berglund, H. (2004) His tag effect on solubility of human proteins produced in Escherichia coli: a comparison between four expression vectors, *Journal of Structural and Functional Genomics 5*, 217-229.

114.   Pietzsch, M., Wiese, A., Ragnitz, K., Wilms, B., Altenbuchner, J., Mattes, R., and Syldatk, C. (2000) Purification of recombinant hydantoinase and L-N-carbamoylase from Arthrobacter aurescens expressed in Escherichia coli: comparison of wild-type and genetically modified proteins, *Journal of Chromatography, B: Biomedical Sciences and Applications 737*, 179-186.

115.   Chant, A., Kraemer-Pecore, C. M., Watkin, R., and Kneale, G. G. (2005) Attachment of a histidine tag to the minimal zinc finger protein of the Aspergillus nidulans gene regulatory protein AreA causes a conformational change at the DNA-binding site, *Protein Expression and Purification 39*, 152-159.

116.   Schmeisser, H., et al. (2006) Binding Characteristic of IFN-α Subvariants to IFNAR2-EC and Influence of the 6-Histidine Tag, *Journal of Interferon & Cytokine Research 26*, 866-876.

117.   Rogers, K. R., Gillies, K., and Lancaster, J. R., Jr. (1988) Iron-sulfur centers involved in methanogenic electron transfer in Methanobacterium

thermoautotrophicum (delta-H), *Biochemical and Biophysical Research Communications 153*, 87-95.

118. Kunz, R. C., Horng, Y. C., and Ragsdale, S. W. (2006) Spectroscopic and kinetic studies of the reaction of bromopropanesulfonate with methyl-coenzyme M reductase, *Journal of Biological Chemistry 281*, 34663-34676.

119. Schweiger, A., and Jeschke, G. (2001) *Principles of Pulse Electron Paramagentic Resonance*, Oxford Press, Oxford.

120. http://www.esr.ethz.ch

121. Madi, Z. L., Van Doorslaer, S., and Schweiger, A. (2002) Numerical Simulation of One- and Two-Dimensional ESEEM Experiments, *Journal of Magnetic Resonance 154*, 181-191.

122. Jeschke, G., and Schweiger, A. (1995) Hyperfine-correlated electron nuclear double resonance spectroscopy, *Chemical Physics Letters 246*, 431-438.

123. Harmer, J., Finazzo, C., Piskorski, R., Bauer, C., Jaun, B., Duin, E. C., Goenrich, M., Thauer, R. K., Van Doorslaer, S., and Schweiger, A. (2005) Spin density and coenzyme M coordination geometry of the ox1 form of methyl-coenzyme M reductase: A pulse EPR study, *Journal of the American Chemical Society 127*, 17744-17755.

124. Yang, N., Reiher, M., Wang, M., Harmer, J., and Duin, E. C. (2007) Formation of a Nickel-Methyl Species in Methyl-Coenzyme M Reductase, an Enzyme Catalyzing Methane Formation, *Journal of the American Chemical Society 129*, 11028-11029.

125. Goenrich, M., Mahlert, F., Duin, E. C., Bauer, C., Jaun, B., and Thauer, R. K. (2004) Probing the reactivity of Ni in the active site of methyl-coenzyme M reductase with substrate analogues, *Journal of Biological Inorganic Chemistry 9*, 691-705.

126. Lin, S. K., and Jaun, B. (1992) Coenzyme F430 from methanogenic bacteria: mechanistic studies on the reductive cleavage of sulfonium ions catalyzed by F430 pentamethyl ester, *Helvetica Chimica Acta 75*, 1478-1490.

127. Stolzenberg, A. M., and Zhang, Z. (1997) F430 model chemistry. An investigation of nickel complexes as catalysts for the reduction of alkyl halides and methyl coenzyme-M by sodium borohydride, *Inorganic Chemistry 3635*, 593-600.

128. Grabarse, W., Mahlert, F., Duin, E. C., Goubeaud, M., Shima, S., Thauer, R. K., Lamzin, V., and Ermler, U. (2001) On the mechanism of biological methane formation: structural evidence for conformational changes in methyl-coenzyme M reductase upon substrate binding, *Journal of Molecular Biology 309*, 315-330.

129. Grabarse, W., Shima, S., Mahlert, F., Duin, E. C., Thauer, R. K., Ermler, U., Messerschmidt, A., Huber, R., Poulos, T., and Wieghardt, K. (2001) Methyl-coenzyme M reductase, in *Handbook of Metalloproteins*, pp 897-914, John Wiley & Sons, Ltd, Chichester.

130. Andersson, K. K., and Hooper, A. B. (1983) Oxygen and water are each the source of one oxygen atom in nitrite produced from ammonia by Nitrosomonas: nitrogen-15 NMR evidence, *FEBS Letters 164*, 236-240.

131. Hooper, A. B., Maxwell, P. C., and Terry, K. R. (1978) Hydroxylamine oxidoreductase from Nitrosomonas: absorption spectra and content of heme and metal, *Biochemistry 17*, 2984-2989.

132. Terry, K. R., and Hooper, A. B. (1981) Hydroxylamine oxidoreductase: a 20-heme, 200,000 molecular weight cytochrome c with unusual denaturation properties which forms a 63,000 molecular weight monomer after heme removal, *Biochemistry 20*, 7026-7032.

133. Erickson, R. H., and Hooper, A. B. (1972) Preliminary characterization of a variant co-binding heme protein from Nitrosomonas, *Biochim Biophys Acta FIELD Full Journal Title:Biochimica et biophysica acta 275*, 231-244.

134. Andersson, K. K., Kent, T. A., Lipscomb, J. D., Hooper, A. B., and Munck, E. (1984) Moessbauer, EPR, and optical studies of the P-460 center of hydroxylamine oxidoreductase from Nitrosomonas. A ferrous heme with an unusually large quadrupole splitting, *Journal of Biological Chemistry 259*, 6833-6840.

135. Andersson, K. K., Babcock, G. T., and Hooper, A. B. (1991) P460 of hydroxylamine oxidoreductase of Nitrosomonas europaea: Soret resonance Raman evidence for a novel heme-like structure, *Biochemical and Biophysical Research Communications 174*, 358-363.

136. Arciero, D. M., Hooper, A. B., Cai, M., and Timkovich, R. (1993) Evidence for the structure of the active site heme P460 in hydroxylamine oxidoreductase of Nitrosomonas, *Biochemistry 32*, 9370-9378.

137. Prince, R. C., and George, G. N. (1997) The remarkable complexity of hydroxylamine oxidoreductase, *Nature Structural Biology 4*, 247-250.

138. Wehrfritz, J.-M., Reilly, A., Spiro, S., and Richardson, D. J. (1993) Purification of hydroxylamine oxidase from Thiosphaera pantotropha. Identification of electron acceptors that couple heterotrophic nitrification to aerobic denitrification, *FEBS Letters 335*, 246-250.

139. Otte, S., Schalk, J., Kuenen, J. G., and Jetten, M. S. M. (1999) Hydroxylamine oxidation and subsequent nitrous oxide production by the heterotrophic ammonia oxidizer Alcaligenes faecalis, *Applied Microbiology and Biotechnology 51*, 255-261.

140. Schalk, J., De Vries, S., Kuenen, J. G., and Jetten, M. S. M. (2000) Involvement of a novel hydroxylamine oxidoreductase in anaerobic ammonium oxidation, *Biochemistry 39*, 5405-5412.

141. Jetten, M. S. M., De Bruijn, P., and Kuenen, J. G. (1997) Hydroxylamine metabolism in Pseudomonas PB16: involvement of a novel hydroxylamine oxidoreductase, *Antonie van Leeuwenhoek 71*, 69-74.

142. Holmes, A. J., Costello, A., Lidstrom, M. E., and Murrell, J. C. (1995) Evidence that particulate methane monooxygenase and ammonia monooxygenase may be evolutionarily related, *FEMS Microbiology Letters 132*, 203-208.

143. Bergmann, D. J., Zahn, J. A., Hooper, A. B., and Dispirito, A. A. (1998) Cytochrome P460 genes from the methanotroph Methylococcus capsulatus Bath, *Journal of Bacteriology 180*, 6440-6445.

144. Bergmann, D. J., Hooper, A. B., and Klotz, M. G. (2005) Structure and sequence conservation of hao cluster genes of autotrophic ammonia-oxidizing bacteria: Evidence for their evolutionary history, *Applied and Environmental Microbiology 71*, 5371-5382.

145. Zahn, J. A., Duncan, C., and DiSpirito, A. A. (1994) Oxidation of hydroxylamine by cytochrome P-460 of the obligate methylotroph Methylococcus capsulatus Bath, *Journal of Bacteriology 176*, 5879-5887.